

# Constraint-based modeling of astrocyte metabolism in neuropsychiatric disorders

*by Anirudh Chellappa*

---

**Submission date:** 27-Sep-2023 12:20PM (UTC+0530)

**Submission ID:** 2178335405

**File name:** Thesis\_for\_plagiarism.docx (5.54M)

**Word count:** 23111

**Character count:** 144584

## 1. Introduction.

20

Psychiatric disorders, encompassing conditions like bipolar disorder (BD), schizophrenia (SCZ), major depressive disorder (MDD), obsessive-compulsive disorder (OCD), substance abuse disorder (SUD), etc., contribute significantly to morbidity<sup>1</sup> and mortality<sup>2</sup> globally, and has a profound impact on an individual's daily life. While twin studies have shown high heritability<sup>3</sup>, most psychiatric disorders do not align with the Mendelian monogenic model; rather, they arise from multifactorial causes influenced by multiple genes<sup>4</sup>. Psychiatric symptoms transcend contemporary diagnostic boundaries. In the case of BD and SCZ, there's a significant overlap in terms of clinical symptoms<sup>5</sup>, genetics<sup>6-8</sup>, brain structure anomalies<sup>9,10</sup>, cellular/molecular factors<sup>11,12</sup>. Despite available treatments, there's variability in responses and potential side effects. Predicting the course of the illness and treatment response upon patients' arrival at the clinic remains challenging<sup>13,14</sup>. Genome-wide association studies (GWAS) and sequencing studies have been successful in identifying thousands of genetic variants associated with various psychiatric disorders<sup>15,16</sup>. However, translating the genetic insights into clinical risk assessment and treatment prediction remains elusive. The main reason for this is our limited foundational understanding of the biological pathways, networks, cell-types and neuronal/glial circuits that these genes operate on. Genomic discoveries on psychiatric disorders, particularly BD and SCZ, tend to converge on altered synaptic pathways in specific excitatory and inhibitory neurons<sup>17-19</sup>. However, there's growing recognition that glial cells, especially astrocytes, through non-cell autonomous functions, mediate neuronal function and contribute to the etiology of BD and SCZ<sup>12,20-22</sup>.

Astrocytes constitute around 20-30% of CNS cell count<sup>23</sup> and play a vital role in maintaining CNS homeostasis. They provide trophic support to neurons<sup>24</sup>, facilitate synapse formation and pruning during development<sup>25</sup>, and form physical contacts with the vasculature enabling metabolite and ion exchange<sup>26</sup>. Historically, astrocyte subtypes have been known to occupy specific brain areas<sup>27,28</sup>, however more recently, it is shown that astrocytes exhibit transcriptomic and functional diversity across brain regions and even within cortical layers<sup>28,29</sup>. These cells are crucial for brain energy metabolism, which is substantial, accounting for 20-25% of the body's energy consumption<sup>30</sup>. Astrocytes primarily generate ATP through glycolysis, releasing lactate into the extracellular space<sup>31-35</sup>. They regulate the balance in the extracellular environment, sensing messenger molecules like glutamate<sup>36</sup>, ATP<sup>37</sup>, D-Serine<sup>38</sup>, potassium<sup>39</sup>, nitric oxide<sup>40-42</sup>, hydrogen peroxide<sup>43,44</sup>, and ammonia<sup>45</sup>. Although glucose metabolism is key, research emphasizes the significance of lipid metabolism in maintaining brain equilibrium, especially through astrocytic fatty acid oxidation (FAO)<sup>46</sup>. Astrocytic networks contribute to brain activity, plasticity, and behavior<sup>47</sup>. Astrocytes operate within defined territories<sup>48</sup>, and it is essential for them to form functional networks that are essential for complex behaviors. And finally, these cells

exhibit diverse responses to various pathological conditions, including acute infection<sup>49-51</sup>, injury<sup>52-54</sup>, and diseases like Huntington's<sup>55,56</sup>, Alzheimer's<sup>57,58</sup>, Parkinson's<sup>59</sup>, glioblastoma<sup>60</sup>, but are also implicated in psychiatric disorders including BD<sup>61-64</sup> and SCZ<sup>20-22,65-67</sup>.

## 2. Review of literature.

### 2.1. Psychiatric disorders.

Psychiatric disorders are a group of mental health conditions characterized by persistent changes in behavior, thoughts, moods, and emotions that can have a profound impact on an individual's daily life. They significantly contribute to morbidity<sup>1</sup> and mortality<sup>2</sup> globally, imposing a considerable burden on individuals and society. Onset usually occurs during adolescence or young adulthood, leading to prolonged periods of illness. Those with severe mental illness (SMI) often face lower socioeconomic status<sup>3</sup>, experience stigma<sup>70</sup>, and are more prone to substance use<sup>71</sup> and somatic disease<sup>72</sup>, all of which<sup>83</sup> negatively impact their well-being and quality of life. Individuals with SMI have an average life expectancy about 10 years shorter than the general population<sup>2,73</sup>, with excess mortality attributed to physical health issues, especially cardiovascular disease<sup>74,75</sup> and mental health-related causes like suicide<sup>76</sup>. Psychiatric disorders could be classified into different categories, including mood disorders (e.g., depression, bipolar disorder), anxiety disorders (e.g., generalized anxiety disorder, panic disorder), impulse control disorders (e.g., attention-deficit/hyperactivity disorder), substance use disorders (alcohol and drug abuse<sup>49</sup> with or without dependence), and psychotic disorders (e.g., schizophrenia). The median lifetime prevalence estimates for mood disorders are 3.3-21.4%, for anxiety disorders are 4.8-31.0%, for impulse control disorders are 0.3-25.0%, for substance use disorders are 1.3-15.0%, and for psychotic disorders are 3.06-3.48%, as estimated by epidemiology studies<sup>77,78</sup>. The prevalence of these conditions can vary depending on the population, but overall, psychiatric disorders account for a significant amount of lived years with disability. The urgent need to improve mental health care has been emphasized by the World Health Organization<sup>79</sup>.

In terms of treatment, psychiatric disorders are managed through a combination of medication and therapy. Antidepressant medications<sup>80</sup>, such as selective serotonin reuptake inhibitors (SSRIs), can be effective in treating depression, while mood stabilizers<sup>81</sup> and antipsychotics<sup>13</sup> are commonly used to manage BD and SCZ, respectively. Psychotherapy, such as cognitive behavioral therapy (CBT)<sup>82</sup>, can also help individuals manage their symptoms, learn coping strategies, and improve their overall quality of life. Electroconvulsive therapy (ECT)<sup>83</sup> is a treatment that involves applying electrical stimulation to the brain through electrodes placed on the scalp, and is typically considered a last resort for patients who have not responded to other treatments such as medications, psychotherapy or other forms of brain stimulation. While existing treatments may have clinically meaningful effects in psychiatric disorders<sup>83,84</sup>, they are rarely curative, leading to relapses and adverse effects experienced by many patients, and therapeutic non-response is common<sup>13,14</sup>. Inadequate therapeutic options can largely be attributed to the limited understanding of the causes of mental illness, despite intensive research efforts over

<sup>3</sup> decades. Psychiatric nosology still relies on traditional diagnostic distinctions based on clinical observations. The current leading diagnostic classification systems, the International Classification of Diseases<sup>85</sup> and the Diagnostic and Statistical Manual of Mental Disorders<sup>86</sup>, primarily diagnose psychiatric disorders based on signs and symptoms, lacking objective biomarkers, which makes clinical psychiatry more susceptible to unwanted variability in both diagnostic and therapeutic decision-making<sup>87</sup>. Although the present diagnostic categories are clinically useful, there is little evidence to suggest that they represent truly discrete entities with natural boundaries<sup>88,89</sup>, as indicated by high comorbidity and shared symptomatology across different mental disorders<sup>90,91</sup> and high heterogeneity within diagnostic categories<sup>92</sup>.

<sup>36</sup> Genetics play a significant role in the development of psychiatric disorders<sup>93</sup>. The history of psychiatry is intimately connected to heredity. Mental illnesses' tendency to run in families was observed by early physicians and later systematically evaluated through twin<sup>94</sup>, family<sup>95-97</sup>, and adoption<sup>98</sup> genetic epidemiological studies in the 20th century. This exceptional body of evidence revealed that common psychiatric disorders are moderately to strongly heritable, providing a significant etiological clue for the field<sup>3</sup>. However, it is now understood that these genetic effects are relatively small and non-deterministic<sup>4</sup>: most individuals with a strong family history are not affected, similar to observations in many complex biomedical diseases. Additionally, most psychiatric disorders do not necessarily show a consistent pattern within families. For instance, relatives of individuals with SCZ have increased risks not only for SCZ but also for various other conditions like BD, MDD and autism<sup>99,100</sup>. The wide range of clinical presentations and varying courses seen in many common psychiatric disorders align with the notion of complex and relatively small genetic effects. In particular, adult-onset common psychiatric disorders often exhibit development within normal limits, although higher cognitive functions may be impaired to some extent<sup>101</sup>. It is also important to note that genetics alone do not determine the development<sup>26</sup> of a psychiatric disorder. Environmental factors, such as trauma<sup>102</sup>, stress<sup>103</sup>, and substance abuse<sup>104</sup>, can also contribute to the onset of these conditions.

<sup>3</sup> A better understanding of the underlying biological mechanisms is needed to improve the care and prevention of mental illness. However, challenges in studying the living human brain and uncertain validity of animal models of mental illness have limited progress in biological research in psychiatry<sup>105</sup>. As a result, there have been no major therapeutic advances in psychiatry in the past decades<sup>106</sup>, and current attention is focused on potential new treatment options, such as repurposing existing drugs like ketamine<sup>107</sup> or psychedelics<sup>108</sup>. Nevertheless, the substantial heritability of psychiatric disorders<sup>3,109</sup> indicates that genetic research could provide valuable pathobiological insights and help in understanding gene-environment interplay and environmental effects.

Despite the high expectations<sup>79</sup> for psychiatric genetics with the increasing availability of DNA sequencing technologies in the second half of the 20th century, a false start occurred in the 1990s and early 2000s. Findings from the candidate gene approach lacked reproducibility, leading to decreased confidence<sup>87</sup> in discovering mental illness genes<sup>110,111</sup>. However, major breakthroughs occurred with the sequencing of the human genome in 2003<sup>112</sup>, and the establishment of reference datasets documenting human genetic variation across different populations<sup>113,114</sup>. These advancements allowed for a systematic exploration of DNA sequence variants associated with human traits and diseases.<sup>2</sup> Since then, a steady and accelerating progress in human genetics<sup>115</sup> has been observed, driven by a combination of technological innovations, more advanced statistical analytical tools, reduced costs for genotyping and sequencing DNA, enhanced knowledge about the genome, and increased international collaboration. Psychiatric genetics has been at the forefront of these efforts, recognizing the importance of assembling large-scale case-control cohorts of psychiatric disorders to reliably identify genetic variants, most of which have very weak effects. These efforts have gradually led<sup>2</sup> to the discovery of multiple genetic risk variants for mental illness<sup>15,16</sup> (Fig.S1). Despite major advances<sup>2</sup> in our understanding of the genetic architecture of mental illness over the last decade, these discoveries have not yet translated into improved care for individuals with mental illness, which remains the key challenge for the field.

Gaining insights into the underlying<sup>3</sup> etiology of illness is one of the key aims of human genetics, informing the development of new therapeutic interventions and aiding biomarker identification. However, translating genetic findings into biological mechanisms is not straightforward. A complete mechanistic<sup>3</sup> understanding of a disorder's genetic risk architecture necessitates identifying the specific causal variant underlying a genetic signal, determining the functional impact of the genetic variant, and understanding how all the genetic risk variants collectively influence biological pathways in specific cell-types, tissues, and organs, throughout developmental stages, and in conjunction with environmental factors<sup>116,117</sup>. This presents a considerable challenge, requiring comprehensive animal studies, cell-biology experiments, and advanced computational approaches. The current mechanistic interpretation is also limited by the incomplete understanding of the physiological role of most genes and proteins, including their interactions within signaling networks and pathways<sup>118</sup>.

## 2.2. Bipolar disorder.

2

Bipolar disorder (BD) is a severe psychiatric illness characterized by manic/depressive episodes and persistent neurocognitive impairments<sup>119</sup>, affecting 0.5% of the population (ca. 7 million in India)<sup>120</sup>. It is a significant cause of disability, morbidity, and mortality (15% die by suicide)<sup>121</sup>. The concept of BD was originally included in the idea of manic-depressive illness put forth by Kraepelin in 1899<sup>122</sup>. This included both single and recurring forms of MDD and BD. In 1957, Leonard proposed that BD-I and MDD were separate syndromes<sup>123</sup>, which was confirmed by family studies showing that relatives of BD-I patients had a 10-fold increased risk of BD and an increased risk of MDD, while relatives of MDD patients had elevated rates of MDD but only slightly higher rates of BD than those of control relatives<sup>124</sup>. Both twin and adoption studies indicate that genetics play an important role in BD, with heritability estimates ranging from 0.59 to 0.87 in twin studies<sup>125-127</sup>. Family/genetic strategies have also been used in efforts to validate potential subtypes of BD. The results of most such studies have been mixed, but supporting evidence is available for early versus late age at onset<sup>128</sup>, lithium responsivity<sup>129</sup>, psychotic BD<sup>130</sup>, puerperal mania<sup>131</sup>, comorbidity with panic disorder<sup>132</sup>, a preponderantly depressed vs. preponderantly manic course<sup>133</sup> and unipolar mania versus typical BD<sup>134</sup>. A large literature has examined the relationship between BD-I and BD-II disorder, requiring, respectively, full manic versus hypomanic episodes. Recent genetic studies have shown that BD-I has a higher single-nucleotide polymorphism (SNP) heritability and a higher genetic correlation with SCZ, while BD-II has a much higher genetic correlation with MDD<sup>135</sup>.

### 2.2.1. Genomics of bipolar disorder.

Advances in genotyping technology have made it possible to assay common variants in large-scale case-control studies, known as genome-wide association studies (GWAS). To date, there have been numerous GWAS studies performed on BD<sup>136-139</sup>, with the largest and most recent conducted by the Psychiatric Genomics Consortium (PGC) reporting 64 genetic loci linked to BD through analysis of 41,917 BD patients and 371,549 controls<sup>17</sup>. The genes identified include those involved in ion channels, neurotransmitter transporters, and synaptic components. On the other hand, the Bipolar Sequencing Consortium (BSC), despite having a sample of 13,933 cases and 14,422 controls, had not found significant associations with any specific gene but showed promising aggregate results: novel singleton protein truncating variants in genes intolerant to loss-of-function mutations are enriched in BP patients<sup>140</sup>. However, the BD genetic studies have several limitations. Firstly, the studies have limited power and have only identified a small portion (3.3% SNP heritability) of the genetic risk factors for BD. Secondly, most samples used in the studies have minimal phenotypic information, which can lead to less specific findings and lower heritability estimates. Thirdly, the studies have been mainly conducted using European populations, leading to uncertainty in how the findings can be applied to other populations and

potentially exacerbating healthcare disparities. Finally, the distribution of clinical features in BD patients may differ between human populations, highlighting the need for greater genetic diversity in research. To further the discovery of common and rare variants, more samples are required, and greater ancestral diversity should be prioritized.

#### 2.2.2. Clinical management of bipolar disorder.

Clinically, BD is characterized by mood swings with the patient alternating between mania and depression<sup>119</sup>. Managing BD effectively requires controlling these mood episodes and preventing relapse. Mood stabilizing agents are used for this purpose, with lithium (Li<sup>+</sup>) being the first-line mood stabilizer. Li<sup>+</sup> has been used since 1949<sup>141</sup>, and is the only effective drug for preventing suicides<sup>81,142</sup> and improving cognition<sup>143</sup> in BD patients. While Li<sup>+</sup> can be highly effective, not all patients respond to it: approximately 30% of patients have an excellent response, 30% show a partial response, and 40% are resistant to treatment and are considered non-responders, making their clinical management difficult<sup>144</sup>. When treating a chronic illness, being able to predict a patient's response to treatment is crucial for effective management. Without this capability, treatment often involves trial and error, leading to uncontrolled disease and a negative impact on long-term prognosis. The selection of mood stabilizers for BD is similarly challenging. Several studies have tried to link clinical parameters to response to Li<sup>+</sup> treatment, but the predictive power of these remains limited<sup>145</sup>. To be able to predict a patient's response to Li<sup>+</sup> would greatly benefit clinical management.

#### 2.2.3. Mechanisms of action of Lithium (Li<sup>+</sup>) in bipolar disorder.

The reason for the inability to predict responses to Li<sup>+</sup> is due to a lack of understanding of its mechanisms of action. It is believed that Li<sup>+</sup> affects brain cells by altering ongoing molecular processes, leading to changes in cellular function. The mechanisms of action of Li<sup>+</sup> in the brain is thought to be highly complex, inducing a multitude of effects on the protein expression, neurotransmission, circadian biology, ion transport, etc<sup>146</sup>. Two main proteins, inositol monophosphatase (IMPA1)<sup>147</sup> and glycogen synthase kinase-3 (GSK3)<sup>148</sup>, have been proposed as candidate targets, with others also being considered. Both of these proteins are inhibited at <sup>65</sup>Li<sup>+</sup> concentrations that approximate therapeutic blood levels, which are 0.5-1 mEq/L<sup>149</sup>. The 'inositol depletion' hypothesis, proposed by Berridge *et al.*<sup>150</sup>, suggests that Li<sup>+</sup>'s effectiveness in treating BD depends on inhibiting IMPA1, reducing inositol supply for phosphatidylinositol (PI) synthesis. Li<sup>+</sup>'s inhibition of IMPA1 shows unusual uncompetitive kinetics, and is seen only when the IMPA1 substrate inositol 1-phosphate (IP1) accumulates in cells. This mechanism implies selective inhibition in cells like neurons with high PI turnover. While a knockout of IMPA1 in mice suggested altered inositol signaling<sup>151</sup>, a suitable mouse model for BD remains elusive. GSK3 inhibition, instead of IMPA1, has been emphasized by researchers over the years<sup>152</sup>, but GSK3 inhibitors haven't progressed to BD clinical trials. Notably, amphibian studies indicated that Li<sup>+</sup>'s effects could be blocked by

inositol supplementation<sup>153</sup>. Observations in yeast<sup>154</sup> and mammalian neurons<sup>155</sup> demonstrated that GSK3 positively regulates myo-inositol 1-phosphate synthase, a key enzyme in inositol's de novo synthesis, further suggesting inositol homeostasis plays a vital role in Li+’s action. Inositol and GSK3 have been the main focus in understanding Li+’s mechanisms of action, emphasizing the pressing need for systematic and unbiased investigations to explore additional pathways involved.

### 2.3. Shared genetic risk and biology between bipolar disorder and schizophrenia.

Substantial overlap between BD and SCZ has been demonstrated by genetic and epidemiological studies, with a genetic correlation of around 0.6–0.7 for common variation<sup>6</sup>, along with high relative risks (RR) among relatives of both BD and SCZ patients (RRs for parent/offspring: BD/BD: 6.4, BD/SCZ: 2.4; SCZ/BD: 5.2, SCZ/SCZ: 9.9)<sup>156</sup>. Despite shared genetics and symptomatology, the current diagnostic systems<sup>86,88</sup> maintain historical distinctions from the late 19th century<sup>6</sup> presenting BD and SCZ as separate entities based on clinical presentation. BD is marked by predominant mood symptoms, mood-congruent delusions, and episodic course, while SCZ is seen as a prototypical psychotic disorder. These distinctions were initially suggested in the late 1950s and gained acceptance<sup>5</sup>. Syndromes like SCZ, BD, and MDD were separated based on symptom patterns and illness trajectory. However, features such as psychosis, mood dysregulation, and cognitive impairments were recognized to transcend diagnostic boundaries. Yet, uncertainties remain about whether these syndromes represent distinct entities, share foundations, or are different variations of an underlying disease due to the unknown biological understanding. For e.g., over time, the diagnosis for an individual patient has the potential to shift from BD to SCZ, or the other way around. These characteristics imply that the two disorders could potentially occupy distinct segments within a spectrum of psychosis. Research until the last decade indicated varying degrees of familial and genetic overlap for pairs of these disorders, and supports diagnostic boundaries between SCZ and BD, and BD and MDD<sup>125,157</sup>, but also implicate correlated familial and genetic liabilities<sup>125,156</sup>. Several genetic variants conferring risk for both SCZ and BD were also identified<sup>136,158,159</sup>.

However, the breakthrough came in 2013 when a study integrated SNP data from five neuropsychiatric disorders - autism spectrum disorder (ASD), attention deficit-hyperactivity disorder (ADHD), BD, MDD, and SCZ—in 33,332 cases and 27,888 controls<sup>7</sup>. This marked the first time all five conditions were simultaneously studied in a single GWAS. The study identified significant SNPs at four loci: regions on chromosomes 3p21 and 10q24, along with genes *CACNA1C* and *CACNB2*, related to L-type voltage-gated calcium channels. This suggests that genetic variation in fundamental systems like calcium channel signaling elevates the risk of general susceptibility to neuropsychiatric disorders, and a combination of other genetic and non-genetic risk factors guides this susceptibility towards specific disorder development.

In 2018, a more extensive and detailed genetic analysis of BD and SCZ, including 53,555 cases (20,129 BD, 33,626 SCZ) and 54,065 controls, along with 28 subphenotypes of BD (n=24) and SCZ (n=4), identified 114 shared genome-wide significant loci across these disorders<sup>8</sup>. While the study did indicate a substantial shared genetic risk, it also showcased that specific locations contribute to the observed differences in characteristics within these disorders.

The subphenotype examination indicated a significant positive correlation between i) BD PRS and manic symptoms in SCZ cases<sup>6</sup> and ii) BD PRS and psychotic attributes in BD patients. Additionally, the study noticed a significant increase in SCZ PRS in i) BD cases with psychotic traits, and ii) SCZ cases with increased negative<sup>6</sup> symptoms. This was the first study that discovered distinct genomic locations distinguishing BD and SCZ, uncovering polygenic elements underlying numerous symptom dimensions. These findings emphasize the utility of genetics and deep clinical phenotyping to guide symptomatology and potentially treatment in such complex traits.

While the shared genetic aspect is significant, studies also point to genetic architecture differences between these two disorders<sup>160,161</sup>. A polygenic<sup>6</sup> risk score (PRS) derived from a case-only SCZ versus BD GWAS correlated significantly with SCZ or BD diagnosis in an independent sample<sup>161</sup>, indicating that differences between disorders have a genetic basis. SCZ patients show an enrichment of rare, moderate to highly penetrant copy-number variants (CNVs), de novo CNVs and somatic CNVs<sup>162-168</sup>, while CNV involvement in BD is less clear<sup>169</sup> and perhaps limited to schizoaffective cases<sup>170</sup>. Although the role of de novo single nucleotide variants (SNVs) in BD and SCZ has been explored in a limited number of studies, enrichment in pathways linked to the postsynaptic density has been reported for SCZ but not BD<sup>171,172</sup>. Identifying disorder-specific variants and quantifying the contribution of genetic variation to<sup>6</sup> specific symptom dimensions remain important questions that will help comprehend dimensions of the disorders beyond dichotomous diagnosis. For example, it is known that SCZ patients with more manic symptoms have higher polygenic risk for BD<sup>161</sup>. These findings highlight shared genetic foundations for symptoms across disorders and might help stratify patients by genetic liability to symptom dimensions, thus informing disease course and treatment.

The genetic liability shared by SCZ and BD also manifests in terms of structural brain abnormalities, encompassing smaller<sup>9</sup> total brain and hippocampal sizes on average, along with larger ventricular sizes, reduced white matter volumes, and common regions of thinner cortex, across both SCZ and BD<sup>10,173-179</sup>. Nonetheless, disorder-specific irregularities were also noted, where the genetic liability for SCZ correlated with thicker right parietal cortex, while the genetic liability for BD linked to larger intracranial volume (ICV)<sup>180</sup>. Whether it is genetic, brain imaging, or cellular/molecular studies, first-degree relatives (FDRs) of patients can represent individuals with a familial susceptibility to the disorder, devoid of confounding factors such as medication or duration of illness. Thus, they offer distinct insight into how familial risk for the disorder influences the brain. Nonetheless, only a few studies have directly compared brain structure between FDRs-BD and FDRs-SCZ, usually in cohorts of moderate<sup>9</sup> sizes<sup>177,180-184</sup>. These studies revealed both distinct and overlapping brain irregularities for FDRs-SCZ and FDRs-BD, with findings being more accentuated in FDRs-SCZ than FDRs-BD.

However, it wasn't until 2019 when a comprehensive multicenter meta-analysis of magnetic resonance imaging (MRI) datasets, encompassing harmonized global and subcortical brain measures<sup>28</sup>, was undertaken, including data from a substantial number of participants, totaling 6,008 individuals (1,228 FDRs-SCZ, 852 FDRs-BD, 2,246 control subjects, 1,016 patients with SCZ, 666 patients with BD), hailing from 34 family cohorts associated with SCZ and/or BD<sup>9</sup>. This endeavor employed standardized methods to assess the patterns and extent of brain deviations in FDRs-BD and FDRs-SCZ, thus achieving increased power and generalizability. The outcomes revealed that FDRs-BD exhibited significantly larger intracranial volume (ICV), while FDRs-SCZ displayed reduced thalamic volumes when compared with control subjects. The findings suggested that despite their shared genetic liability, FDRs-SCZ and FDRs-BD manifest distinct structural brain irregularities, particularly in ICV. This divergence might suggest that the neurodevelopmental paths leading to brain abnormalities in SCZ or BD could be distinct.

The common variants reported by GWAS<sup>17,185,186</sup>, along with rare variants from exome sequencing<sup>171,187,188</sup> and transcriptomic analyses of post-mortem brains<sup>189,190</sup>, have consistently pinpointed synaptic function as a significant risk pathway in both BD and SCZ. With the potential for this to be manifested in molecular alterations within synapses of patients affected by these disorders, and considering advancements in biochemical fractionation for purifying<sup>17</sup> synapses and mass spectrometry-based proteomics<sup>191-193</sup>, a comprehensive, in-depth, and unbiased proteomic profiling of synaptic fractions derived from the dorsolateral prefrontal cortex (DLPFC) of individuals with BD and SCZ was undertaken in 2023<sup>11</sup>, as a follow-up to uncover the molecular basis of the past decade's genomic findings. The research unveiled highly comparable alterations in several proteins and molecular pathways within human BD and SCZ<sup>17</sup> synapses. These pathways notably encompassed synaptic function, revealing a decline in glutamate receptors (including AMPA, NMDA, and Kainate receptors), molecules within the glutamatergic signaling pathway (such as PLCB1 and APP), and postsynaptic scaffolding proteins (like HOMER1 and SHANK3). Surprisingly, the study also identified proteins associated with mitophagy, ribophagy, and aggrephagy, alongside other processes like enhanced vesicle tethering and proteins linked to forward and retrograde secretory trafficking, mitochondrial respiration, and mRNA translation, all disrupted within synapses of SCZ and BD patients.

These findings were in line with an earlier study from 2018<sup>12</sup>, which had the goal of examining the cortical molecular pathology across five major neuropsychiatric disorders (ASD, SCZ, BD, MDD, and alcoholism) through the meta-analysis of gene expression microarray datasets. The results unveiled a significant overlap in gene expression patterns among ASD, SCZ, and BD, as well as SCZ, BD, and MDD. Moreover, the study suggested a gradient of down-regulated synaptic genes, with ASD having the highest down-regulation, followed by SZ and BD. While BD and SCZ appeared notably similar in terms of synaptic

malfunction, MDD exhibited no synaptic pathology. However, MDD did show dysregulation in HPA-axis and hormonal signaling, which was absent in the other disorders. The data suggests that the degree of sharing of dysregulation in gene expression is related to polygenic overlap across disorders, suggesting a significant causal genetic component. Both the synapse proteomics<sup>11</sup> and the transcriptome meta-analysis<sup>12</sup> studies provide a comprehensive view of the neurobiological architecture of major neuropsychiatric illnesses, and demonstrates convergence but also specificity at the level of molecules and biological pathways.

## 2.4. Cell-types implicated in bipolar disorder and schizophrenia.

The genetic architectures of complex brain disorders<sup>11</sup> are closely linked to the genes whose expression defines specific brain cell-types<sup>194</sup>, and connecting the genomic results to cellular studies is crucial for prioritizing cells underlying the genes<sup>85</sup> of such complex phenotypes<sup>195,196</sup>. The largest and most recent BD GWAS hits were enriched in both inhibitory (medium spiny neurons/MSNs, striatal interneurons) and excitatory (pyramidal neurons SS, pyramidal neurons CA1) neurons over other cell-types within cortical and subcortical brain regions in mice<sup>17</sup>. Using human brain samples, the signal enrichment was observed in hippocampal pyramidal neurons and prefrontal cortex and hippocampal interneurons<sup>17</sup>.

In the<sup>11</sup> case of SCZ GWAS, akin to BD, using mice scRNA-seq data<sup>19</sup>, the hits were enriched in both excitatory (glutamatergic pyramidal neurons from the cortex and hippocampus) and inhibitory (cortical interneurons and MSNs) cells, and notably less consistent with embryonic<sup>11</sup> progenitor, or glial cells<sup>186</sup>. Using human scRNA-seq data<sup>197</sup>, the enrichment was observed in excitatory (glutamatergic neurons from the cerebral cortex, hippocampus-pyramidal CA1 and CA3 cells, and granule cells of dentate gyrus) and inhibitory (cortical interneurons) cells<sup>186</sup>. In MDD GWAS, unlike SCZ or BD, the enrichment was limited to cortical interneurons and embryonic midbrain neurons<sup>19</sup>, but also to neuroblasts<sup>18</sup>. The molecular targets of antipsychotic medications, as defined by pharmacology, were also linked to the<sup>11</sup> same cell-types as those associated with the schizophrenia GWAS findings, including the neocortical S1 pyramidal cells, MSNs, hippocampal CA1 pyramidal cells, and cortical interneurons<sup>19</sup>.

Striatal MSNs have been of interest to SCZ due to several factors: i) their involvement in expressing dopamine type 2 and type 1 receptors (Drd2, Drd1), with Drd2 being a common target for effective antipsychotic medications<sup>198</sup>; ii) enrichment of MSNs through SCZ GWAS findings<sup>19</sup>; and iii) the significant overlap between antipsychotic-induced differentially expressed genes (DEGs) in mice striatum and the genes implicated in SCZ GWAS<sup>199</sup>. Drawing from these rationales, a recent investigation conducted single-cell RNA-seq analysis to scrutinize DEGs within distinct striatal cell-types in C57BL/6 mice subjected to chronic exposure to a typical antipsychotic (haloperidol), an atypical antipsychotic (olanzapine), or a placebo<sup>200</sup>. The study determined that, for olanzapine, genes specifically upregulated in MSNs exhibited significantly greater overlap with the most recent SCZ GWAS discoveries. Nevertheless, when considering rare genetic variations, there was no convergence of any DEG (whether related to MSNs or other cell-types) with genes identified in a meta-analysis of SCZ WES study by the Schizophrenia Exome Sequencing Meta-analysis (SCHEMA) consortium<sup>187</sup>. These findings underscore a fundamental link between SCZ GWAS findings and genes upregulated in MSNs following exposure to olanzapine.

Glial cells (astrocytes, oligodendrocytes, and microglia) did not show enrichment for the most recent GWAS findings in BD or SCZ. However, a study in 2014<sup>20</sup>, utilizing the PGC1 SCZ GWAS data<sup>158</sup>, did reveal notable associations between expert-curated astrocyte and oligodendrocyte gene sets and the risk to SCZ. Similarly, analyses of transcriptome data from psychiatrically ill postmortem brains did reveal up-regulation of astroglial gene sets, potentially representing astrocytosis or activation, in SCZ, BD and ASD<sup>12,21</sup>. More recently, by integrating the latest SCZ GWAS findings with the transcriptome data of induced neurons from healthy human donors, co-cultured with murine glial cells, the study found significant correlations between variants adjacent to astrocyte-related genes and SCZ, which suggests that astrocytes might induce transcriptional programs related to SCZ in neurons<sup>22</sup>.

## 2.5. Astrocytes.

Astrocytes, constituting <sup>18</sup> significant cellular proportion in the central nervous system (CNS), account for 20-40% of the total <sup>18</sup> CNS cell count<sup>23</sup>, depending on the species under investigation. Together with other brain and spinal cord glial cells (oligodendrocytes and microglia), the CNS's homeostasis is maintained by astrocytes throughout development<sup>27,201</sup>, normal physiology, and aging<sup>202</sup>. Astrocytes also play their roles in higher order functions like learning and memory<sup>203</sup>, control of emotional states<sup>204</sup>, sensory-motor responses<sup>205</sup> and decision making<sup>206</sup>. Despite profound changes occurring in response to disease<sup>207-215</sup>, astrocytes remain <sup>1</sup> a fundamental element of the brain's usual environment. Notably, they offer essential trophic support to neurons<sup>24</sup>, facilitate synapse formation, function and pruning during development<sup>25</sup>, and form extensive networks with vasculature for metabolite uptake and distribution within the CNS<sup>26</sup>.

<sup>18</sup> Core homeostatic functions in the brain are performed by astrocytes, making them <sup>1</sup> an integral part of the blood-brain barrier (BBB)<sup>216</sup>. They sense and respond to peripheral insults like inflammation<sup>217</sup> while taking up metabolites to fuel the brain<sup>218</sup>. Specifically, glucose is taken up from the bloodstream, stored as glycogen, or converted into lactate to support active neurons through the astrocyte-neuron lactate shuttle<sup>219</sup>. This metabolite shuttle is closely tied to an antioxidant exchange system involving glutathione, ensuring homeostatic control of neuronal redox stress through astrocyte-mediated shuttling of glutathione precursors to neurons<sup>220</sup>. Moreover, astrocytes can uptake and metabolize synaptically released neurotransmitters<sup>221</sup>, partially contribute to the glymphatic system via aquaporin 4 (AQP4) channels<sup>222</sup>, and phagocytose synapses<sup>223,224</sup>. With each astrocyte connecting to thousands of synapses in rodents and millions in humans<sup>48,225</sup>, they have a far-reaching capacity to interact with numerous cells in the CNS, hinting at the possibility of integrating neuronal signaling and circuit functions<sup>201,226</sup>.

<sup>1</sup> Astrocytes are derived from radial glial cells at the ventricular zone around embryonic day 18 in mice (approximately 16-18 weeks in human gestation), coinciding with the end of neurogenesis, until approximately post-natal day <sup>7</sup><sup>227,228</sup>. Following maturation, they spread throughout the entire brain, forming distinct domains due to contact inhibition between their processes. This maturation gives rise <sup>2</sup> various astrocyte subtypes occupying specific brain areas<sup>27,28</sup>. Conventionally, they were categorized as either grey matter, protoplasmic astrocytes, or white matter, fibrous astrocytes based on location and morphology<sup>229</sup>, but this oversimplified classification underestimates their true heterogeneity. In reality, astrocytes exhibit transcriptomic and functional diversity across brain regions and even within cortical layers<sup>28,29</sup>. While the exact mechanisms behind this maturational diversity remain unclear, it is believed to arise, in part, from their derivation from different precursors and the cues they receive from neurons and neuronal activity<sup>230-232</sup>.

In the CNS, various markers are utilized at the gene and protein level to characterize astrocytes, such as GFAP, vimentin, ALDH1L1, GLAST, AQP4 and S100 $\beta$ <sup>233,234</sup>. However, finding a perfect and specific cellular marker for all astrocytes is challenging as it depends on the context, CNS region, and methods employed. GFAP<sup>18</sup> for example, exhibits heterogeneity at the protein level<sup>233</sup>, and ALDH1L1 provides a homogeneous driver for genetically controlled reporters but has limited detection through immunofluorescence. Moreover, using Aldh1l1 as a driver in knockout/knockdown experiments raises concerns due to its high expression in the liver<sup>235</sup>. Continued exploration into astrocyte functions will be facilitated by the discovery of new markers for regionally constrained, developmentally regulated, or heterogeneous reactive populations of astrocytes. Moreover, these more specific markers will reveal potential novel druggable targets, aiding in the treatment of CNS diseases without a current cure.

Astrocytes, like other non-neuronal cells in the CNS, showcase rapid and diverse responses to various pathological insults, whether triggered by acute infection<sup>49–51</sup> or injury<sup>52–54</sup>, or linked to diseases like Huntington's<sup>55,56</sup>, Alzheimer's<sup>57,58</sup>, Parkinson's<sup>59</sup> and glioblastoma<sup>60</sup>. Traditionally, researchers examined astrocyte reactivity by observing morphological changes and GFAP upregulation<sup>236</sup>. However, recent attention revolves around uncovering the precise external molecular mediators driving these reactions and the internal pathways orchestrating changes at the transcriptomic, proteomic, morphological, and functional levels<sup>237–240</sup>. While some studies have defined specific changes, many have reported profound alterations in a few parameters. The field has flourished, embracing insights ranging from morphological shifts and cytoskeletal element upregulation to alterations in specific cell functions<sup>241</sup>. Astrocyte subtypes' various responses seem to fit within a triangle of 'normal physiological,' 'pathological trophic,' and 'pathological toxic,' with infinite possibilities in between<sup>242</sup>. Interestingly, what may seem toxic in one context might offer trophic support in another, revealing further intricacies. For comprehensive understanding, a collaborative endeavor is needed to unite modern discoveries with historical literature, spanning disease, sex<sup>243</sup>, CNS region<sup>23</sup>, circadian rhythm<sup>244,245</sup>, and species<sup>246</sup>. Embracing this contextual heterogeneity is pivotal to grasp the mechanisms behind how and why astrocyte subsets respond to diseases.

Recent discoveries have provided valuable insights into the specific functions, markers, spatial localization, and distinct subtypes of astrocytes that respond to various conditions in both permanent and transient ways. For example, during inflammation, reactive<sup>18</sup> astrocytes swiftly alter gene expression, which returns to baseline levels within days<sup>237,247</sup>. In contrast, acute axonal injuries lead to astrocyte proliferation, forming enduring 'scar' or 'border' structures that can persist for decades in human patients<sup>248</sup>. While we comprehend much about astrocytes' vital role in normal health, there are still crucial gaps in understanding their function during disease, infection, and injury. Questions remain about the number,

duration, and consistency of reactive astrocyte populations across species, sex, brain regions, and different disease states<sup>242</sup>. While we have some knowledge of astrocyte-specific pathways and non-cell-autonomous molecules driving certain reactive states, a comprehensive unification of functional changes with transcriptomic and proteomic analyses is needed to further our understanding.

### 2.5.1. Astrocyte metabolism.

Astrocytes assume pivotal roles in governing brain energy metabolism, significantly influencing brain functions, encompassing memory<sup>249–251</sup>, neuroprotection<sup>252</sup>, resistance to oxidative stress<sup>253–255</sup>, and maintenance of homeostatic equilibrium<sup>218</sup>. The brain's energy requisites are substantial, constituting a continuous allocation of 20–25% of the entire body's energy consumption<sup>30</sup>. The brain's energy provision closely intertwines with neuronal activity<sup>256</sup>, underpinning the origins of signals detected by widely used functional brain imaging methods, including functional magnetic resonance imaging and positron emission tomography<sup>257–260</sup>. Notably, the orchestration of neuroenergetic coupling falls within the purview of astrocytes, accomplished through glutamate uptake, triggering astrocytic aerobic glycolysis, and culminating in glucose uptake and the release of lactate<sup>261,262</sup>, an operation christened the "Astrocyte Neuron Lactate Shuttle"<sup>263</sup>. This mechanism is complemented by neurotransmitters such as noradrenaline and Vasoactive Intestinal Peptide, invoking glycogen mobilization—exclusively ensconced within astrocytes—ultimately resulting in lactate release<sup>264–266</sup>. The consequential transfer of lactate to neurons is then used as a rapid energy source, following conversion to pyruvate<sup>267</sup>. Furthermore, lactate doubles as a signaling agent<sup>268,269</sup>, modulating neuronal excitability<sup>270–272</sup>, homeostasis<sup>273</sup>, and the expression of vital survival and plasticity genes<sup>203,274,275</sup>, suppresses interferon<sup>276</sup>, modifies histone<sup>277</sup>, activates GPCRs<sup>278</sup>, upregulates kinases<sup>279</sup>, controls Mg<sup>280</sup> and Fe<sup>281</sup>, links cannabis to social behavior<sup>282</sup>, inhibits proteases<sup>283</sup>, stabilizes HIF<sup>284</sup>, and activates electron transport chain (ETC)<sup>285</sup>. An important observation underscores the gradual decline of glycolysis in astrocytes and more broadly, cerebral glucose metabolism, particularly in the context of aging<sup>286–288</sup> and age-associated neurodegenerative disorders, exemplified by AD<sup>289–292</sup>.

In the normal functioning of the brain, astrocytes and neurons forge a complex and interdependent relationship. This serves a dual purpose: the upkeep of neuronal functionality, as well as providing vital sustenance to brain metabolism<sup>293–297</sup>. Predominantly, the central nervous system's aerobic metabolism is steered by neurons due to their considerable ATP prerequisites, notably during neuronal activation<sup>298</sup>. In contrast, astrocytes carve a more modest metabolic niche, essential for mitigating the fluctuations in neurons' interactions with the bloodstream<sup>299</sup>. In conjunction, astrocytes contribute significantly to maintaining the blood-brain barrier, an intricate structure that facilitates glucose conveyance to the extracellular arena, emerging as the primary initial metabolite for

the brain<sup>300-302</sup>. Additionally, astrocytes stockpile glycogen, offering a buffer against hypoglycemia<sup>303,304</sup>. The crux of astrocyte metabolism centers on deriving ATP via complete glycolysis, culminating in the expulsion of lactate into the extracellular domain<sup>31-35</sup>. Remarkably, extracellular lactate levels within the human brain outpace systemic levels<sup>305,306</sup>, imparting substantial support to neuronal aerobic metabolism, complementing the direct usage of glucose by neurons. The interaction between astrocytic lactate expulsion and neuronal uptake orchestrates an intricate equilibrium in response to neuronal activation timelines<sup>33,307</sup>.

Astrocytes adeptly oversee the equilibrium within the extracellular space. Their sensitivity to heightened neuronal metabolic requirements is accomplished through an array of intercellular messenger molecules, including glutamate<sup>36</sup>, ATP<sup>37</sup>, D-Serine<sup>38</sup>, potassium<sup>39</sup>, nitric oxide ( $\text{NO}_{10}^{40-42}$ ), hydrogen peroxide ( $\text{H}_2\text{O}_2$ )<sup>43,44</sup>, and ammonia<sup>45</sup>. The functionality of mitochondria and the citric acid cycle (also known as the tricarboxylic acid cycle [TCA]) within astrocytes substantially diverges from that observed in neurons. Astrocytic metabolism prioritizes synthetic or cataplerotic pathways, crucial for generating glutamine, for neuronal use<sup>295,301,302,308</sup>. A notable facet of astrocytic activity revolves around the absorption of glutamate, arising from neuronal synaptic spillover<sup>309</sup>. Swift glutamate absorption, facilitated by transporters within astrocytes, moderates the synaptic activity of glutamate<sup>309</sup>, akin to the role of acetylcholinesterase at neuromuscular junctions<sup>310</sup>. This dynamic cycle reaches its zenith with the expulsion of glutamine by astrocytes, indispensable for the subsequent regeneration of neuronal glutamate. Much of this glutamine originates from the astrocytic TCA cycle through  $\alpha$ -ketoglutarate ( $\alpha$ -KG) synthesis. Consequently, astrocytes predominantly generate ATP through anaerobic glycolysis and lactate expulsion (while concurrently generating ATP through the TCA cycle). In contrast, neurons primarily thrive on a foundation of aerobic mitochondrial metabolism. This inherent resilience against oxygen deprivation is exemplified by the well-acknowledged ability to culture astrocytes (or astrocytoma cells) for up to 24 hours using adult brain tissue, and even cadaveric sources. This striking contrast is highlighted by neurons' inability to endure more than 3 to 5 minutes in an oxygen-depleted environment<sup>311</sup>.

While glucose catabolism is the primary energy source in the CNS, ongoing research underscores the significance of lipid metabolism in maintaining brain equilibrium. Around 20% of brain oxidative energy in rat brains is attributed to fatty acid oxidation (FAO)<sup>46</sup>. As the brain ages, there's an observed rise in the utilization of free fatty acids and ketone bodies<sup>312</sup>, possibly due to decreased glucose efficiency linked to aging and neurodegenerative diseases<sup>313</sup>. Interestingly, an essential component of the mitochondrial trifunctional protein complex in the FAO cycle<sup>314</sup>, hydroxyacyl-CoA dehydrogenase/3-ketoacyl-CoA thiolase/enoyl-CoA hydratase  $\alpha$  (HADHA), is mainly colocalized with GFAP+ astrocytes<sup>315</sup>, implying astrocytes as the primary site of brain FAO<sup>46</sup>. This suggests that

1 astrocytic lipid metabolism might contribute to neurological diseases such as neurodegenerative disorders and brain injury. In essence, lipid droplets (LDs) are primarily generated to serve as fuel for  $\beta$ -oxidation<sup>316,317</sup>. Hyperactive neurons seem to channel excess/toxic fatty acids to astrocytic LDs for energy production via mitochondrial  $\beta$ -oxidation<sup>255</sup>, possibly due to higher expression of FAO genes in astrocytes compared to neurons<sup>318</sup>. Furthermore, upregulated astrocyte-specific energy production through FAO protects against ischemic stroke-induced damage<sup>315</sup>. Thus, astrocytic mitochondrial  $\beta$ -oxidation of LDs appears to both shield neurons from FA toxicity and provide energy. Although post-ischemic reactive astrocytes' upregulation of lipid metabolism might be beneficial<sup>237</sup>, there's a duality in their role, as seen in an HD mouse model where astrocytic shifts from glycolysis to FAO led to increased ROS-induced damage<sup>319</sup>. This suggests that the role of astrocyte LDs could either drive neuroprotection or contribute to neurodegenerative disorders, necessitating further investigation into the factors behind these varying effects on reactive astrocyte phenotypes.

5 Astrocytic networks play a significant role in being a key contributor to brain activity, plasticity, and behavior<sup>47</sup>. Because astrocytes claim their own tight and isolated territories<sup>48</sup>, it is essential for them to operate cohesively as functional networks to maintain complex behaviors. The spotting of astrocyte networks, intimately linked with neuronal circuits<sup>320</sup>, has pushed us to rethink how metabolic interactions between neurons and astrocytes might operate in the brain. In a groundbreaking 2008 paper, Nathalie Rouach and Christian Giaume uncovered that energetic metabolites are supplied through groups of connected astrocytes, more efficiently reaching distantly located sites with high neuronal demand<sup>301</sup>. They noted that two gap-junction subunit proteins (connexin 43, Cx43; connexins 30, Cx30) offer an activity-dependent pathway for transporting energetic metabolites from blood vessels to far-off neurons. Intriguingly, this trafficking of metabolites is regulated by glutamatergic synaptic activity, and directly delivering glucose or lactate to an astrocyte can uphold glutamatergic synaptic transmission even without external glucose. Subsequent studies have consistently supported these early findings and validated that astroglial metabolic networks have a crucial role in supporting complex behaviors and are disrupted in various brain diseases. Among these complex behaviors, sleep is universal across vertebrate and invertebrate animals. Adenosine acts as a transmitter that drives the need for sleep following extended wakefulness<sup>321</sup>. In 2009, experiments hinted that astrocytes might be the source of adenosine, which then influences neuronal A1 receptors to induce sleep<sup>322</sup>. This marked one of the earliest experimental instances of active glial participation in mammalian behavior<sup>256</sup>. Nearly a decade later, the same group offered evidence that an astrocyte network functioning in the lateral hypothalamus and mediated by Cx43 played a critical role in transporting lactate needed for the proper functioning of orexin neurons, a subset of neurons involved in the circadian sleep/wake cycle and arousal<sup>323</sup>. Efficiently delivering energy substrates via

gap junction-mediated astrocytic networks stands as a leading contender to effectively fulfill neuronal energy needs during activity.

### 2.5.2. Astrocyte dysfunction in psychiatric disorders.

Multiple lines of evidence indicate astrocyte dysfunction in BD<sup>61-64</sup> and SCZ<sup>20-22,65-67</sup>. However, the need for astrocyte research in psychiatric disorders, which has traditionally been neurocentric, is best explained by the following narrative. Despite the findings from GWAS, exome studies, CNV studies, and functional genomics data related to BD and SCZ constantly pointing towards synaptic pathways<sup>17,164,186,187,324</sup>, particularly in specific excitatory and inhibitory neurons<sup>17,186</sup>, the alterations in neuronal components alone do not provide a comprehensive explanation for the synaptic alterations or the behavioral and cognitive deficits observed in BD and SCZ. For instance, efforts aimed at correcting the neuronal dendritic abnormalities, impaired synaptic plasticity and neurotransmitter imbalance in mouse models of Down syndrome and Fragile X syndrome (FXS), have only achieved partial restoration of the cognitive impairments<sup>325-328</sup>, highlighting the need for exploring alternative mechanisms contributing to cognitive dysfunction. Research conducted over the past decade has introduced the concept of the tripartite synapse, encompassing the presynaptic and postsynaptic neuronal elements along with perisynaptic astrocytes. It has become increasingly evident that interactions between neuronal and astrogial components develop during the postnatal developmental phase, and astrocytes play a critical role in regulating early neurodevelopmental processes<sup>38,329-334</sup>. Dysfunctions in the morphological and functional maturation of astrocytes may lead to abnormal neurodevelopmental processes implicated in the pathogenesis of BD/SCZ, such as mitochondrial biogenesis, synaptogenesis, and the modulation of glutamatergic and dopaminergic transmission<sup>65</sup>.

The astrocyte genotype determines neuronal firing, and consequently, could influence psychiatric disorders through non-cell autonomous mechanisms. While this concept was originally demonstrated through mouse models of FXS<sup>335</sup>, a monogenic form of ASD, findings from rodent studies do not always corroborate human biology. However, only recently, these mechanisms were also demonstrated in human models of FXS, through a series of neuron-astrocyte co-culture experiments<sup>336</sup>. In these experiments, when control neurons were co-cultured with FXS-astrocytes i.e., astrocytes obtained from human induced pluripotent stem (iPS) cells lacking the fragile-X mental retardation protein (FMRP), significant differences were observed in the firing patterns of neurons, resulting in short bursts. However, this phenotype was rescued when FXS-neurons were cultured with healthy astrocytes. Furthermore, the study suggested that one of the molecules involved in this rescue might be S100 $\beta$ , a protein that is secreted by astrocytes and taken up by neurons. Indeed, this discovery holds significance not only in the realm of basic biology but also in the context of potential therapeutics. It suggests that while directly correcting neurons may be challenging,

it might be possible to modulate astrocytic activity, which could, in turn, influence neuronal function and offer a therapeutic avenue for psychiatric phenotypes.

Although there have been numerous indications of impaired astrocyte metabolism in BD and SCZ from post-mortem brain studies<sup>337</sup>, it wasn't until 2018 that the first evidence emerged, showing that the knockout of Disrupted-In-Schizophrenia-1 (DISC1), a gene historically linked to SCZ, BD, and depression due to its highly penetrant ultra-rare chromosomal translocation<sup>338</sup>, resulted in decreased levels of the glucose transporter 4 (GLUT4), reduced glucose uptake, and diminished lactate production by primary astrocytes. These metabolic phenotypes in DISC1 knockout mice were associated with altered affective behaviors and impaired spatial memory, which were subsequently restored through systemic lactate treatment<sup>66</sup>. Despite this important discovery connecting a robust genetic signal (DISC1 translocation) to astrocyte metabolism, such comprehensive analyses have yet to be conducted, at scale, for ~200 GWAS signals implicated in SCZ/BD, and investigate their impact on astrocytic phenotypes.

#### 2.5.3. Influence of Li+ on astrocyte metabolism.

Increasingly, it is being known that Li+ might have an influence on glial cells, especially astrocytes<sup>339-341</sup>. Stable isotope-resolved metabolomics (SIRM) approach showed that Li+ enhanced glycolytic and Krebs cycle activity in both astrocytes and neurons<sup>14</sup>, specifically the anaplerotic pyruvate carboxylation (PC). The study also showed that Li+ stimulated the extracellular release of 13C labeled -lactate, -alanine (Ala), -citrate, and -glutamine (Gln), specifically by astrocytes<sup>340</sup>. It has also been shown that concentration of myo-inositol is higher in astrocytes than in neurons, and has been widely considered an astroglial metabolic marker<sup>342</sup>. In addition, cortical neuron cultures do not express the enzyme myo-inositol phosphate synthase (MIP-synthase), but rather depend on extracellular supply of myo-inositol<sup>343</sup>. In-vitro studies have shown that astrocytes are metabolically involved in the maintenance of the ionic and osmotic environment of the CNS. Increase in activity of oxidative enzymes (succinic dehydrogenase, DPN-diaphorase, etc.) in astrocytes has been associated with salt concentrations (NaCl, MgCl<sub>2</sub> and LiCl) of the environment, and this was considered a specific metabolic response which was seen only in astrocytes<sup>341</sup>. Overall, these observations make astrocytes more attractive and a probable candidate for Li+'s action leading to myo-inositol homeostasis in the brain, compared to neurons.

## 2.6. Metabolism.

Metabolism converts available nutrients, whether present in the culture media or within the cellular microenvironment, into various forms of usable resources, including energy, biomass, signaling molecules, structural lipids, etc. This process relies on a network of enzymatic reactions that generate and consume metabolites, typically with a molecular weight of <1500 Da.<sup>294</sup> In a metabolic reaction, each metabolite must have both a source and a sink, and, under steady-state, the sum of incoming fluxes must equal the sum of outgoing fluxes<sup>345</sup>. The complexity of the metabolic network varies significantly across organisms, ranging from approximately 500 reactions in the case of *E. coli* to approximately 10,000 reactions in any mammalian cell. Nevertheless, metabolites remain largely consistent across the spectrum of life forms<sup>346</sup> which underscores the universal need for nucleotides and amino acids to synthesize DNA, RNA, and proteins in all organisms, whether they are bacteria or humans.

The essential building blocks of a cell's fundamental biomass components are comprised of 100 conserved, abundant, and high-flux metabolites, including intermediates from glycolysis, the pentose phosphate pathway (PPP), the tricarboxylic acid (TCA) cycle, along with amino acids, and nucleotides, that play a pivotal role in both the synthesis and breakdown of biomass constituents. In contrast to this finite core involved in energy metabolism, the realm of small molecules within biological systems is extensive. It encompasses internally generated metabolites, including substances that activate or inhibit enzymes, modulators of macromolecule modifications, signaling molecules like neurotransmitters and hormones, and structural and energy storage compounds like lipids. All of these molecules hold vital functional roles within living organisms<sup>347</sup>.

Beyond known metabolites, there is substantial interest in the unknown metabolome<sup>348</sup>. While the full set of genes and proteins in an organism can be revealed by WGS, the full set of metabolites remains ill-defined, due to the catalytic potential of uncharacterized proteins, enzyme promiscuity, and the diversity of metabolic inputs coming from nutrition. Furthermore, most mass spectrometry (MS) peaks lack annotations<sup>349</sup>, although many of these are analytical artifacts<sup>350</sup>. This has reignited enthusiasm for the detection and annotation of the unknown metabolome.

### 2.6.1. Tools to study metabolism.

With the advancements in mass spectrometry (MS) and nuclear magnetic resonance (NMR) spectroscopy, significant progress has been achieved in the last decade towards conducting comprehensive studies of metabolism. This includes not only measuring the relative abundance of intracellular metabolite pools but also monitoring metabolite labeling using stable isotope tracers, which can further provide insights into pathway activities<sup>351</sup>.

Quantifying metabolite concentrations through metabolomics provides only part of the picture; it doesn't capture the metabolic flux, which represents the flow of metabolites through a biochemical network<sup>352</sup>. Understanding flux is crucial for assessing reaction rates, pathway activity, and nutrient utilization. It's important to note that changes in flux levels don't always correspond to alterations in metabolite concentrations, and vice versa. In the realm of metabolism, this is akin to distinguishing between cars on a highway and cars stuck in traffic. If we take a snapshot of the cars on the road and merely count them, it won't reveal whether there's heavy traffic or if the road is just heavily used. Similarly, metabolite concentrations in a cell can rise due to fast synthesis or slow degradation<sup>353</sup>. As metabolite concentrations and fluxes offer complementary information, a comprehensive understanding of metabolism necessitates exploring both aspects.

Metabolic fluxes are experimentally inferred through stable isotope tracing, involving the tracking of the fate of non-radioactive isotopically enriched nutrients like <sup>13</sup>C, <sup>2</sup>H and <sup>15</sup>N tracers. This method offers two advantages: firstly, unlike radioisotopes, stable isotopes do not undergo radioactive decay, and secondly, it enables the quantitative assessment of label incorporation into multiple downstream products simultaneously<sup>347</sup>. However, this technique hasn't been as democratized as metabolomics due to the expertise needed in computational modeling for interpreting labeling data.

Nonetheless, important biological insights have been gained through isotope tracing experiments, with most developments occurring in the field of cancer metabolism. Notable anecdotes include the infusion of uniformly labeled [ $\text{U-}^{13}\text{C}$ ] glucose and lactate in glioblastoma<sup>354</sup> and non-small cell lung adenocarcinoma (NSCLC)<sup>355,356</sup> patients, respectively, and analyzing the isotope labeling patterns in intraoperative tumor resections revealed local uncoupling of glycolysis (pyruvate reduction to lactate or the "Warburg effect") and the TCA cycles (TCA cycle-mediated <sup>13</sup>C glucose oxidation) in tumor tissues. Further tracer infusion studies in mice showed that circulating lactate directly provides carbon to the TCA cycle<sup>357</sup>. Likewise, infusion of [ $\text{U-}^{13}\text{C}$ ] glucose in patients with clear cell renal cell carcinoma (ccRCC) undergoing nephrectomy demonstrated increased glucose contribution to glycolysis and lactate but decreased contribution to downstream TCA metabolism, consistent with highly glycolytic ccRCC tumors with impaired glucose oxidation<sup>358</sup>. In more recent studies, the infusion of [ $\text{U-}^{13}\text{C}$ ] lactate in mice revealed that slower TCA flux and ATP production were distinctive features of primary solid tumors, as opposed to metastases<sup>359</sup>. This observation was further substantiated in subsequent human studies, using intraoperative infusions of [1,2-<sup>13</sup>C] acetate and [ $\text{U-}^{13}\text{C}$ ] glutamine in ccRCC patients, which found that ccRCC metastases exhibited increased labeling of TCA intermediates compared to primary ccRCCs<sup>360</sup>.

<sup>7</sup> While MS offers excellent sensitivity and can determine both the total enrichment of a metabolite pool and the contributions of each isotopolog ( $M+0, M+1, M+2 \dots M+i$ ) to the pool, it does not report the precise position of  $^{13}\text{C}$  within the metabolite. This limitation is noteworthy because a metabolite with  $i$  carbons has  $i+1$  isotopologs but  $2^i$  labeled forms (isotopomers) when considering the position of each  $^{13}\text{C}$ . In contrast, NMR has been the preferred analytical method for isotopomer analysis because the local magnetic environment around an atomic nucleus corresponds to a predictable position on a chemical shift spectrum, thereby reporting the  $^{13}\text{C}$  position within a molecule<sup>361</sup>. However, NMR generally does not report all possible isotopomers and has lower sensitivity compared to MS.

The knowledge of the position of  $^{13}\text{C}$  within the metabolite pool holds significance, as exemplified in the context of the TCA cycle<sup>362</sup>. The entry of carbon into the TCA cycle predominantly occurs through acetyl-CoA, which primarily originates from pyruvate dehydrogenase (PDH), fatty acid or ketone oxidation, or anaplerotic pathways supplied by pyruvate carboxylation and the oxidation of specific amino acids and other fuel sources. The specific  $^{13}\text{C}$  isotopomers present in TCA intermediate metabolites encode valuable information regarding the relative contributions of diverse acetyl-CoA sources, anaplerosis, pyruvate recycling, and cycle turnover. Furthermore, as the cycle advances, the positions of the  $^{13}\text{C}$  atoms within these intermediates undergo changes, a crucial aspect often overlooked by conventional MS isotopolog analysis, resulting in the omission of significant data<sup>363</sup>. Recent advancements in isotopomer analysis have seen notable progress. For instance, a LC-MS/MS-based approach has been recently devised with the specific aim of quantifying all individual isotopomers of glutamate and aspartate, showcasing its superiority over rudimentary isotopolog analysis, evidenced through investigations into the metabolism of cancer cells in culture, as well as in the context of tumors developing in mice and patients<sup>363</sup>.

### <sup>31</sup> 2.6.2. Constraint-based reconstruction and analysis (COBRA).

The complexity of directly measuring metabolic flux in mammalian systems *in vivo* is compounded by the challenges associated with isotope tracing. These challenges primarily relate to the scalability of tracer experiments, particularly when attempting to perform isotopomer analysis for all potential nutrient sources, in parallel, within a specific tissue. Additionally, it's worth noting that these experiments are demanding, and the expertise needed to generate and interpret these datasets is relatively limited, restricted to only a few laboratories worldwide. Conversely, with the ever-expanding volume of high-dimensional 'omic data, particularly transcriptomic and proteomic data, numerous computational modeling algorithms ranging from stochastic/deterministic kinetic models<sup>364,365</sup>, Boolean/rule-based models<sup>366,367</sup> to statistical/probabilistic models<sup>368,369</sup>, have been developed and applied to interrogate metabolism directly from these datasets.

One such method would be the constraint-based modeling, which has been applied to analyze biochemical reaction networks for more than 32 years<sup>370</sup>.

Sequencing whole genomes<sup>112,371</sup> enabled the development of constraint-based models (CBMs), at genome-scale, also known as genome-scale metabolic models (GSMMs), which represents the complete metabolic gene repertoire for assessing phenotypic functions<sup>372</sup>. Crucially, metabolic reactions in CBMs are directly linked to the genotype of the specific cell-type, allowing predictions of gene knockouts, specifically those encoding metabolic enzymes and transporters<sup>373,374</sup>. These models at the genome-scale facilitate the examination of the organization of cellular behavior, from pathway structure<sup>375</sup> to adaptive evolution<sup>376</sup>, and most significantly, the metabolic fluxes<sup>377</sup>.

The development of CBMs has been grounded in several foundational principles or axioms<sup>378</sup>. Firstly, cells can be likened to a chemical factory, where the synthesis, degradation, and interconversions of molecules can be described using simple chemical equations. Secondly, cells operate within various constraints, including physico-chemical constraints such as stoichiometry and mass balance, topological constraints like molecular crowding and steric clashes, environmental constraints including nutrient availability, and regulatory constraints like allosteric inhibition. Lastly, cells evolve under selection pressure, optimizing for one or multiple objectives such as growth, protein synthesis, or the production of a specific metabolite, all while adhering to the aforementioned constraints. While each of these axioms may appear straightforward individually, when considered collectively, they form the foundational basis of constraint-based reconstruction and analysis (COBRA). This framework enables the mechanistic representation and modeling of genotype-to-phenotype relationships, at least in terms of metabolic phenotypes.

The process of network reconstruction is at the core of CBMs<sup>379</sup>. The reconstruction involves systematically gathering the parts like i.e., metabolites, reactions, and the genes/proteins that govern these reactions. Additionally, it entails representing this information in a chemically consistent format. To be more specific, a bottom-up reconstruction is a two-dimensional portrayal of the metabolic genome. It includes a parts list, with reactions and metabolites as rows, and the connections between them, represented as columns through stoichiometric coefficients. These components are sourced from an annotated genomic sequence, meaning we collect a list of all open reading frames (ORFs) associated with enzymes and metabolite transporters. Furthermore, we obtain these components, to the best of our ability, through extensive manual curation of the literature to identify any missing, blocked reactions, or dead-end metabolites. It's essential to keep in mind that no reconstructions or models are ever truly complete or perfect, emphasizing the idea that the map is not the territory.

However, the metabolic reconstruction of the target cell by itself does not provide information about the flow of metabolites occurring inside the cell. For instance, specific metabolic fluxes within the cell may be of interest, such as determining how many carbons in a TCA intermediate come from glucose versus ketone bodies. Alternatively, given a pool of pyruvate, it may be important to understand how much is converted into circulating lactate versus how much enters mitochondria for oxidation. Numerous mathematical methods have been developed to infer the flow of metabolites through the metabolic network, and one such technique is flux balance analysis (FBA)<sup>380</sup> ([Fig.S3](#)).

Analysis of metabolic networks, using FBA or otherwise, starts with a stoichiometric matrix, which is the core component of any metabolic reconstruction. This matrix contains stoichiometric coefficients for each metabolite, indicating how these metabolites are either consumed (indicated by a negative sign) or produced by reactions within the system. To convert the reconstruction<sup>29</sup> into a mathematical model, an assumption is made that the system has reached a steady state, where the sum of incoming fluxes equals the sum of outgoing fluxes in the network. In other words, for a given metabolite, the sum of fluxes producing the metabolite is equal to the sum of fluxes utilizing the metabolite, ensuring that no metabolite accumulates<sup>51</sup> within the cell. This balance can be expressed as "input-output = 0," represented as a dot product of the stoichiometric matrix [S] and the flux vector [v], where  $S \cdot v = 0$ . This multiplication results in a system of linear equations. Since this system is underdetermined, meaning the number of unknown variables is much greater than the number of equations, it has infinitely many solutions. To select a specific solution or explore the solution space, this can be transformed into an optimization problem, where one can through some pre-existing knowledge of the target cell/organism<sup>381</sup>, for example, maximize the production of a metabolite 'B' i.e., maximize the flux through the reaction 'B2' which synthesizes 'B'. This optimization is performed subject to constraints, including the steady-state mass balance represented by  $S \cdot v = 0$ , which cannot be violated. Additional inequality constraints can also be imposed on reactions, like setting uptake rates within a specific range or defining a reaction being reversible or irreversible, among other possibilities. The result is a theoretically feasible metabolic flux distribution, indicating the rate of each reaction within the metabolic network. It's essential to note that in FBA, the flux distribution is often non-unique, but the objective value is unique. This means that multiple alternative optimal solutions can have the same objective value, reflecting the existence of a system or cell in different functional states when optimizing for a specific objective, whether it's biomass, the secretion of a metabolite like lactate, or another criterion.

The choice of optimization algorithm depends on the specific objective and constraints in the problem ([Fig.S4](#)). FBA employs linear programming (LP)<sup>63</sup> algorithms to optimize a linear combination of fluxes, making it suitable for predicting the minimum and maximum flux through a particular reaction in the network. However, FBA predictions often do not align

well with experimental growth rates or flux values, especially when attempting to predict knockout phenotypes. To address this limitation, in 2002, Church/Segre introduced the minimization of metabolic adjustment (MOMA) approach based on quadratic programming (QP)<sup>374</sup>. MOMA operates on the principle that knockout flux distributions should not deviate significantly<sup>75</sup> from wild-type flux distributions in the solution space. This boils down to minimizing the Euclidean distance between the wild-type and knockout FBA solutions, and since this objective includes a quadratic term, QP is used to solve it. Unlike FBA, the Euclidean distance minimization in MOMA yields a unique solution. Similarly, the Regulatory on/off minimization (ROOM) algorithm developed by Shlomi/Ruppin shares the core concept of MOMA but utilizes mixed-integer linear programming (MILP)<sup>382</sup>. Additionally, there are nonlinear programming (NLP) algorithms available with nonlinear constraints and objectives. It's important to note that for LP, QP, and MILP methods, the optimal solution always resides at the corners or periphery of the solution space, forming an n-dimensional convex polytope, where n represents the number of fluxes. This convex solution space guarantees optimal solutions for LP, QP, and MILP. In contrast, NLP may not guarantee solutions due to challenges associated with local minima.

Over the last two decades, numerous metabolic reconstructions of cell-types and organisms have been published and made accessible to the public. While the majority of these reconstructions are designed for prokaryotic microorganisms<sup>373,377</sup>, reconstructions are available for eukaryotes as well such as yeast<sup>383</sup>, worm<sup>384,385</sup> and human<sup>386,387</sup>. Moreover, these reconstructions serve as a scaffold/framework, against which comprehensive 'omic data can be mapped. For example, Recon3D, is the most comprehensive knowledge repository of human metabolism<sup>387</sup>. It can be customized for a specific cell/tissue in a specific phenotype-of-interest, such as when a specific gene is knocked out. This customization process involves using datasets related to gene expression (transcriptome) and protein levels (proteome). Various computational methods have been developed to overlay 'omic data onto these metabolic reconstructions<sup>388-391</sup>, resulting in a sub-network that eventually forms a specialized metabolic model tailored to a specific cell-type, tissue, or phenotype. One of the advantages of CBMs is that it can describe the metabolic state of cells at a steady state without the need for detailed knowledge of enzymatic kinetics<sup>392</sup>, which is difficult to estimate at a network level. CBMs/GSMMs have been extensively used in the past decade to explain not only human metabolism in general<sup>387</sup> but also the effects of human disease phenotypes<sup>393-396</sup>.

## 2.7. Rationale for the study.

The role of astrocyte metabolism in psychiatric disorders (BD, SCZ), neurodegeneration (AD), and the response to treatment (Li+) in BD, is poorly understood, despite multiple lines of evidence indicating dysfunction of astrocytes<sup>20-22,61-66,339</sup>. To shed light on potential metabolic mechanisms associated with these phenotypes, we embarked on an unbiased investigation of astrocyte metabolism. The key idea that led to this body of work was the utilization of metabolic modeling principles and publicly available 'omic data to investigate metabolic phenotypes in astrocytes, and ask questions within the context of neuropsychiatric disorders. Given that directly screening metabolic pathways in astrocytes, whether *in vivo* or *in vitro*, is a substantial undertaking, we opted for metabolic modeling, which can describe the metabolic state of cells at a steady state without the need for detailed knowledge of enzymatic kinetics. Among the available metabolic modeling tools, the COBRA framework<sup>392</sup> was chosen as the most advanced and preferred option due to its exceptional scalability, which would be difficult to achieve solely through conventional wet-lab experiments. Furthermore, it stands out as one of the few modeling methods that integrates high-throughput 'omic data with theoretical principles, utilizing straightforward mathematics. This enables the simulation of numerous knockout conditions rapidly, facilitating the generation<sup>36</sup> of hypotheses that could potentially guide experimental investigations. Notably, to the best of our knowledge, this body of work represents the first exploration of cellular metabolism in psychiatric phenotypes using constraint-based modeling.

## 2.8. Preview of dissertation.

Metabolic modeling was employed to ask if there are metabolic phenotypes in astrocytes that are i) specific to BD patients who do not respond to Li+ treatment, ii) shared between BD and SCZ patients, and iii) observed as a consequence of LoF mutations implicated in BD, SCZ and AD patients. The key data substrate for the first two questions were phenotype-specific transcriptomes from iPS-astrocytes derived from BD, SCZ, and control subjects<sup>62,67</sup>, while for the latter question, the data substrate was solely genetic, specifically the knowledge of LoF mutations identified by WES of patients diagnosed with SMI (BD & SCZ)<sup>397,398</sup> and AD<sup>399</sup>. However, all three inquiries were dependent on the generation of astrocyte metabolic models in the first place. To accomplish this, we combined the human metabolic knowledge base 'Recon3D' with publicly available transcriptome data from astrocytes of BD & SCZ patients, and healthy controls, alongside glial proteomic data from healthy controls. This amalgamation allowed us to derive phenotype-specific metabolic models of human astrocytes. Subsequently, we engaged in meticulous manual curation of relevant literature to identify metabolic functions pertinent to astrocytes. These tasks were then evaluated in all metabolic models while adhering to appropriate nutrient media constraints. Metabolic flux distributions between the healthy and disease models were compared, along with specific filtering criteria, to identify metabolic phenotypes associated with our inquiries.

### 3. Aims and objectives.

46

- To generate genome-scale metabolic models (GSMMs) of human astrocytes using publicly available 'omic data obtained from psychiatrically ill patients (BD, SCZ) and healthy controls ([Figure.1](#)).
- To identify the astrocytic metabolic phenotypes associated with treatment responsiveness to Li+ in BD, but also to explore the shared metabolic phenotypes between BD with SCZ ([Figure.1](#)).
- To identify the astrocytic metabolic phenotypes associated with LoF mutations implicated in neuropsychiatric disorders (SMI), and neurodegenerative disorders (AD) ([Figure.5](#)).

The specific objectives were as follows:

#### 3.1. Deriving the human astrocyte metabolic models.

- a. Pre-processing and quality control of public data.
- b. Integrating phenotype-specific transcriptomes and glial proteome data with Recon3D.
- c. Expanding draft metabolic models through manual curation of literature.
- d. Imposing experimental nutrient uptake constraints.

#### 3.2. Using the models to identify disrupted metabolic fluxes in BD (Li+ Responders and Non-Responders) and SCZ patients' astrocytes.

- a. Setting up the analytical methods to solve metabolic models.
- b. Filtering reactions relevant to phenotype-of-interest.
- c. Metabolic-subSystem enrichment analysis (MSEA).
- d. Identifying disruptions that are significant across modules.

#### 3.3. Using the models to identify the impact of LoF mutations implicated in SMI and AD.

- a. Curating the genes with LoF mutations implicated in SMI and AD.
- b. Setting up the analytical method to simulate the effects of LoF mutations on the metabolic models.
- c. Identifying the fluxes disrupted by LoF mutations.

Objectives 3.1 and 3.2 will be executed in [Section 4](#), while objectives 3.3 will be executed in [Section 5](#).

#### 4. Metabolic modeling of astrocytes in bipolar disorder and schizophrenia.

##### <sup>44</sup> 4.1. Introduction.

Bipolar disorder (BD) is a severe psychiatric illness characterized by manic/depressive episodes and persistent neurocognitive impairments<sup>3</sup>, affecting 0.5% of the population (ca. 7 million in India)<sup>4</sup>. It is a significant cause of disability, morbidity, and mortality (15% die by suicide)<sup>5</sup>. Lithium (Li+), a WHO “essential medicine”, is the only effective drug for preventing suicides<sup>27,28</sup> and improving cognition<sup>29</sup> in BD patients. There are many biochemical pathways which have been implicated in the pathobiology of BD and the mechanisms of Li+, including the inositol metabolism, cyclic nucleotide metabolism, glycogen synthase kinase 3β signaling, glutamate pathways, and circadian clock systems<sup>146</sup>. However, the exact mechanisms are enigmatic leading to absence of predictive markers.

Astrocyte <sup>45</sup>dysfunction has been implicated in BD<sup>61,62</sup> and also in the mechanisms of action of Li+<sup>339,340</sup>. Stab<sup>14</sup>isotope-resolved metabolomics (SIRM) approach showed that Li+ enhanced glycolytic and Krebs cycle activity in both astrocytes and neurons<sup>14</sup> especially the anaplerotic pyruvate carboxylation (PC). The study also showed that Li+ stimulated the extracellular release of <sup>13</sup>C labeled -lactate, -alanine (Ala), -citrate, and -glutamine (Gln), specifically by astrocytes<sup>340</sup>. It has also been shown that concentration of myo-inositol is higher in astrocytes than in neurons, and has been widely considered an astroglial metabolic marker<sup>342</sup>. In addition, cortical neuron cultures do not express the enzyme myo-inositol phosphate synthase (MIP-synthase), but <sup>13</sup>rather depend on extracellular supply of myo-inositol<sup>343</sup>. In-vitro studies have shown that astrocytes are metabolically involved in the maintenance of the ionic and osmotic environment of the CNS. Increase in activity of oxidative enzymes (succinic dehydrogenase, DPN-diaphor<sup>13</sup>e, etc.) in astrocytes has been associated with salt concentrations (NaCl, MgCl<sub>2</sub> and LiCl) of the environment, and this was considered a specific metabolic response which was seen only in astrocytes<sup>341</sup>. Overall, these observations make astrocytes more attractive and a probable candidate for Li+'s action leading to myo-inositol homeostasis in the brain, compared to neurons.

Because screening for these metabolic pathways in astrocytes, *in vivo* or *in vitro*, is a substantial task, we adopted an alternative, computational approach to ask if there are metabolic phenotypes in astrocytes that are i) specific to BD patients who do not respond to Li+ treatment, and ii) shared between BD and SCZ patients ([Fig.1](#)). First<sup>80</sup> by integrating publicly-available transcriptomics and proteomics data with the constraint-based reconstruction and analysis (COBRA) framework<sup>392</sup>, we have derived GSMMs of astrocytes obtained from BD, SCZ patients and healthy controls. We improved upon prior brain metabolic models by extensive manual curation of literature to identify the metabolic functions and extracellular nutrient uptake constraints relevant to astrocytes. In BD, we

derived separate metabolic models for Li+ responders and non-responders to analyze metabolic fluxes related to treatment<sup>24</sup> responsiveness. Despite the shared clinical symptomatology, genetics and biology between BD and SCZ, there is limited evidence supporting the effectiveness of Li+ as a standalone treatment for SCZ patients<sup>400</sup>. To explore the specificity of Li+'s efficacy in BD compared to SCZ, we hypothesized that it might be reflected at the molecular/metabolic level, and thus we derived metabolic models of astrocytes from SCZ patients, particularly monozygotic twin pairs (SCZ twins and Healthy twins), along with matched controls. And subsequently, by using diverse analytical methods we have identified metabolic fluxes that are specifically disrupted in the astrocytes of BD, BD-Responders, BD-NonResponders and SCZ Twins, as compared to healthy/control models, thereby gaining insights into the differences between these conditions.

One of the advantages of GSMM is that it can describe the metabolic state of cells at a steady state without the need for detailed knowledge of enzymatic kinetics<sup>392</sup>, which is difficult to estimate at a network level. Modeling studies like this have been extensively used in the past decade to explain not only human metabolism in general<sup>387</sup> but also the effects of human disease phenotypes<sup>393-396</sup>.

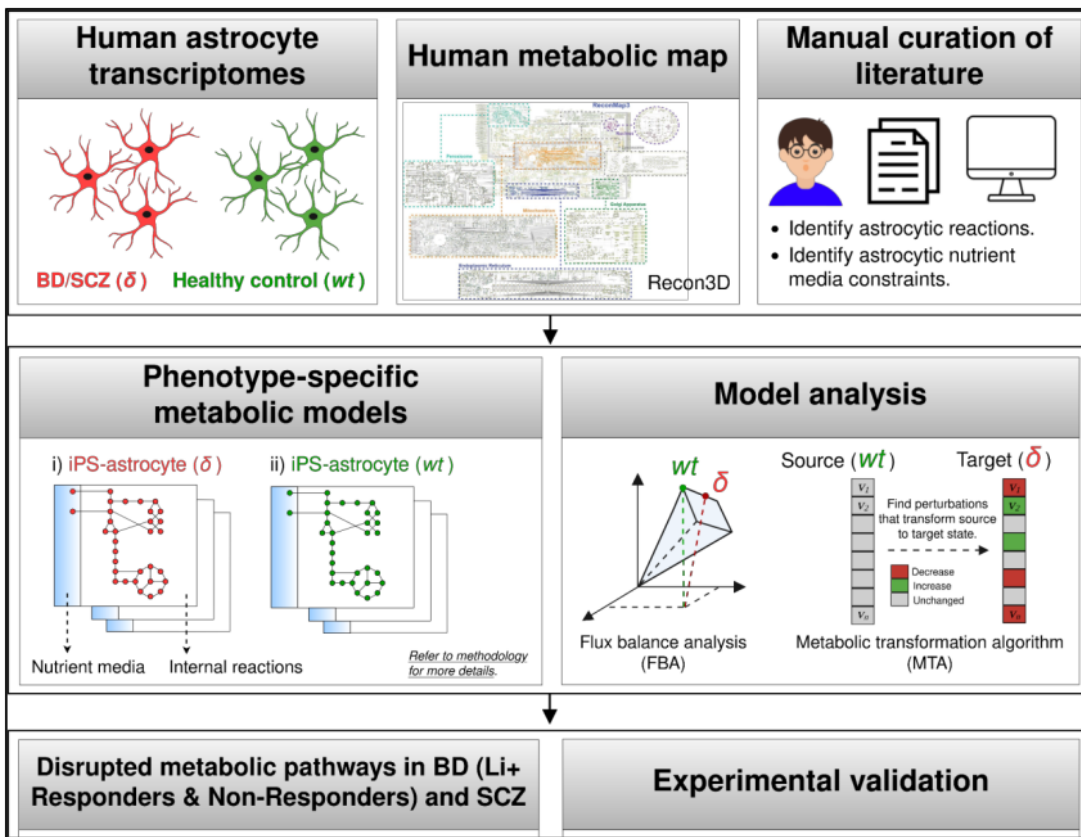


**Figure 1. Graphical abstract. Metabolic modeling of astrocytes in BD and SCZ.**

Firstly, GSMMs of astrocytes from BD, SCZ patients, and healthy controls were constructed by integrating publicly-available transcriptomics data, proteomics data with the constraint-based reconstruction and analysis (COBRA) framework. Separate metabolic models for Li+ responders and non-responders were derived to analyze metabolic fluxes related to treatment responsiveness. Metabolic models of astrocytes from SCZ patients were derived to explore the shared metabolic phenotypes with BD. Enhancements to previous brain metabolic models were achieved through comprehensive manual curation of literature, identifying relevant metabolic functions and extracellular nutrient uptake constraints relevant to astrocytes. Subsequently, diverse analytical methods were employed to identify disrupted metabolic fluxes in astrocytes from BD, BD-Responders, BD-NonResponders and SCZ Twins.

## 4.2. Materials and methods.

### <sup>1</sup> 4.2.1. Key resources table

REAGENT or RESOURCE	REFERENCE	IDENTIFIER or LINK
<b>Data</b>		
Zhang, Human Primary Astrocyte, RNA-Seq	<sup>401</sup>	GSE73721
Vadodaria, Human iPSC Astrocyte, BD/Ctrl, RNA-Seq	<sup>62</sup>	GSE157509
Koskuvi, Human iPSC Astrocyte, SCZ/Ctrl, RNA-Seq	<sup>67</sup>	GSE191248
Human glia, Proteomics (semi-quantitative immunohistochemistry abundance)	<sup>402</sup>	<a href="https://www.proteinatlas.org/download/normal_tissue.tsv.zip">https://www.proteinatlas.org/download/normal_tissue.tsv.zip</a>
Recon3D	<sup>387</sup>	<a href="https://www.vmh.life/#downloadview">https://www.vmh.life/#downloadview</a>
<b>Software and Algorithms</b>		
FastQC	-	<sup>1</sup> <a href="https://www.bioinformatics.babraham.ac.uk/projects/fastqc/">https://www.bioinformatics.babraham.ac.uk/projects/fastqc/</a>
Cutadapt	-	<a href="https://cutadapt.readthedocs.io/en/stable/">https://cutadapt.readthedocs.io/en/stable/</a>
HISAT2	<sup>403</sup>	<a href="http://daehwankimlab.github.io/hisat2/">http://daehwankimlab.github.io/hisat2/</a>
Samtools	<sup>404</sup>	<a href="http://samtools.sourceforge.net/">http://samtools.sourceforge.net/</a>
Cufflinks	<sup>405</sup>	<sup>24</sup> <a href="http://cole-trapnell-lab.github.io/cufflinks/">http://cole-trapnell-lab.github.io/cufflinks/</a>

<sup>24</sup> org.Hs.eg.db	-	<a href="https://bioconductor.org/packages/release/data/annotation/html/org.Hs.eg.db.html">https://bioconductor.org/packages/release/data/annotation/html/org.Hs.eg.db.html</a>
<sup>31</sup> COBRA Toolbox v3.0	392	<a href="https://opencobra.github.io/cobratoolbox/stable/">https://opencobra.github.io/cobratoolbox/stable/</a>
iMAT	388	-
GIMME	391	-
MBA	389	-
FastCore	390	-
Metabolic Transformation Algorithm (MTA)	393,406,407	<a href="https://github.com/ImNotaGit/MTA">https://github.com/ImNotaGit/MTA</a>
Gurobi optimizer	-	<sup>71</sup> <a href="https://www.gurobi.com/">https://www.gurobi.com/</a>
MATLAB R2015b	-	<a href="https://in.mathworks.com/products/matlab.html">https://in.mathworks.com/products/matlab.html</a>
<sup>53</sup> R version 3.6.3	-	<a href="https://www.r-project.org/">https://www.r-project.org/</a>
Custom scripts for model generation and analysis	This study	<a href="https://github.com/anin90/AstroModel">https://github.com/anin90/AstroModel</a>

#### 4.2.2. Dataset overview.

Three previously published <sup>23</sup> transcriptome datasets: "Zhang"<sup>401</sup>, "Vadodaria"<sup>62</sup>, "Koskuvi"<sup>67</sup>, were utilized. In Zhang, the astrocytes were purified from mice, human fetal, and adult brain tissues using immunopanning. The mi<sup>86</sup> data were excluded from our analysis leaving us with 41 human subjects including <sup>23</sup> six fetal astrocyte samples, 12 adult astrocyte samples, eight glioblastoma multiforme (GBM) or sclerotic hippocampal samples, four whole human cortex samples, and 11 human samples of other purified CNS <sup>55</sup> cell-types. Healthy astrocytes, except for the GBM and sclerotic samples, were obtained from fetal brain tissue from elective pregnancy terminations at 17–20 gestational weeks or healthy temporal lobe cortices from patients undergoing neurological surgeries. In Vadodaria, the astrocytes were derived from iPS cells generated from fibroblasts of BD patients (n=5), which includes both Li+ responders

(n=3) and non-responders (n=2), as well as healthy controls (n=4). The astrocytes were differentiated for five weeks, and subsequently stimulated with 10 ng/mL IL-1 $\beta$  or phosphate buffered saline (PBS) for 5h, followed by RNA-Seq. Similarly, in Koskuvi, the astrocytes were derived from iPS cells generated from fibroblasts of monozygotic twin pairs discordant for SCZ (n=4), which includes both healthy twins (HT, n=4) and SCZ twins (ST, n=4), as well as age- and sex- matched healthy controls (n=6). RNA was extracted from the monolayer culture of iPS-derived astrocytes (150 DIV i.e., days in vitro), followed by RNA-Seq. All three datasets were uniformly processed using a consensus set of tools. After processing and quality control, "Zhang" was used to derive metabolic models of primary astrocytes, while "Vadodaria" and "Koskuvi" were used to derive metabolic models of iPS-astrocytes.

#### 4.2.3. Pre-processing and quality control of public data.

##### 4.2.3.1. RNA-sequencing.

Transcriptome data (FastQ) were obtained by downloading from public repositories (Zhang/Vadodaria/Koskuvi). The non-human samples, if any, were removed from Zhang, Vadodaria and Koskuvi.

FastQC (<http://www.bioinform.cs.babraham.ac.uk/projects/fastqc>) was used to assess the quality of the reads and Cutadapt (<https://cutadapt.readthedocs.io/en/stable/>) was used to remove adapter contamination. HISAT2<sup>403</sup> was used to align the filtered reads to the human reference genome (GRCh37). Samtools<sup>404</sup> was used for SAM to BAM conversion and sorting. Cufflinks<sup>405</sup> was used to estimate gene-level expression (FPKM), and gene symbols were annotated for NCBI Entrez IDs using org.Hs.eg.db. The non-specific genes i.e., same gene symbol mapping to multiple Entrez IDs or multiple symbols mapping to the same ID were excluded. For Zhang, Vadodaria and Koskuvi, the genes with FPKM  $\geq 0.1$  in at least 50% of all samples were considered, resulting in 13,423, 14,543 and 16,724 genes respectively.

##### 4.2.3.2. Proteomics.

The human cortical glial proteomics data from the human protein atlas (HPA)<sup>402</sup> were utilized to provide further evidence of expression in Zhang, Vadodaria and Koskuvi. The reliability scores ('Enhanced', 'Supported', 'Approved', or 'Uncertain') and the semi-quantitative nature of the immunohistochemistry protein abundance ('High', 'Medium', 'Low') were retained<sup>408</sup>.

#### 4.2.4. Metabolic modeling of astrocytes.

##### 4.2.4.1. Integration of phenotype-specific astrocyte transcriptomes with Recon3D.

Recon3D<sup>387</sup>, the latest human metabolic reaction library, was used to extract draft metabolic models. While all the samples in the Zhang, Vadodaria, and Koskuvi datasets were

processed (FASTQ to FPKM), only a subset of samples was chosen from each dataset for metabolic modeling. In Zhang, only cortical astrocytes from adult samples ( $n=12$ ) were included. In the Vadodaria dataset, only PBS treated iPS-astrocytes from BD patients ( $n=5$ ) and healthy controls ( $n=4$ ) were considered. However, in the Koskuvi dataset, the entire dataset, including iPS-astrocytes from SCZ twin pairs ( $n=4$ ) and healthy controls ( $n=6$ ), was utilized for modeling. In Vadodaria, the BD patient data was further divided into Li+ responders ( $n=3$ ) and non-responders ( $n=2$ ) for modeling treatment responsiveness. In Koskuvi, the monozygotic twin pairs were further divided into SCZ twins ( $n=4$ ) and healthy twins ( $n=4$ ) for modeling the effects of familial/genetic risk. Genes that were detected in the transcriptome ( $n=13,423$ , Zhang;  $n=14,543$ , Vadodaria;  $n=16,724$ , Koskuvi) but had 'uncertain' reliability in the HPA glial proteome were excluded, resulting in a subset of genes that were "transcriptome & proteome" evident ( $n=4,105$ , Zhang;  $n=4,040$ , Vadodaria;  $n=4,203$ , Koskuvi). Metabolic models for eight distinct phenotypes were obtained by constraining Recon3D with the transcriptome data of:

1. Zhang: Primary astrocytes (Primary-Ctrl),
2. Vadodaria: iPS-astrocytes from Healthy controls (iPS-Ctrl-a),
3. Vadodaria: iPS-astrocytes from BD patients (iPS-BD),
4. Vadodaria: iPS-astrocytes from BD patients - responders (iPS-BD-R),
5. Vadodaria: iPS-astrocytes from BD patients - non-responders (iPS-BD-NR),
6. Koskuvi: iPS-astrocytes from Healthy controls (iPS-Ctrl-b),
7. Koskuvi: iPS-astrocytes from monozygotic twin pairs - SCZ twins (iPS-ST),
8. Koskuvi: iPS-astrocytes from monozygotic twin pairs - Healthy twins (iPS-HT).

The genes were mapped to reactions using the function *mapExpressionToReactions* in COBRA Toolbox. The reactions were associated with a core reaction set ( $n=1843$ , Zhang;  $n=1765$ , Vadodaria;  $n=1836$ , Koskuvi). Different variants of the model extraction methods (MEMs) such as iMAT<sup>388</sup>, GIMME<sup>391</sup>, MBA<sup>389</sup> and FastCore<sup>390</sup> were considered. Both absolute (abs) and normalized (norm) FPKM values were used to generate the metabolic models. Three gene expression thresholds ( $FPKM_{abs}$ ,  $FPKM_{norm.t1}$ ,  $FPKM_{norm.t2}$ ) were used, and for each of them, the high-confidence (HC), medium-confidence (MC) and inactive (IA) reactions were defined as follows,

a.)  $FPKM_{abs}$ :

$$\begin{aligned} G_i &= \text{rowMax}_i(\text{abs}(FPKM)) \\ HC &\leftarrow \text{if } G_i > 2 \\ MC &\leftarrow \text{if } 2 \geq G_i \geq 0.1 \\ IA &\leftarrow \text{if } G_i < 0.1 \end{aligned}$$

b.)  $FPKM_{norm.t1}$ :

```

 $G_i = \text{rowMax}_i(\text{quantilenorm}(\log_{10}(FPKM + 1)))$ 
 $HC \leftarrow \text{if } G_i > 50\text{th percentile}(G)$ 
 $MC \leftarrow \text{if } 50\text{th percentile}(G) \geq G_i \geq 25\text{th percentile}(G)$ 
 $IA \leftarrow \text{if } G_i < 25\text{th percentile}(G)$ 

```

c.)  $FPKM_{norm.t2}$ :

```

 $G_i = \text{rowMax}_i(\text{quantilenorm}(\log_{10}(FPKM + 1)))$ 
 $HC \leftarrow \text{if } G_i > 25\text{th percentile}(G)$ 
 $MC \leftarrow \text{if } 25\text{th percentile}(G) \geq G_i \geq 10\text{th percentile}(G)$ 
 $IA \leftarrow \text{if } G_i < 10\text{th percentile}(G)$ 

```

Where  $G_i$  is the maximum expression value of the  $i^{th}$  gene across all samples. The above thresholds were also used to define inactive reactions (IA), unless manual curation of literature dictated otherwise.

Draft metabolic models of astrocytes were generated from the transcriptomes of eight phenotypes (Primary-Ctrl, iPS-Ctrl-a, iPS-BD, iPS-BD-R, iPS-BD-NR, iPS-Ctrl-b, iPS-ST and iPS-HT) using four MEMs (iMAT, GIMME, MBA, and FastCore) across three gene expression thresholds ( $FPKM_{abs}$ ,  $FPKM_{norm.t1}$ ,  $FPKM_{norm.t2}$ ). iMAT and MBA require a 'medium-confidence' threshold to be defined by users, while GIMME and FastCore do not. The MEMs maximize the number of high-confidence and minimize the number of medium-confidence reactions in their output models. The 24 models that captured the least fluxInconsistent reactions, the highest number of core reactions, and the highest overlap with astrocytic reactions (n=649) from Lewis et al. 2010, for each of the eight phenotypes, were chosen for further expansion.

#### 4.2.4.2. Manual curation of astrocytic reactions for the expansion of draft metabolic models and defining model function tests.<sup>35</sup>

Extensive manual curation of the literature was conducted to identify biochemical reactions (n=159) in astrocytes, which exhibited behavioral, cellular, or molecular phenotypes upon disruption. Their rationale for inclusion, along with PMIDs supporting and refuting their activity in astrocytes, was also provided. Most of the literature evidence was derived from studies on rodent models. While these curated reactions were mostly part of Recon3D, a significant number of them were not detected by the automated model extraction methods (MEMs) across all 24 models. Consequently, it became necessary to identify the missing metabolites and reactions, conduct gap-filling, and incorporate these reactions into the models. As part of this effort, an additional extracellular compartment 'synapse' [s], along with exchange (n=15) and transport reactions (n=14), were included in the 'Primary-Ctrl' models to capture astrocyte-synapse metabolic crosstalk (Fig.S5). However, the synaptic

compartment and corresponding reactions were not included in the iPS-astrocyte models. Additionally, the curated reactions were also used as model function tests (MFTs), ensuring that all 24 models carried non-zero flux through the curated reactions, subject to nutrient media constraints.

#### 4.2.4.3. Imposing astrocytic nutrient uptake constraints.

A crucial assumption was made that culture media components exist in systemic circulation<sup>409</sup>, traverse the blood-brain barrier (BBB), and are accessible for astrocyte uptake. Hence, the 'Primary-Ctrl' models' extracellular compartment [e] was constrained by all metabolites and ions that i) constitute the astrocyte sustenance medium (ASM)<sup>410</sup>, and ii) cross the blood brain barrier (BBB)<sup>411</sup>. The remaining iPS-astrocyte models' extracellular [e] compartments were constrained by ASM alone, representing culture media conditions (Fig.S5). The metabolic components of the ASM, which consists of Neurobasal medium, Minimum Essential Medium - Non-Essential Amino Acids Solution, GlutaMAX Supplement, and N-2 Supplement, were obtained from the Thermo Fisher Scientific™ website. The metabolic components of the BBB were obtained from Thiele et al.<sup>411</sup>. There are 22 components that overlap between the ASM (n=44) and BBB (n=45). To simulate nutrient uptake, all nutrient uptakes in the model except for the 67 exchanges added to the extracellular compartment [e], for which uptake rates were set to -10mmol/gDw/h, were set to 0.

#### 4.2.5. Identifying disrupted reactions & subSystems in BD and SCZ astrocyte metabolic models.

##### 4.2.5.1. Flux balance analysis (FBA)

A metabolic network consisting of  $m$  metabolites<sup>48</sup> and  $n$  reactions is represented by a stoichiometric matrix  $S$  where  $S_{ij}$  represents the stoichiometric coefficient of metabolite  $i$  in reaction  $j$ .<sup>25</sup> The flux vector for each reaction in the network is represented by  $v$ . Flux balance analysis (FBA) assumes a steady-state mass balance wherein the sum of the input flux equals the sum of the output flux. This follows<sup>32</sup> as,  $dx_i / dt = 0$  i.e. the change in concentration of the  $i^{th}$  metabolite over time is zero<sup>380</sup>. Flux variability analysis (FVA) was used to calculate the minimum and maximum flux through each reaction in all five metabolic models subject to constraints,

$$\min/\max c^T x, \text{s.t. } s.v = dx/dt = 0, \quad (1)$$

$$v_{min} \leq v_j \leq v_{max}, \quad (2)$$

where the equation (1) corresponds to the steady-state mass-balance constraints, whereas equation (2) corresponds to the reaction directionality and capacity constraints. The ratio of flux span ( $FSr$ )<sup>412</sup> for each reaction was calculated as follows,

$$FSr (\text{healthy vs disease}) = \frac{abs(FVAm_{j,\text{healthy}} - FVAm_{j,\text{disease}})}{abs(FVAm_{j,\text{disease}} - FVAm_{j,\text{healthy}})}, \quad (3)$$

where  $FVAm_{\text{max}}$  and  $FVAm_{\text{min}}$  are the maximum and minimal flux through the  $j^{\text{th}}$  reaction in the model.  $FSr$  can be calculated only for those reactions that are captured by both the models under comparison. The reactions with  $FSr > 1.5$  and  $< 0.8$  were identified for each phenotype-of-interest (n=4 i.e., BD; BD\_Responder; BD\_NonResponder; SCZ-Twin), and subsequently considered for downstream analysis.

#### 4.2.5.2. Metabolic transformation algorithm (MTA)

The metabolic transformation algorithm (MTA)<sup>393,406,407</sup> identifies reactions in a metabolic network whose inhibition facilitates a transformation between two metabolic states (e.g., from diseased to healthy states, or vice-versa). The inputs to MTA are i) the transcriptomic measurements of the source and target states, and ii) the reference metabolic model. For each transformation analysis, MTA follows a two-step process: i) determining the flux distribution of the source metabolic state ( $v^{ref}$ ) using iMAT followed by ACHR sampling of the solution space. ii) determining the set of genes whose expression is significantly elevated or reduced between the source and target states. Using i) and ii), MTA computes a transformation score for each of the metabolic reactions in the cell, and usually, the 10-20% reactions with the highest MTA score contain promising candidate targets. For each phenotype-of-interest, we ran MTA twice, by swapping the source and the target states. E.g., in order to identify the reactions relevant to BD, we identified the reactions that transformed i) "iPS-Ctrl" to "iPS-BD", and ii) "iPS-BD" to "iPS-Ctrl". For either runs, the top 20% predictions were first identified, and subsequently their union sets were considered for downstream analysis.

#### 4.2.5.3. Filtering reactions relevant to phenotype-of-interest.

From the reactions as identified by FVA ( $FSr > 1.5$ ;  $FSr < 0.8$ ) or MTA (top 20%), filters were applied to select for reactions that were relevant to the phenotype-of-interest (Table 1). While defining the filters, it was important to consider the fact that the treatment responders and the non-responders together comprise the BD cohort. Hence the fluxes relevant to "BD\_R" and "BD\_NR" can share overlaps with "BD". A detailed protocol is provided in [supplementary section 7.1](#).

Phenotype-of-interest	Filtering criteria
-----------------------	--------------------

BD <sup>a</sup>	Specifically disrupted in "iPS-Ctrl vs iPS-BD" & unchanged between control models.
BD-Responder <sup>b</sup>	Specifically disrupted in "iPS-Ctrl vs iPS-BD-Responder" & unchanged between control models.
BD-NonResponder <sup>c</sup>	Specifically disrupted in "iPS-Ctrl vs iPS-BD-NonResponder" & unchanged between control models.
SCZ-Twin <sup>d</sup>	Specifically disrupted in "iPS-Ctrl vs iPS-SCZ-Twin" & unchanged between control models.

<sup>a</sup>Can share overlaps with BD-Responder, BD-NonResponder and SCZ-Twin.  
<sup>b</sup>Can share overlaps with BD and SCZ-Twin but not with BD-NonResponder.  
<sup>c</sup>Can share overlaps with BD and SCZ-Twin but not with BD-Responder.  
<sup>d</sup>Can share overlaps with BD, BD-Responder and BD-NonResponder.

Table 1. Reaction filtering criteria. "Unchanged between control models" means the reactions that were not found to be disrupted in "iPS-Ctrl vs Primary-Ctrl".

#### 4.2.5.4. Metabolic subSystem enrichment analysis (MSEA).

To test for enrichment of disrupted metabolic subSystems, a hypergeometric test was applied to each subSystem, and the P-value was calculated for each subSystem using the *phyper* function in R as below,

$$\text{phyper}(x - 1, m, n - m, k, \text{lower.tail} = \text{FALSE}) \quad (4)$$

56

Where  $n$  is the number of all reactions in the model,  $k$  is the number of the disrupted reactions within each tested subSystem,  $m$  is the total number of reactions within each disrupted subSystem, and  $x$  is the overlap size between  $k$  and  $m$ . This was followed by multiple-testing corrections using the Benjamini-Hochberg false discovery rate<sup>413</sup>, and subSystems with  $P_{FDR} < 0.05$  were considered as significant.

#### 4.2.5.5. Identifying disruptions that are significant across modules.

Here, a 'module' was defined as the list of subSystems that were predicted to be significant by MSEA, using either of the analytical approaches i.e., FBA/MTA. E.g. 'FVA\_BD\_NR\_norm\_t1' is a module - where 'FVA' is the analytical method, 'BD\_NR' is the phenotype-of-interest and 'norm\_t1' is the gene expression thresholding of the metabolic model. For each phenotype-of-interest (BD, BD-Responder, BD-NonResponder and SCZ-Twin), we generated six modules (i.e., derived using three expression thresholds and two analytical methods), and identified the subSystems that were disrupted in at least two or more modules.

34

#### 4.2.6. Data, figures and code availability.

34

This study did not generate experimental data. Raw transcriptome data used in this study were publicly available. Figure panels were generated either programmatically in R or using [BioRender.com](#) (full license) and [Diagrams.net](#) (open source). All original code has been deposited at GitHub (<https://github.com/anin90/AstroModel>) and will be made publicly available. References and identifiers are provided in the [key resources table](#).

### 4.3. Results.

#### 4.3.1. Deriving and testing the human astrocyte metabolic models. ([Figure 2](#))

Draft metabolic models of astrocytes (n=56) were extracted for eight distinct phenotypes, including BD patients (iPS-BD, iPS-BD-R, iPS-BD-NR), SCZ twin (iPS-ST), healthy twin (iPS-HT) and healthy controls (Primary-Ctrl, iPS-Ctrl-a, iPS-Ctrl-b), by using transcriptome data and glial proteomics data as a constraint on the Recon3D human metabolic knowledgebase. The gene expression threshold determines the model contents, and there's no one model that's poised to explain the underlying biology<sup>414</sup>. Hence, three metabolic models were derived for each of the eight phenotypes by using different FPKM thresholds. Of the 56 models, only the iMAT-derived models (n=24) satisfied our selection criteria and only those were further expanded (refer Methodology section 3.3. for more details). First, the properties of the 24 models, before (preExpansion) and after expansion (postExpansion), were evaluated ([Fig. 2.a-e](#)). The final models (i.e., postExpansion) consisted of 5,342–6,305 reactions and 3,679–4,273 metabolites. The flux inconsistency, which refers to the blocked reactions, ranged between ~22-29% in the final models, which is primarily driven by the nutrient media constraints, as opposed to zero blocked reactions in the draft models due to the unconstrained nutrient media. This constraint was necessary to ensure that the final models operated solely on physiologically relevant nutrient media conditions. The core reactions captured by all models ranged between ~70-98%, and the Lewis et al. astrocytic reactions captured by all models ranged between ~40-53%. The literature curated reactions (n=159) were also used as “metabolic tasks”, and all 24 models passed ~90-93% of the tasks. A comparison was performed between our models (This Study, n=24) and previously published mass-action models of brain metabolism<sup>394,415-418</sup> (Predecessor, n=11) ([Fig. 2.f-g](#)). The growth in the size of the models over time is mainly due to the ongoing development of larger metabolic knowledge bases like Recon3D. Overall, the statistics indicated that our models do recapitulate astrocyte physiology; were in-par with its equivalents<sup>394</sup> and were ready to be deployed for downstream analysis. We have provided the comprehensive details of all 24 models on Github for open access for the scientific community.

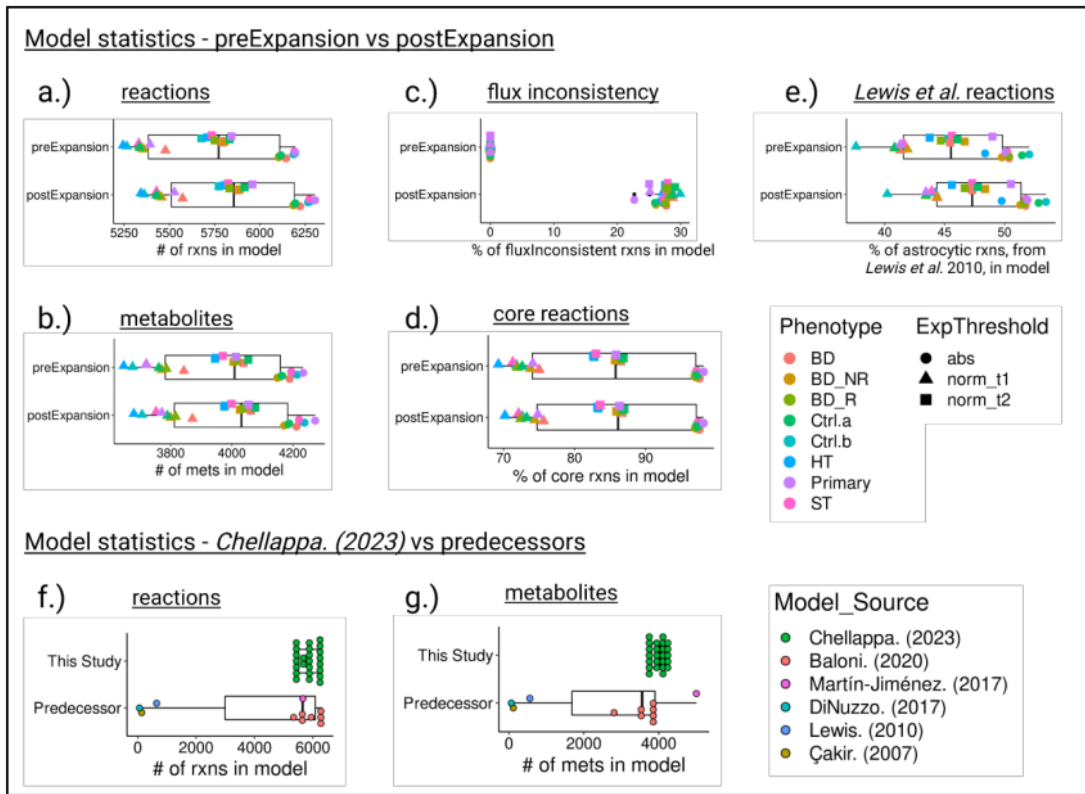


**Figure 2: Model statistics.** (a-e) Differences in model statistics observed between the iMAT-derived draft models (preExpansion, n=24) and the final models (postExpansion, n=24) of astrocyte metabolism, that were generated for five phenotypes across three gene expression thresholds. The model statistics include the # of reactions, # of metabolites, % of flux inconsistent reactions, % of core reactions and % of astrocytic reactions (Lewis et al. 2010), captured in the respective models. (f-g) Differences in model statistics observed between the models that were derived as a part of this study (This Study, n=24) and those captured by previous studies (Predecessor, n=11). Because the reconstructions of most predecessors were not publicly accessible, except for Lewis et al. (2010) and Baloni et al. (2020), the comparison was conducted solely based on the number of reactions and metabolites.

#### 4.3.2. Metabolic subsystems disrupted in BD & SCZ patients' astrocytes ([Figure 3](#))

To identify fluxes that are disrupted in our phenotypes-of-interest (BD, BD-Responder, BD-NonResponder and SCZ-Twin), the models (n=24) were first divided into groups based on their FPKM thresholds (n=3). This resulted in five models within each group. The flux distributions of the models within each group were analyzed using two methods - FVA and MTA. Filters were applied to select for reactions that were relevant to each phenotype-of-interest, followed by Metabolic-subSystem enrichment analysis (MSEA). The metabolic subsystems that were disrupted ( $P_{FDR} < 0.05$ ) in at least two or more modules were identified (Refer to the Methodology section 3.4. for more details). Thirteen subsystems were predicted to be disrupted by at least two or more modules across either of the four phenotypes-of-interest ([Fig.3.a](#)). However, none of these disruptions were found to be significant across all six modules while considering the  $mean(P_{FDR}) < 0.05$ .

##### 4.3.2.1. Slower PI-cycle in Li+ Non-Responder astrocytes. ([Figure 3](#))

Eight subsystems were predicted to be specifically disrupted in the Li+ non-responders models, while three subsystems were specifically disrupted in the Li+ responders models. There were no subsystems disrupted across both Li+ responders and non-responders ([Fig.3.b](#)). Among the eight disrupted subsystems in non-responders, inositol phosphate (IP) metabolism was captured by two modules ([Fig.3.a](#)). The flux through the reactions in this pathway (n=4) was reduced, indicating slower synthesis rates compared to the Li+ responder and the control models ([Fig.3.c-d](#)). The myo-inositol 1-phosphate phosphatase (MI1PP/IMAPase, catalyzing  $IP_1 \rightarrow$ Inositol), one of the four disrupted reactions in the IP metabolism, has a long-standing association with Li+'s mechanisms of action<sup>150</sup>. The "inositol depletion" hypothesis posits that the depletion of inositol by Li+ reduces the brain excitability in BD<sup>150</sup>. And this may happen through the ability of Li+ to,

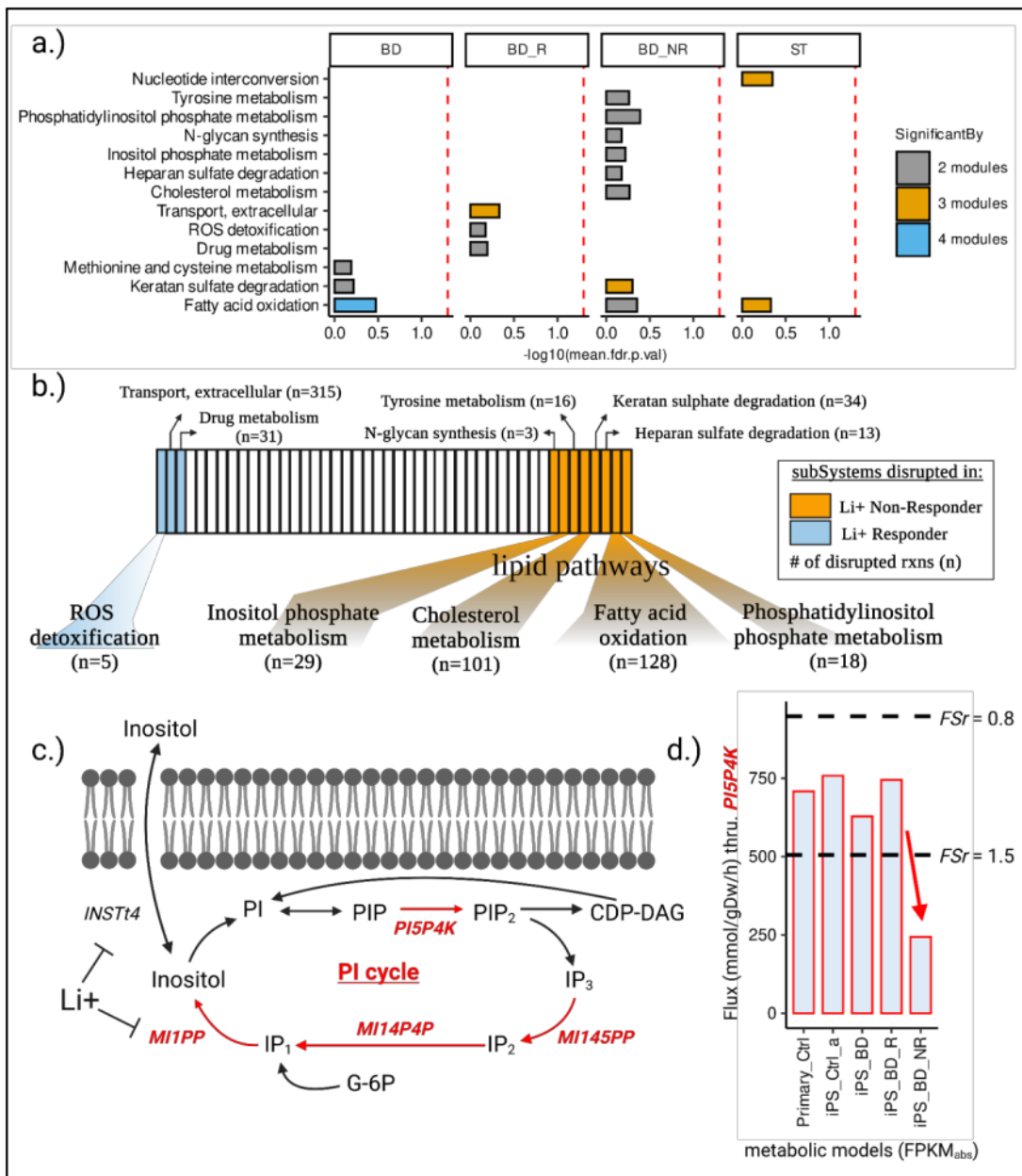
1. Inhibit MI1PP activity<sup>150</sup>,
2. Inhibit plasma membrane inositol transporters<sup>419</sup>,
3. Regulate the rate of inositol synthesis<sup>420</sup>.

Our models also predict slower syntheses of phosphoinositide (PI5P4K, catalyzing  $PIP \rightarrow PIP_2$ ) and phosphoinositols (MI145PP, catalyzing  $IP_3 \rightarrow IP_2$ ; and MI14P4P, catalyzing  $IP_2 \rightarrow IP_1$ ), specifically in Li+ non-responder ast<sub>40</sub>cytes ([Fig.3.c](#)). This seems to be consistent with Sade *et al.*<sup>151</sup>, which suggests that Li+ affects the entire phosphatidylinositol (PI) signaling system in tw<sub>40</sub> ways: first, by depleting inositol, thereby reducing phosphoinositide levels; and second, by elevating inositol monophosphate levels, leading to phosphoinositols accumulation.

Regardless of the molecular mechanisms of Li<sup>+</sup> action, in BD patients inositol concentrations can change, and may be further altered by Li<sup>+</sup> treatment<sup>421</sup>. In contrast to the majority of metabolism studies that focus on metabolite concentrations, our model predictions are exclusively on fluxes, which represent the rates of reactions, and alterations in flux levels do not always indicate changes in metabolite concentrations<sup>353</sup>. Metabolite concentrations in a cell can increase due to fast synthesis or slower degradation processes. As a result, two interpretations can be derived from our model prediction of slower rates of synthesis of inositol, PIP<sub>2</sub>, IP<sub>2</sub> and IP<sub>1</sub>, specifically in Li<sup>+</sup> non-responders:

1. Our models challenge the depletion hypothesis, expecting a faster PI cycle (specifically a higher flux through MI1PP and PI5P4K) for its metabolites (inositol and PIP<sub>2</sub>) to accumulate in BD patients. This implies that there may be other factors contributing to the slower PI cycle observed in Li<sup>+</sup> non-responders.
2. Alternatively, the slower PI cycle could be indicative of lower enzyme concentrations that hinder the actions of Li<sup>+</sup> and subsequently impact the responsiveness in BD patients. It is important to note that the slower PI cycle is only observed in the models of Li<sup>+</sup> non-responders, while in Li<sup>+</sup> responders, the inositol fluxes remain unaffected. This might suggest that the levels of inositol monophosphatase (IMPAse), and/or the other enzymes in the PI cycle, may be maintained at a higher level in Li<sup>+</sup> responders, facilitating the desired response.

While the latter explanation appears to be the most plausible and parsimonious based on our predictions, experimental validation is necessary to confirm these hypotheses. Our models successfully capture the disruption of the PI signaling system, a well-known aspect of Li<sup>+</sup> biology<sup>151,421</sup>. This validation enhances trust in the model predictions, and justifies further investigation of the novel predictions, such as the involvement of remaining seven disrupted subsystems in Li<sup>+</sup> non-responders that may not have been previously reported in the literature regarding BD/Li<sup>+</sup> biology.

**Figure 3: Disrupted metabolic subsystems in BD and SCZ patients' astrocytes.**

**(a)** Metabolic subsystems (n=13) predicted to be disrupted by at least two or more modules in any of the four target phenotypes (BD, BD-Responder, BD-NonResponder, and SCZ-Twin). **(b)** Metabolic subsystems predicted to be disrupted by at least two or more modules in Li+ responders (n=3) and non-responders (n=8). The value 'n' represents the total number of disrupted reactions within each subsystem, captured by any of the six modules. **(c)** Metabolic

fluxes (n=4) through the inositol phosphate metabolism (PI cycle) were found to be reduced (red) specifically in Li<sup>+</sup> non-responder metabolic models. **(d)** Bar plot highlighting the reduced flux through Phosphatidylinositol-5-Phosphate 4-Kinase (PI5P4K), specifically within the Li<sup>+</sup> non-responder metabolic model.

#### 4.3.2.2. Other pathways disrupted in Li<sup>+</sup> Non-Responder astrocytes ([Figure 3](#))

Apart from inositol phosphate metabolism, the disrupted subsystems in BD-NR comprised fatty acid oxidation (FAO), cholesterol metabolism, phosphatidylinositol phosphate metabolism, tyrosine metabolism, N-glycan synthesis, keratan sulfate degradation and heparan sulfate degradation ([Fig. 3.b](#)). However, the association of these biochemical pathways to mood/psychotic disorders remains patchy. The disruption of FAO was particularly intriguing, as it was the only disruption observed across the other two phenotypes-of-interest, BD (four modules) and SCZ (three modules) ([Fig. 3.a](#)). In all three contexts (BD, BD-NR and SCZ), disruptions in FAO were observed in both mitochondria and peroxisomes, indicating alterations in medium chain, long chain, and very-long chain fatty acids. The involvement of fatty acid oxidation (FAO) in psychotic disorders' etiology or treatment response is supported by sparse and inconsistent evidence<sup>422</sup>. The inconsistencies observed in these studies can be attributed to confounding factors such as medication usage, lifestyle, etc. Moreover, many of these studies investigated fatty acid alterations in peripheral samples like erythrocyte membranes, which may not necessarily corroborate findings from post-mortem brains or iPS-cells obtained from psychiatrically ill patients. However, in a recent bioinformatics study, ~250 'seeded co-expression networks' were constructed across 11 brain regions and 1113 samples with the aim of identifying the network of coregulated MDD GWAS genes, and the prefrontal cortex co-expression networks of FADS1 (fatty acid desaturase 1) and ZKSCAN8 (zinc finger with KRAB and SCAN domains 8) were found to be significantly associated with suicidal ideation<sup>64</sup>. Interestingly, these networks functionally converge on fatty acid metabolism specifically in astrocytes. Furthermore, in the same study, biased astrocytic states in MDD were identified through network-based clustering of single nucleus RNA sequencing (snRNA-seq) data. This represents one of the first pieces of evidence indicating the involvement of fatty acid metabolism in a psychiatric disorder, stemming from a systematic secondary analysis of a psychiatric GWAS. Another recent study revealed that the brain critically depends on the astrocytic oxidative phosphorylation (OxPhos) to break down fatty acids and maintain lipid balance. And disrupted astrocytic OxPhos led to the accumulation of lipid droplets (LD) and subsequent neurodegeneration, resembling key aspects of Alzheimer's disease (AD)<sup>423</sup>, which exhibits shared biology with BD and SCZ. However, the disruptions in OxPhos fluxes were not predicted by our models, likely due to degeneracy in metabolic networks<sup>424</sup>, where a phenotype may not be apparent due to compensatory fluxes mediated through other genes/reactions.

#### 4.3.2.3. Identifying links between PI-cycle and other disrupted lipid pathways in Li+ Non-Responder astrocytes. ([Figure 4](#))

To investigate the potential coupling of PI-cycle disruptions with other seven disrupted pathways in the Li+ non-responders, the wiring diagram of pathways/fluxes feeding into and out of inositol metabolism was reconstructed ([Fig. 4](#)). Subsequently, the disrupted fluxes were mapped onto the wiring diagram - limited to inositol metabolism, cholesterol metabolism, and FAO, considering tractability and the close links between these three pathways. The wiring diagram revealed that fatty acids (FAs) feed into the inositol cycle through diacylglycerol (DAG), however, our models did not predict disruptions in DAG synthesis or utilization reactions. This could be attributed either to the degeneracy in metabolic networks, or limitations of metabolic models (or mass-action models in general) to encompass other biological mechanisms that may lead to the observed metabolic phenotype. The output of FAO is acetyl-CoA, which feeds into cholesterol biosynthesis through HMG-CoA and Mevalonate in the endoplasmic reticulum (ER). As anticipated, our models predicted disruption in the final steps of cholesterol metabolism, particularly slower fluxes through the conversion of lanosterol to cholesterol, and subsequent interconversions of cholesterol and cholestryl esters, in the ER. The disruption of brain lipid metabolism in psychoses has been inconsistent in the literature, akin to FAO, and necessitates systematic re-investigations<sup>425</sup>. However, the slower turnover of fatty acyl-coAs and cholestryl esters suggests the possibility of disruptions in the biogenesis of lipid droplets (LDs), which are critical for lipid and energy homeostasis<sup>316,426</sup>. Accumulation of LDs has been observed in astrocytes under stress<sup>427</sup>, and in the context of AD, astrocytes expressing the risk variant APOE4 form large LDs with impaired turnover and increased peroxidation sensitivity<sup>428</sup>. However, there is no literature evidence for alterations in LDs in the context of psychotic or mood disorders.

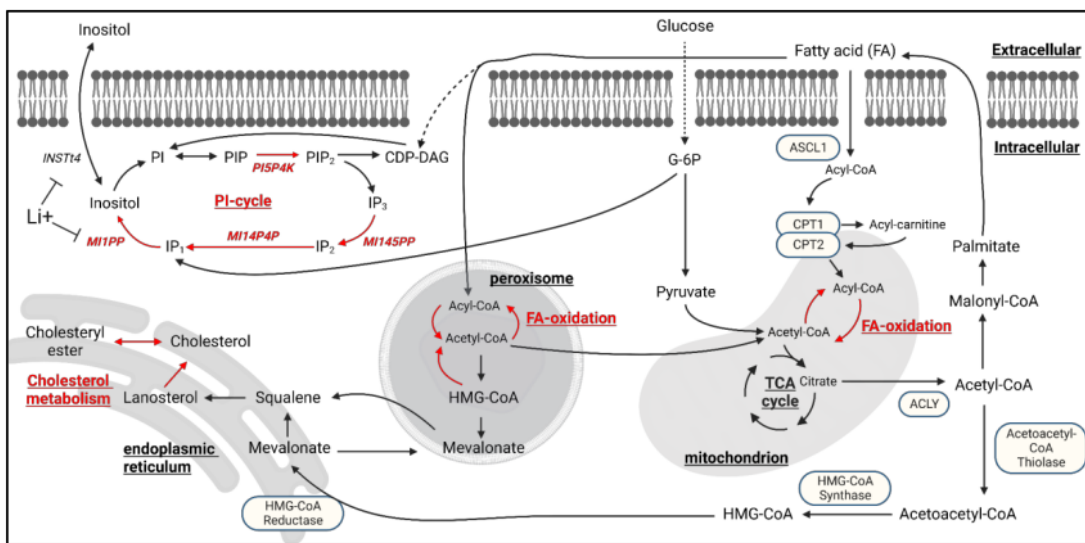


**Figure 4: Wiring diagram illustrating the metabolic coupling of inositol metabolism with FAO and cholesterol metabolism.**

Disruptions (highlighted in red) are distributed across various compartments, including the ER, peroxisome, mitochondrion and cytosol. In order to accommodate multiple subsystems, the presented diagram does not encompass all intermediate reactions, reflecting the adage that the map is not the territory.

#### 4.4. Discussion.

By utilizing publicly available 'omic data and applying principles of metabolic modeling, an inquiry was made into the existence of metabolic phenotypes in astrocytes that are: i) unique to BD patients who do no response to Li<sup>+</sup> treatment, and ii) common to both BD and SCZ patients. This was accomplished by first deriving phenotype-specific metabolic models of astrocytes from BD & SCZ patients, and healthy controls, followed by extensive manual curation of astrocyte literature to identify relevant metabolic tasks, which were subsequently tested in all models subject to appropriate nutrient media constraints, and finally comparing the metabolic flux distributions between the *wt* (Ctrl) and  $\delta$  (BD/SCZ) models. Specific filtering criteria were applied to identify the disrupted fluxes in four of the phenotypes that are of interest to us including BD, BD-Responder, BD-NonResponder and SCZ-Twin ([Fig.1](#)). The key findings are noted as follows. Eight metabolic pathways were identified as being specifically disrupted in astrocyte models of Li<sup>+</sup> non-responsive BD patients. Among these, four pathways were directly linked to lipid metabolism, encompassing inositol phosphate metabolism, FAO, cholesterol metabolism, and phosphatidylinositol phosphate metabolism. Furthermore, it was observed that FAO was the sole pathway disrupted in the astrocyte models of both BD and SCZ patients. Key hypotheses, for experimental validation, were formulated based on our model predictions, as outlined below:

1. Slower rates of FAO were observed in BD, BD-NonResponder, and SCZ-Twin astrocytes. To verify this, the levels of acylcarnitine or carnitine palmitoyltransferase I (CPT1), a rate-limiting step in FAO<sup>429</sup>, can be assessed in astrocytes from both BD and SCZ patients, as this pathway exhibited disruption in both phenotypes.
2. Slower turnover of cholesteryl esters and fatty acyl-coAs in BD-NonResponder astrocytes suggests potential disruptions in the biogenesis/expansion of LDs. This can be explored by profiling LDs<sup>317</sup> in astrocytes from BD patients.
3. Maintaining a faster astrocytic inositol synthesis rate (i.e., an accelerated PI cycle) might be a necessary condition for Li<sup>+</sup> responsiveness in BD. This can only be tested through stable-isotope tracing experiments, probing inositol metabolism using <sup>13</sup>C-labeled myo-inositol<sup>430</sup>, in BD patients' astrocytes.

Although there is evidence of astrocyte dysfunction in BD<sup>61-64</sup> and SCZ<sup>20-22,65-67</sup>, the unbiased genomic studies, especially GWAS findings, for these conditions do not converge on astrocytes. Instead, they tend to converge on synaptic pathways in specific excitatory and inhibitory neurons<sup>17,186</sup>. Nevertheless, we chose to model astrocyte metabolism in this study for specific reasons:

1. GWAS, exome, CNV studies, along with functional genomics data related to BD and SCZ typically converge on synaptic pathways<sup>17,164,186,187,324</sup>, and these pathways are influenced by the presynaptic exocytosis of synaptic vesicles containing neurotransmitters<sup>431</sup> (glutamate, GABA, dopamine, serotonin, norepinephrine, histamine, acetylcholine, etc) and the subsequent detection of these neurotransmitters by postsynaptic receptors<sup>432</sup>. As a corollary, neurotransmitter homeostasis is maintained through astrocytic regulation of signaling molecules including lactate<sup>31–35</sup>, glutamate<sup>36</sup>, ATP<sup>37</sup>, D-Serine<sup>38</sup>, potassium<sup>39</sup>, nitric oxide (NO)<sup>40–42</sup>, hydrogen peroxide (H<sub>2</sub>O<sub>2</sub>)<sup>43,44</sup> and ammonia<sup>45</sup>. Notably, all of the neurotransmitters and signaling molecules mentioned are ‘metabolites’ themselves originating from intracellular metabolic pathways. In essence, GWAS hits associated with BD and SCZ have an impact on synaptic metabolite signaling, a system that is under the regulatory influence of astrocytes<sup>433</sup>.
2. GWAS explains only a small portion of heritability, with SNP-based heritability ( $h^2_{SNP}$ ) estimates on the liability scale for BD and SCZ at 20.9%<sup>17</sup> and 24.4%<sup>186</sup>, respectively, compared to overall heritability estimates from twin and population-based studies ranging from 60% to 85% for both conditions<sup>434</sup>. This missing heritability is, in part, explained by rare SNVs and CNVs contributing to the liability of BD and SCZ. Therefore, it is crucial to integrate GWAS results with whole exome and CNV studies, perform meta-analyses, and then evaluate the enrichment of cell-types and pathways, rather than dismissing astrocytes and other glial cell-types solely based on current GWAS outcomes.
3. While the concept of brain cell-type serving as the primary GWAS readout is appealing, it presupposes that the genetic architectures of complex brain disorders closely align with the genes whose expression maps to specific cell-types<sup>18,19,194</sup>. However, cell-types are defined not only by their transcriptional states but also by epigenomic regulation<sup>435–439</sup>, translational control<sup>440</sup>, structural proteome<sup>441</sup>, protein interaction networks<sup>442,443</sup>, metabolite signaling<sup>353,444,445</sup>, and more. The interplay of genetics and the environment affects each of these layers of information. For example, we lack an understanding of how common genetic variations identified by GWAS affect the brain's metabolic environment in SCZ/BD patients and, if they do, which particular cell-types are affected. Therefore, it is imperative to construct reference maps encompassing some or all of these layers of information and subsequently integrate the genomic findings to prioritize cell-types, rather than disregarding specific cell-types like astrocytes solely because GWAS genes exhibit low expression levels in astrocytes and higher levels in certain excitatory and inhibitory neurons.

Metabolic models of astrocytes were derived and analyzed for distinct BD subtypes (Li+ responder vs non-responder), with the expectation that this approach could potentially elucidate variations associated with Li+ response. Remarkably, it was indeed demonstrated that the disruption of the PI signaling system, well-known to be implicated in BD but also altered by Li+ treatment, was specifically captured by the astrocyte models representing Li+ non-responders. This successful validation served to bolster confidence in the model predictions and justified further exploration of the novel insights they offered. Nevertheless, it is essential to acknowledge that individuals clinically categorized as Li+ non-responders might also belong to the subset of BD patients with more severe symptoms, such as an increased frequency of manic episodes. Hence, our findings could potentially reflect severity rather than intrinsic factors mediating treatment responsiveness (genetics, family history, etc).

20

Our findings should be viewed in light of several limitations:

1. Quantitative metabolic data was not directly used for deriving the models. Instead, astrocyte RNA-Seq and glial proteomics data served as constraints, albeit with weak correlations to metabolite levels and fluxes. For a more comprehensive analysis of metabolic flux<sup>446</sup>, it would be ideal to constrain the models using metabolomics, physiological nutrient uptake rates, and metabolic dry-weight of astrocytes from BD, SCZ, and control subjects.
2. Although astrocyte-synapse metabolic interactions were incorporated in all Primary astrocyte models (n=3), they represented only 29 exchange and transport reactions, in contrast to the ~5,000–6,000 internal astrocytic reactions. The extensive model size led to degeneracy, which might prevent the models from effectively capturing true synaptic disruption events.
3. For FVA, conducting statistical analysis directly on flux values posed challenges due to the uniqueness of objective values. Repeating the simulation with the same constraints consistently yielded identical results through the objective function.

## 5. Identifying the metabolic effects of LoF mutations implicated in neuropsychiatric and neurodegenerative disorders.

### 5.1. Introduction.

Neuropsychiatric disorders like BD and SCZ, as well as neurodegenerative disorders such as AD, have a strong genetic component and complex inheritance patterns. GWAS studies provide some insights but fall short of explaining the full heritability of these conditions. To address this gap, extensive sequencing efforts are being carried out globally by consortia like the PGC<sup>93</sup>, BSC<sup>140</sup>, SCHEMA<sup>187</sup>, and the Alzheimer's Disease Sequencing Project (ADSP)<sup>447,448</sup>. These projects involve large case-control studies, with samples primarily representing European populations, to identify rare coding variants that could account for the missing heritability. Similar initiatives are underway in India, focusing on WES of multiplex families diagnosed with SMI (BD and SCZ)<sup>397,398</sup>, and AD<sup>399</sup> as part of the "Accelerator Program for Discovery of Brain Disorders Using Stem Cells (ADBS)" longitudinal study<sup>449</sup>. These efforts have uncovered rare LoF variants with relatively larger effects, some of which are unique to Indian patients and not reported in reference databases like gnomAD<sup>450</sup>. Many of these LoF mutations are private to individual families, suggesting recent founder events. While these sequencing efforts hold promise in addressing the missing heritability problem in oligogenic disorders, they are often underpowered and do not provide insights into the cellular and molecular effects of these variants. Given that many of these cohorts, both in India<sup>449</sup> and globally<sup>22,451</sup>, collect biological material from patients and controls to derive iPS-cells for future research, we saw an opportunity to use computational models, that were built as a part of [Section 4](#), to predict the cellular-level impacts of these LoF mutations. These predictions can generate testable hypotheses, which could be experimentally validated, especially using iPS-cells generated from the same patients.

The human astrocyte metabolic models, developed in [Section 4](#), were employed to investigate potential metabolic phenotypes in astrocytes resulting from LoF mutations implicated in SMI and AD, but also PD, which was included as certain genes linked to this neurodegenerative disorder were known to specifically affect astrocytes, serving as a positive control. The approach involved computationally inducing and simulating the effects of these LoF mutations on their target enzymes/transporters within the 'control' astrocyte metabolic models. This process resembled an *in silico* CRISPR screening but focused on metabolic phenotypes. Due to the limited scope of these metabolic models, which encompassed enzymes and transport proteins, it was anticipated that only a subset of the implicated genes in these disorders would be amenable to analysis. By comparing flux levels between the wild-type (wt) and LoF models, valuable insights were gained into the distinctions between these conditions.

## 5.2. Materials and methods.

A collection of genes ( $n=154$ ) implicated in various neuropsychiatric disorders (SMI, AD, and PD) was curated. This analysis was specifically restricted to the genes identified from in-house studies on SMI ( $n=120$ )<sup>397,398</sup> and AD ( $n=26$ )<sup>399</sup>, as well as the genes known to impact astrocytes in PD ( $n=8$ )<sup>452</sup>. The cobratoolbox's *findRxnsActiveWithGenes* function was utilized to map individual genes to their corresponding reactions in the control metabolic models, namely the 'Primary-Ctrl' and 'iPS-Ctrl-a' models that were generated using the 'abs' gene expression threshold (refer to [Section 4.2.](#) for details). Among the 154 genes, those that were not captured by Recon3D or the two control metabolic models, were excluded from this analysis ([Fig.5.](#)). Subsequently, to simulate the LoF of a particular gene, an LoF model was created in which the upper bounds (ub) and the lower bounds (lb) of the mapped reactions were constrained by 50% of wt model's optima, i.e.,

$$ub_{r,LoF} = max_{r,wt}/2, \quad (5)$$

$$lb_{r,LoF} = min_{r,wt}/2, \quad (6)$$

Afterward, both the *LoF* and *wt* models underwent FVA, and reactions with  $FSr > 1.5$  and  $< 0.8$  in the LoF condition were determined for each gene included in this analysis. The perturbation class of the disrupted reactions was annotated as 'DirectMapping' if the reaction was directly mapped by the gene, or as 'Cascade' if the reaction was captured as a consequence of the disruption of another 'DirectMapping' reaction. This information indicates whether the disruption was limited to the reaction directly catalyzed by the gene itself (DirectMapping) or if it led to a domino effect (Cascade).

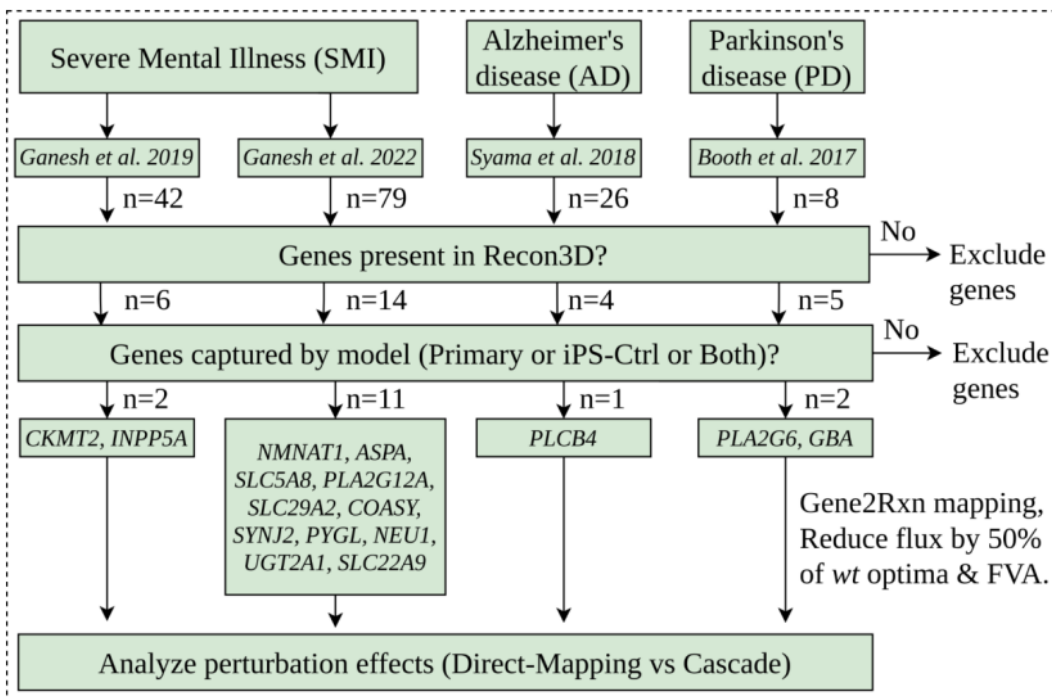


**Figure 5: Identifying the metabolic effects of LoF mutations in SMI, AD, and PD.**

The astrocyte metabolic models (Primary and iPS-Ctrl-a) were used to study the metabolic phenotypes of LoF mutations observed in neuropsychiatric and neurodegenerative disorders. This was performed using a curated collection of genes (n=154) implicated in various neuropsychiatric (SMI<sup>397,398</sup> (n=120) and AD<sup>399</sup> (n=26), as well as genes known to impact astrocytes in PD<sup>452</sup> (n=8). Among the 154 genes, only a subset (n=16) was captured by the astrocyte metabolic models and considered for simulating LoF effects.

### 5.3. Results.

Out of the 154 genes implicated in SMI, AD, and PD, only a subset ( $n=16$ ) was found to be captured by the astrocyte metabolic models (Primary-Ctrl, iPS-Ctrl-a, or both) (Fig.5.). The attrition rate could be attributed to the fact that less than 20% of the human genome encodes metabolic reactions (biosynthesis, breakdown, or transport). For instance, only 2248 genes (as part of Recon3D) from the human genome encode metabolic reactions. Genes captured by Recon3D but unobserved in the astrocyte metabolic models are possibly due to the gene expression threshold used for model extraction, where expression levels of the uncaptured genes fall below the threshold that was used to capture active reactions in the model. The disrupted subsystems, upon the LoF of each of the 16 genes are provided in Table 2. Except for *SLC22A9* and *SLC29A2*, the LoF of the remaining 14 genes did not result in novel disruptions. In this context, "novel disruptions" refer to subsystems distinct from those associated with the 'DirectMapping' reactions. For instance, if gene 'x' maps to reactions annotated for 'subsystems y' in Recon3D, we define novel disruptions as those subsystems (aside from 'y') that experience disruptions when gene 'x' loses its function. This definition takes into account the inherent disruption of subsystem 'y' caused by the LoF of gene 'x', but also negates exchange/transport reactions.

The LoF of *SLC22A9* (implicated in SMI<sup>397</sup>) was particularly interesting as it led to the disruption of cascade reactions in both synthesis and oxidation of FAs (Fig.6), a metabolic phenotype that was also observed in the context of BD, BD-NonResponder, and SCZ-Twin astrocytes (Fig.3a). The LoF of *SLC29A2* (implicated in SMI<sup>397</sup>) was also interesting as it led to the disruption of cascade reactions in nucleotide interconversion (Fig.7), which was also observed in the context of SCZ-Twin astrocytes (Fig.3a). In both scenarios involving the LoF of either *SLC22A9* or *SLC29A2*, the observed metabolic phenotypes, such as the disruption of FA synthesis and oxidation in the case of *SLC22A9*, and nucleotide interconversion in the case of *SLC29A2*, were consistent across both astrocyte metabolic models (Primary-Ctrl and iPS-Ctrl) used for this analysis. Apart from the SLC transporters, the LoF of either of three genes, *INPP5A* (Fig.S18), *SYNJ2* (Fig.S19), and *PLCB4* (Fig.S20) resulted in the disruption of both 'DirectMapping' and 'Cascade' reactions within the inositol phosphate metabolism, a metabolic phenotype that has been implicated in BD/Li<sup>+</sup><sup>421</sup>, but was also observed in BD-NonResponder, from our analysis of Li<sup>+</sup> non-responder astrocyte metabolic models (Fig.3a). *INPP5A* and *SYNJ2* are implicated in SMI<sup>397,398</sup>, and *PLCB4* in AD<sup>399</sup>.

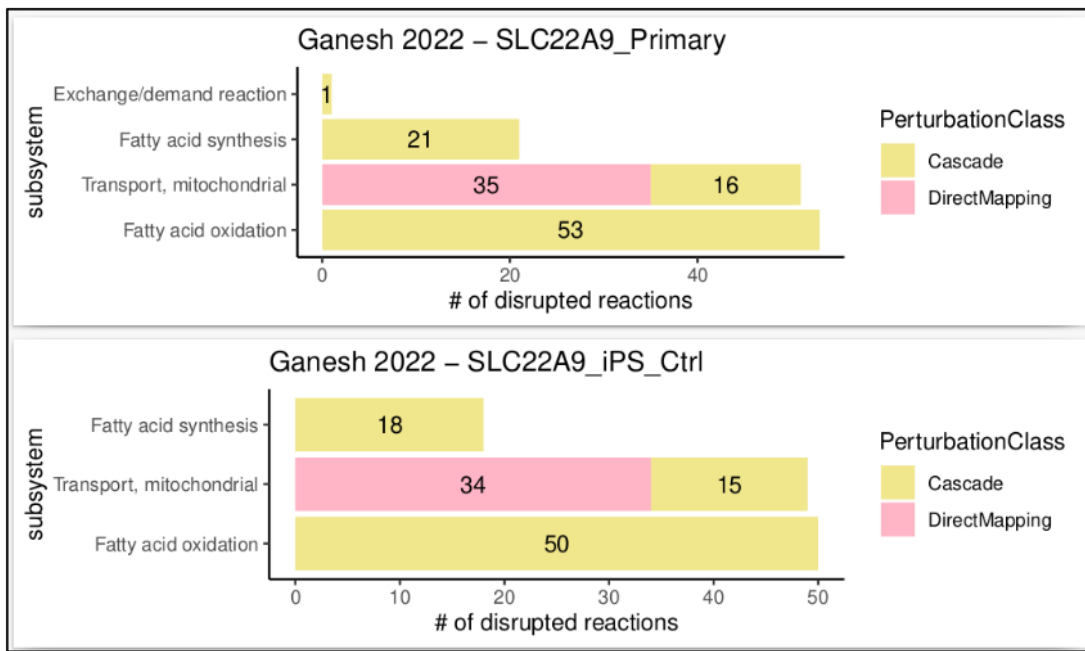


**Figure 6: The LoF of Solute Carrier Family 22 Member 9 (*SLC22A9*).**

The LoF of *SLC22A9*, a gene that directly maps to mitochondrial transport reactions and implicated in SMI<sup>397</sup>, resulted in the disruption of 'Cascade' reactions in both fatty acid synthesis (FAS) and fatty acid oxidation (FAO), in either astrocyte metabolic models (Primary-Ctrl and iPS-Ctrl-a).

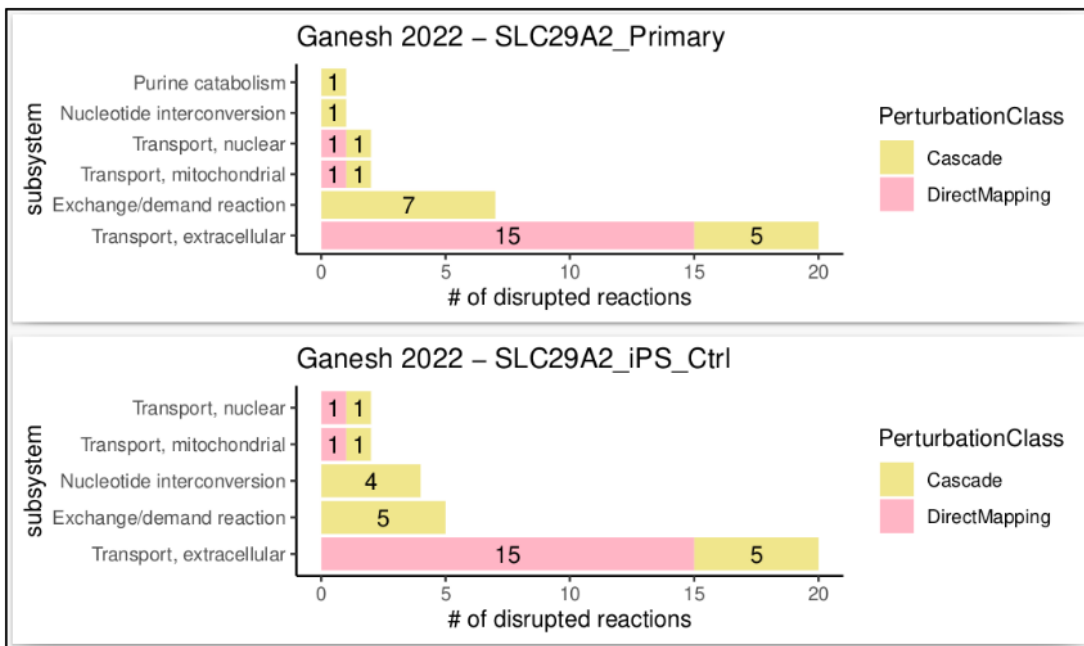


**Figure 7: The LoF of Solute Carrier Family 29 Member 2 (SLC29A2).**

The LoF of *SLC29A2*, a gene that directly maps to nuclear/mitochondrial/extracellular transport reactions and implicated in SMI<sup>397</sup>, resulted in the disruption of 'Cascade' reactions, within Nucleotide interconversion, in either astrocyte metabolic models (Primary-Ctrl and iPS-Ctrl-a). The LoF also resulted in disruption of 'Cascade' reactions, within Purine catabolism, however only in the Primary-Ctrl astrocyte metabolic model, but not in the iPS-Ctrl-a model.

**Table.2:** Metabolic subsystems disrupted upon the LoF of genes (n=16) implicated in SMI, AD, PD:

	Phenotype	Study	Gene Symbol	# of disrupted rxns Primary-Ctrl	disrupted subsystems Primary-Ctrl	# of disrupted rxns iPS-Ctrl-a	disrupted subsystems iPS-Ctrl-a
1.	SMI	Ganesh 2019 <sup>398</sup>	<i>CKMT2</i>	3	Urea cycle	3	Urea cycle
2.	SMI	Ganesh 2019 <sup>398</sup>	<i>INPP5A</i>	9	Inositol phosphate metabolism	6	Inositol phosphate metabolism
3.	SMI	Ganesh 2022 <sup>397</sup>	<i>NMNAT1</i>	6	NAD metabolism Transport, nuclear	7	NAD metabolism Transport, nuclear
4.	SMI	Ganesh 2022 <sup>397</sup>	<i>ASPA</i>	NIL	NIL	NIL	NIL
5.	SMI	Ganesh 2022 <sup>397</sup>	<i>SLC5A8</i>	6	Transport, extracellular	6	Transport, extracellular
6.	SMI	Ganesh 2022 <sup>397</sup>	<i>PLA2G12A</i>	165	Glycerophospholipid metabolism Exchange/demand reaction Transport, extracellular	167	Glycerophospholipid metabolism Exchange/demand reaction Transport, extracellular
7.	SMI	Ganesh 2022 <sup>397</sup>	<i>SLC29A2</i>	33	Transport, extracellular Nucleotide interconversion Transport, mitochondrial Transport, nuclear	33	Transport, extracellular Nucleotide interconversion Transport, mitochondrial Transport, nuclear

					Exchange/demand reaction Purine catabolism		Exchange/demand reaction
8.	SMI	Ganesh 2022 <sup>397</sup>	<i>COASY</i>	7	CoA synthesis CoA catabolism Transport, mitochondrial	7	CoA synthesis CoA catabolism Transport, mitochondrial
9.	SMI	Ganesh 2022 <sup>397</sup>	<i>SYNJ2</i>	5	<sup>41</sup> Inositol phosphate metabolism	<sup>2</sup>	Inositol phosphate metabolism
10.	SMI	Ganesh 2022 <sup>397</sup>	<i>PYGL</i>	5	<sup>41</sup> Starch and sucrose metabolism	2	Starch and sucrose metabolism
11.	SMI	Ganesh 2022 <sup>397</sup>	<i>NEU1</i>	NIL	NIL	NIL	NIL
12.	SMI	Ganesh 2022 <sup>397</sup>	<i>UGT2A1</i>	NIL	NIL	NIL	NIL
13.	SMI	Ganesh 2022 <sup>397</sup>	<i>SLC22A9</i>	126	<sup>39</sup> Fatty acid oxidation Fatty acid synthesis Transport, mitochondrial Exchange/demand reaction	117	<sup>39</sup> Fatty acid oxidation Fatty acid synthesis Transport, mitochondrial
14.	AD	Syama 2018 <sup>399</sup>	<i>PLCB4</i>	4	Inositol phosphate metabolism	4	Inositol phosphate metabolism
15.	PD	Booth 2017 <sup>452</sup>	<i>PLA2G6</i>	164	Glycerophospholipid metabolism Exchange/demand	167	Glycerophospholipid metabolism Exchange/demand

					d reaction Transport, extracellular		nd reaction Transport, extracellular
16.	PD	Booth 2017 <sup>452</sup>	<i>GBA</i>	1	Sphingolipid metabolism	4	Sphingolipid metabolism Transport, lysosomal

#### 5.4. Discussion.

By utilizing the human astrocyte metabolic models that were built as a part of [Section 4](#), an inquiry was made into the existence of metabolic phenotypes in astrocytes that could potentially result from LoF mutations implicated in SMI, AD, and PD. Of the 154 genes implicated in SMI, AD, and PD, only a subset ( $n=16$ ) was found to be captured by the astrocyte metabolic models, of which only two genes, *SLC22A9* and *SLC29A2*, both implicated in SMI<sup>397</sup>, whose LoF resulted in novel disruptions, such as the disruption of FA synthesis and oxidation in the case of *SLC22A9*, and nucleotide interconversion in the case of *SLC29A2*. As mentioned in [Section 4.3.2.2](#), the contribution of FA metabolism towards psychotic disorders is supported by sparse and inconsistent evidence<sup>422</sup>. In the case of nucleotide interconversion, the disrupted fluxes were associated with the pyrimidine salvage. While there is considerable evidence of the involvement of cyclic adenosine monophosphate (cAMP) signaling in BD<sup>453</sup>, and cAMP is synthesized through nucleotide interconversion mechanisms, there is inconsistent evidence of the involvement of pyrimidine/purine analogues in BD or SCZ<sup>454–457</sup>.

It was also observed that the LoF of *INPP5A* and *SYNJ2* (both implicated in SMI), as well as *PLCB4* (implicated in AD), independently resulted in the disruption of inositol phosphate metabolism. It is known that Li<sup>+</sup> enhances cognition in BD patients<sup>143</sup> and, at moderate doses, improves cognitive function and memory performance in AD and mild cognitive impairment (MCI) patients<sup>458</sup>. This effect may be attributed, at least in part, to Li<sup>+</sup>'s ability to downregulate an aberrant level of the inositol trisphosphate (InsP3), in these patients<sup>459,460</sup>. Consequently, it would be interesting to establish a cohort of AD/MCI subjects, including those who did and did not experience cognitive improvement with Li<sup>+</sup>, and conduct genetic and molecular studies, to identify pathways mediating the cognitive outcomes in these patients, but also explore potential overlaps with Li<sup>+</sup> response signatures observed in BD cohorts.

The attrition rate, whereby only 16 out of 154 genes were effectively captured by the models, primarily stems from the fact that less than 20% of the human genome is associated with metabolic reactions. Within this subset of 16 genes, only the LoF of two genes (*SLC22A9* and *SLC29A2*) resulted in novel disruptions. This phenomenon is primarily attributed to the degeneracy in metabolic networks but also the limitations of contemporary GSMMs, which fail to account for other mechanisms such as regulatory constraints and allosteric feedback. These unaccounted factors significantly challenge the capability of GSMMs to capture and explain metabolic phenotypes, solely using mutation information (without 'omic data), in oligogenic disorders like those addressed in this study.

## 6. Summary and future directions.

The role of astrocyte metabolism in psychiatric disorders (BD, SCZ), neurodegeneration (AD), and the response to treatment (Li+) in BD, is poorly understood, despite multiple lines of evidence indicating dysfunction of astrocytes<sup>20-22,61-66,339</sup>. To shed light on potential metabolic mechanisms associated with these phenotypes, we embarked on an unbiased investigation of astrocyte metabolism. Given that directly screening metabolic pathways in astrocytes, whether *in vivo* or *in vitro*, is a substantial undertaking, we opted for an alternative computational approach known as metabolic modeling, which can describe the metabolic state of cells at a steady state without the need for detailed knowledge of enzymatic kinetics<sup>392</sup>.

Metabolic modeling was employed to ask if there are metabolic phenotypes in astrocytes that are i) specific to BD patients who do not respond to Li+ treatment, ii) shared between BD and SCZ patients, and iii) observed as a consequence of LoF mutations implicated in BD, SCZ and AD patients. The key data-substrate for the first two questions were phenotype-specific transcriptomes from iPS-astrocytes derived from BD, SCZ, and control subjects<sup>62,67</sup>, while for the latter question, the data-substrate was solely genetic, specifically the knowledge of LoF mutations identified by WES of patients diagnosed with SMI (BD & SCZ)<sup>397,398</sup> and AD<sup>399</sup>. However, all three inquiries were dependent on the generation of astrocyte metabolic models in the first place. To accomplish this, we combined the human metabolic knowledge base 'Recon3D' with publicly available transcriptome data from astrocytes of BD & SCZ patients, and healthy controls, alongside glial proteomic data from healthy controls. This amalgamation allowed us to derive phenotype-specific metabolic models of human astrocytes. Subsequently, we engaged in meticulous manual curation of relevant literature to identify metabolic functions pertinent to astrocytes. These tasks were then evaluated in all metabolic models while adhering to appropriate nutrient media constraints. Metabolic flux distributions between the healthy and disease models were compared, along with specific filtering criteria, to identify metabolic phenotypes associated with our inquiries.

Our findings indicate a significant distinction between Li+ responders and non-responders based on lipid metabolic phenotypes, with slower flux through inositol, cholesterol, and FAO pathways, specifically in the astrocytes of BD patients who did not respond to Li+. Additionally, we observed that FAO was the sole disrupted pathway in the astrocytes of both BD and SCZ patients. The FAO metabolic phenotype was also associated with the loss of function of *SLC22A9*, a mitochondrial transporter implicated in SMI. Notably, the inositol metabolic phenotype was unique to astrocytes from Li+ non-responders in BD and not observed in SCZ, which might explain the specificity of Li+'s effectiveness in BD compared to SCZ, despite their shared clinical symptoms, genetics, and biology.

There are several avenues for advancing our predictions. Firstly, it's important to note that these are 'predictions' based on computational models, and as a result, we've formulated hypotheses (outlined in [Section 4.4](#)). We have posited that modified metabolism could impact FAO in both BD and SCZ astrocytes, as well as impact LD biogenesis/expansion and PI turnover rates specifically in BD Li+ non-responder astrocytes. All of these hypotheses require experimental validation, and our laboratory<sup>449</sup> is currently in the process of generating iPS-astrocytes from healthy controls, BD patients (both Li+ responders and non-responders), and SCZ patients. Irrespective of which hypothesis is examined (whether it's related to FAO, LDs, inositol, or otherwise), it is imperative to leverage emerging tools for perturbing metabolism<sup>461-463</sup> and examine astrocytic phenotypes, alongside quantifying the absolute metabolite concentrations in iPS-astrocytes through MS.

At a higher level, as discussed in [Section 4.4](#), it becomes crucial to establish a connection between metabolism and genomics. For instance, one could inquire how genomic variations associated with BD/SCZ affect the brain's metabolic landscape and which specific cell-types are implicated. One approach to investigate this would involve utilizing CRISPR-edited mice, targeting the particular genomic loci linked to BD/SCZ, followed by MS imaging (e.g., MALDI-MSI)<sup>464</sup>, to measure metabolite levels *in situ* and examine metabolic heterogeneity within/between brain regions.

Finally, we'd like to reiterate that, all the metabolic models built, along with the accompanying analysis codes, as part of this thesis, are freely accessible for anyone to download at <https://github.com/anin90/AstroModel>. These resources are not restricted to a single use but can be repurposed to explore a multitude of research questions.

## 7. Supplementary: figures, tables, methods.

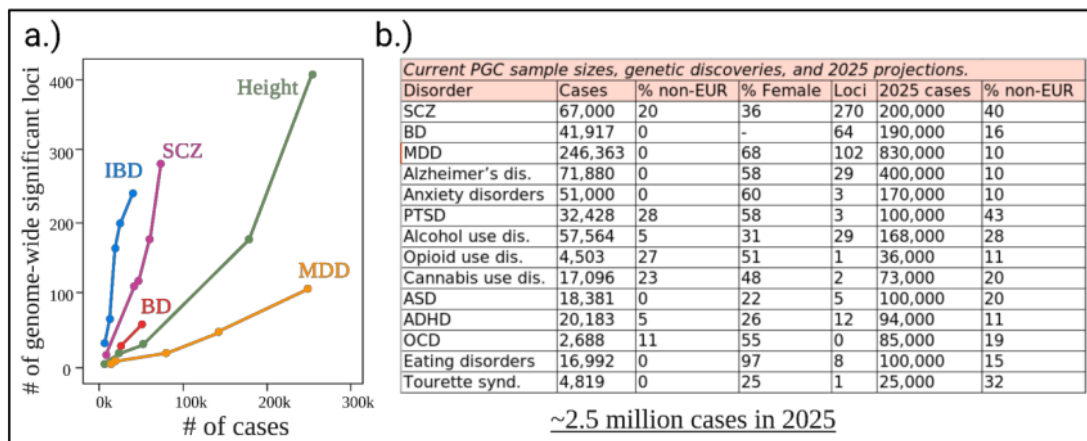


**Figure S1: Psychiatric Genomics Consortium (PGC) - GWAS Discoveries until 2023.**

**a)** Each data point corresponds to a PGC GWAS on conditions including SCZ, BD and MDD, compared to non-psychiatric GWAS such as Inflammatory bowel disease (IBD) and Height. The x-axis displays the number of cases included in the study, while the y-axis indicates the number of GWAS loci identified in that study. **b.)** The table presents current PGC sample sizes, discovered loci, the proportion of non-European samples, proportion of female samples, and projections for 2025 for 14 psychiatric phenotypes. The projections anticipate an increase in the number of cases up to 2.5 million samples.

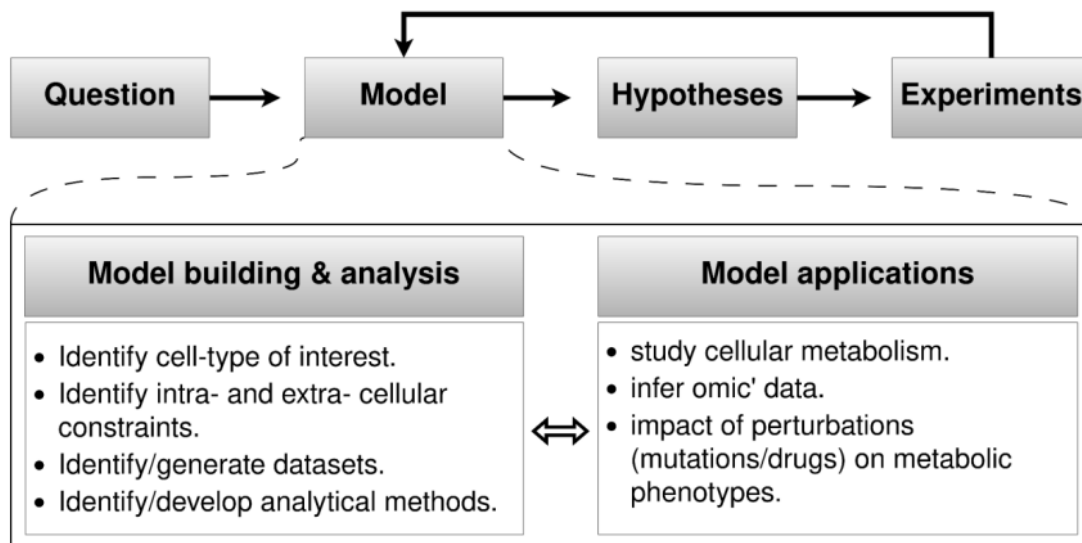


**Figure.S2: Computational modeling to understand cellular metabolism.**

Computational modeling, employed as a tool in scientific research, enables complex systems to be simulated and understood, resulting in the generation of hypotheses that can be tested through real-world experiments. Experimental data validate or refute the predictions generated by these models. This cyclical process of computational modeling and experimental validation fosters an ongoing refinement of hypotheses and models based on observed outcomes. Similar to other scientific inquiries, computational modeling initiates with the formulation of questions or specific applications in mind. The subsequent model building/analysis aligns with the chosen focus. Within the context of my PhD research, questions ranged from investigating the metabolic dependency of Li<sup>+</sup> response in BD, to exploring whether metabolic phenotypes cross-cut related clinical phenotypes like BD and SCZ. Considering the challenges of directly addressing these questions through experiments and capitalizing on public data, my approach involved repurposing publicly accessible 'omic data related to astrocytes, curating biochemical literature to determine the astrocytic constraints, and employing suitable analytical methods, which facilitated the building of computational models of astrocyte metabolism to address these questions comprehensively.

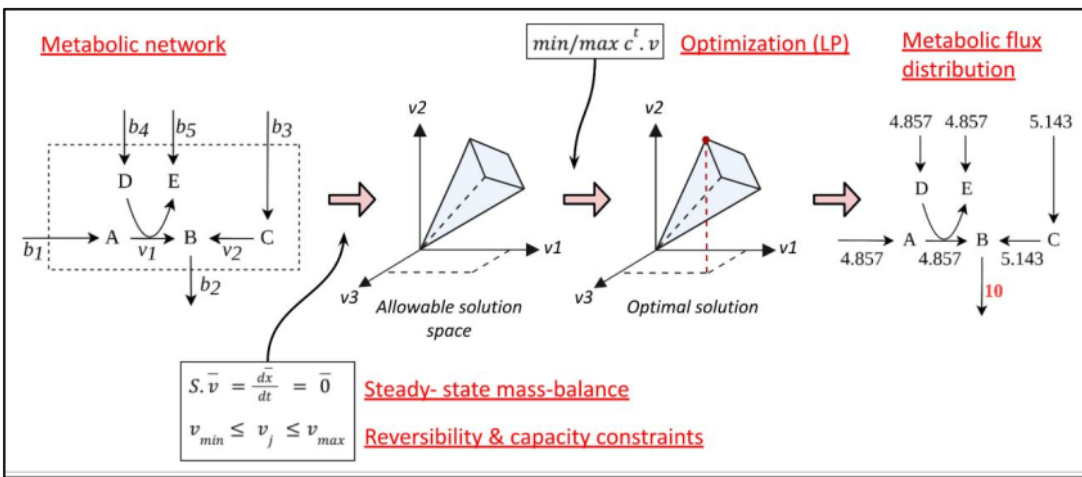
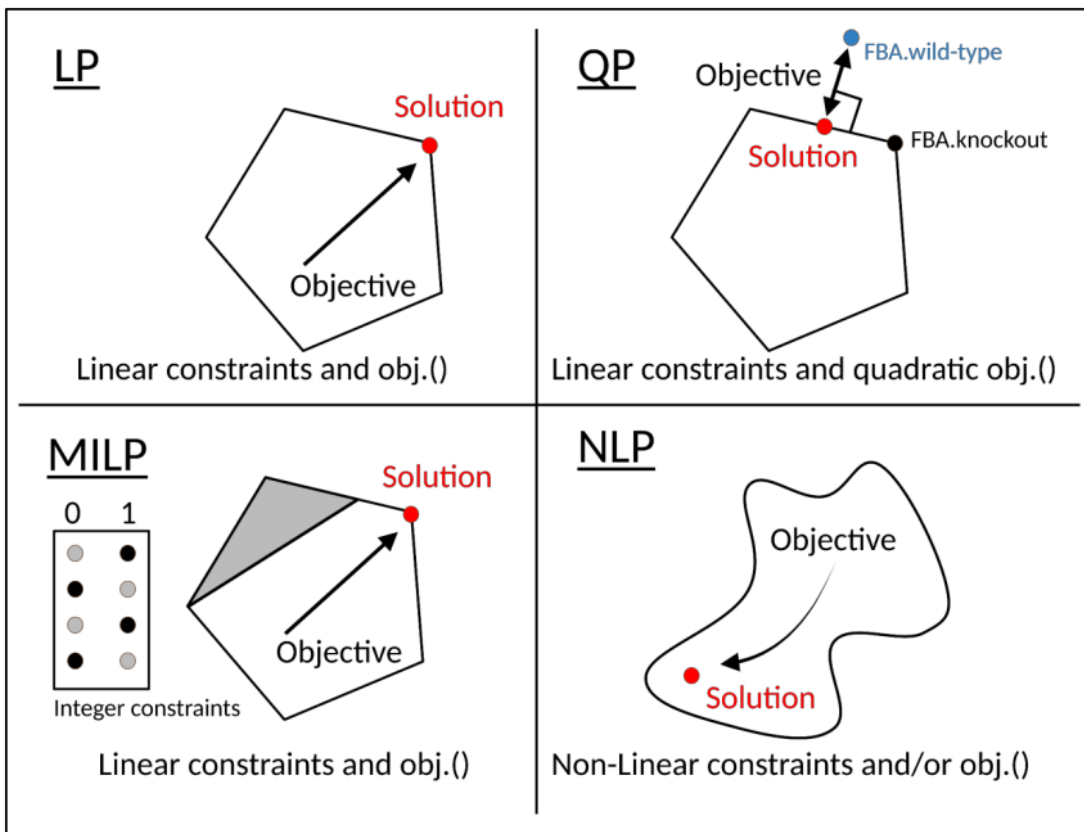


Figure.S3: F<sub>67</sub>x balance analysis (FBA).

Metabolite flow in a metabolic network is examined using flux balance analysis (FBA), involving the stoichiometric matrix containing metabolite coefficients reflecting production and consumption. Assuming steady-state, incoming flux equals outgoing flux, preventing metabolite accumulation. This balance is represented as a dot product between the stoichiometric matrix [S] and the flux vector [v], yielding linear equations. Solving these underdetermined linear equations, where variables exceed equations, results in infinite solutions. Optimization solves this problem by maximizing for an objective function, say metabolite 'B' production or its flux 'b2', subject to constraints including the steady-state mass-balance ( $S.v=0$ ) and further reaction inequalities. The outcome is a theoretically feasible flux distribution, revealing the rates of each reaction within the metabolic network. Notably, the flux distribution in FBA is often not unique, yet the objective value remains consistent. In other words, multiple alternative optimal solutions with the same objective value can coexist within the system. This concept can be likened to a system or cell adopting various functional states while optimizing toward a specific objective. Figure adapted from Raman/Chandra (2009)<sup>465</sup> and Orth/Thiele/Palsson (2010)<sup>380</sup>.



**Figure S4: Major classes of optimization methods.**

The selection of optimization algorithms hinges on the defined objective and constraints. FBA optimizes a linear combination of fluxes using linear programming (LP) algorithms, useful in predicting minimum and maximum flux through reactions. However, FBA predictions may not always align with experimental growth rates or flux values, particularly <sup>59</sup> knockout phenotypes. To address this, the quadratic programming (QP)-based minimization of metabolic adjustment (MOMA) algorithm minimizes the Euclidean distance between knockout and *wt* FBA solutions. QP is chosen due to the quadratic objective. Regulatory on/off minimization (ROOM) shares the concept of MOMA but uses <sup>73</sup> mixed-integer linear programming (MILP). Non-linear programming (NLP) algorithms with nonlinear constraints and objectives also exist. Notably, optimal solutions for LP, QP, and MILP methods lie within the solution space's corners or periphery, whereas NLP may encounter local minima. The convex solution space ensures optimal solutions for LP, QP, and MILP, while NLP might not guarantee solutions due to local minima challenges. Figure adapted from B.O. Palsson's COBRA textbook (2015), Chapter-18<sup>378</sup>.

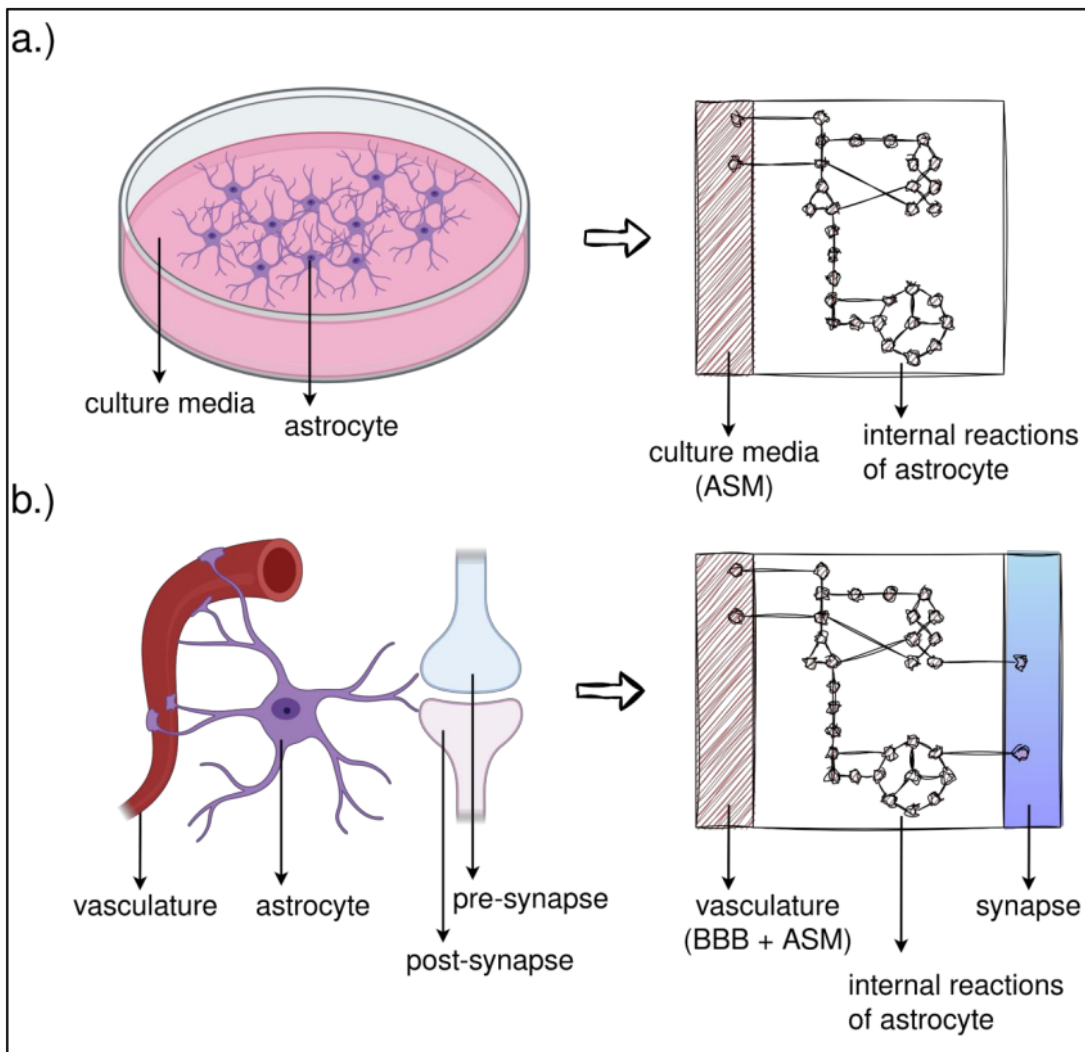


**Figure S5: Conceptualization of astrocyte metabolic models.**

**a.)** In the context of a metabolic model, astrocytes in culture can be envisioned as having an internal reaction space fueled by nutrients from the culture media. The nutrient medium for all iPS-astrocyte models comprises the metabolites and ions constituting the astrocyte sustenance medium (ASM). **b.)** In the context of *in vivo* astrocytes, a crucial assumption was made that culture media components also exist in systemic circulation, traverse the blood-brain barrier (BBB), and are accessible for astrocyte uptake. Consequently, the extracellular compartments of Primary-astrocyte models were constrained by metabolites and ions from both ASM and BBB. An additional synapse compartment is introduced to capture astrocyte-synapse metabolic interactions. This logic informs all Primary-astrocyte models. Further details are available in methodology sections [4.2.4.2](#) and [4.2.4.3](#).

**7.1. Protocol: Filtering reactions relevant to phenotype-of-interest (BD, BD-Responder, BD-NonResponder, SCZ-Twin): expansion of [methodology section 4.2.5.3.](#)**

**7.1.1. Prerequisites: generate FVA and MTA results.**

- i. FVA results - ratio of flux span (FSr) between,
  - o iPS-Ctrl-a and iPS-BD/iPS-BD-R/iPS-BD-NR models. Retain reactions with FSr>1.5 and FSr<0.8. [Script in github.](#)
  - o iPS-Ctrl-b and iPS-ST models. Retain reactions with FSr>1.5 and FSr<0.8. [Script in github.](#)
  - o iPS-Ctrl-a and Primary-Ctrl models. Retain reactions with FSr values between 1.5 and 0.8. [Script in github.](#)
  - o iPS-Ctrl-b and iPS-HT models. Retain reactions with FSr values between 1.5 and 0.8. [Script in github.](#)
  - o iPS-Ctrl-b and Primary-Ctrl models. Retain reactions with FSr values between 1.5 and 0.8. [Script in github.](#)
- ii. MTA results - transformation scores between,
  - o iPS-Ctrl-a  $\rightleftharpoons$  iPS-BD/iPS-BD-R/iPS-BD-NR/Primary-Ctrl models. [Script in github.](#)
  - o iPS-Ctrl-b  $\rightleftharpoons$  iPS-ST/iPS-HT/Primary-Ctrl models. [Script in github.](#)

Prepare the above (i, ii) for models generated using 'abs', 'norm\_t1', and 'norm\_t2' expression thresholds, separately.

### 7.1.2. Filtering reactions: Using FVA Results:

**7.1.2.1. BD, BD-Responder and BD-NonResponder:** This protocol is prepared for replicating [Fig.S6](#), exemplified by analyzing the FVA results from 'abs' models. Similar logic must be extended for 'norm\_t1' ([Fig.S7](#)) and 'norm\_t2' models ([Fig.S8](#)).

- i. Start with four sets:
  - o Reactions with altered rates: iPS-Ctrl-a vs iPS-BD (mentioned as "Ctrl\_vs\_BD" in [Fig.S6](#)).
  - o Reactions with altered rates: iPS-Ctrl-a vs iPS-BD-R (mentioned as "Ctrl\_vs\_BD\_R" in [Fig.S6](#)).
  - o Reactions with altered rates: iPS-Ctrl-a vs iPS-BD-NR (mentioned as "Ctrl\_vs\_BD\_NR" in [Fig.S6](#)).
  - o Reactions with consistent rates: iPS-Ctrl-a vs Primary-Ctrl (mentioned as "Ctrl\_vs\_Primary\_Uncanged" in [Fig.S6](#)).
- ii. Visualize overlap between four sets using R's `upset()` function.
- iii. Apply filtering criteria from [Table.1](#):
  - o Slice relevant subsets (reactions).
  - o In [Fig.S6](#), BD relevant subsets are mentioned in blue, BD-R subsets in green, and BD-NR subsets in red. The union set was considered if multiple subsets per phenotype were found.
- iv. Obtain one reaction set for each phenotype (BD/BD-R/BD-NR). Sets may overlap; refer to [Table.1](#) for overlap criteria.
- v. Perform [Metabolic subSystem Enrichment Analysis \(MSEA\)](#) on the filtered subset of reactions for each of the three phenotypes (BD/BD-R/BD-NR).

Perform step i-iv using this [script in github](#) which also generates [Fig.S6](#), and step v using this [script in github](#). These processes should be iterated for FVA outcomes obtained from 'norm\_t1' and 'norm\_t2' models as well. Modify the script's filename suffix from '\_abs' to '\_norm\_t1' and '\_norm\_t2' to generate results corresponding to the respective conditions.

**7.1.2.2. SCZ-Twin:** This protocol is prepared for replicating [Fig.S9](#), exemplified by analyzing the FVA results from 'abs' models. Similar logic must be extended for 'norm\_t1' ([Fig.S10](#)) and 'norm\_t2' models ([Fig.S11](#)).

- i. Start with three sets:
  - o Reactions with altered rates: iPS-Ctrl-b vs iPS-ST (mentioned as "Ctrl\_vs\_ST" in [Fig.S9](#)).
  - o Reactions with consistent rates: iPS-Ctrl-b vs iPS-HT (mentioned as "Ctrl\_vs\_HT\_Uncchanged" in [Fig.S9](#)).
  - o Reactions with consistent rates: iPS-Ctrl-b vs Primary-Ctrl (mentioned as "Ctrl\_vs\_Primary\_Uncchanged" in [Fig.S9](#)).
- ii. Visualize overlap between three sets using R's upset() function.
- iii. Apply filtering criteria from [Table.1](#):
  - o Slice relevant subsets (i.e., reactions).
  - o In [Fig.S9](#), ST relevant subsets are mentioned in red. The union set was considered if multiple subsets per phenotype were found.
- iv. Obtain one reaction set for the phenotype (ST). Sets may overlap with BD/BD-R/BD-NR; refer to [Table.1](#) for overlap criteria.
- v. Perform [Metabolic subSystem Enrichment Analysis \(MSEA\)](#) on the filtered subset of reactions for the phenotypes (ST).

Perform step i-iv using this [script in github](#) which also generates [Fig.S9](#), and step v using this [script in github](#). These processes should be iterated for FVA outcomes obtained from 'norm\_t1' and 'norm\_t2' models as well. Modify the script's filename suffix from '\_abs' to '\_norm\_t1' and '\_norm\_t2' to generate results corresponding to the respective conditions.

### 7.1.3. Filtering reactions: Using MTA Results:

**7.1.3.1. BD, BD-Responder and BD-NonResponder:** This protocol is prepared for replicating [Fig.S12](#), exemplified by analyzing the MTA results from 'abs' models. Similar logic must be extended for 'norm\_t1' ([Fig.S13](#)) and 'norm\_t2' models ([Fig.S14](#)).

- i. Start with eight sets i.e., the MTA scores for,
  - o  $iPS\text{-}Ctrl\text{-}a \rightleftharpoons iPS\text{-}BD$ . (one set for either direction).
  - o  $iPS\text{-}Ctrl\text{-}a \rightleftharpoons iPS\text{-}BD\text{-}R$ . (one set for either direction).
  - o  $iPS\text{-}Ctrl\text{-}a \rightleftharpoons iPS\text{-}BD\text{-}NR$ . (one set for either direction).
  - o  $iPS\text{-}Ctrl\text{-}a \rightleftharpoons Primary\text{-}Ctrl$ . (one set for either direction).
- ii. Identify reactions with top 20% MTA scores i.e., reactions that facilitate metabolic state transformations for " $iPS\text{-}Ctrl\text{-}a \rightleftharpoons iPS\text{-}BD/iPS\text{-}BD\text{-}R/iPS\text{-}BD\text{-}NR$ ".  
 o For instance, to pinpoint the top 20% of MTA reactions relevant to BD phenotype, run MTA between the  $iPS\text{-}Ctrl\text{-}a$  and  $iPS\text{-}BD$  models. This entails identifying the top 20% of reactions whose knockout transforms  $Ctrl \rightarrow BD$ , as well as the top 20% that transforms  $BD \rightarrow Ctrl$ . Subsequently, take the **union set of the top 20% reactions** from both runs.
- iii. Identify reactions with bottom 80% MTA scores i.e., reactions that do not facilitate metabolic state transformations for  $iPS\text{-}Ctrl\text{-}a \rightleftharpoons Primary\text{-}Ctrl$  models.  
 o Similar to the procedure in (ii), except in this case, focus on the **intersection of the bottom 80% reactions** from both runs, namely  $Ctrl \rightarrow Primary$  and  $Primary \rightarrow Ctrl$ .

The above steps (ii, iii) generates four reaction sets for,

- BD (mentioned as "BD\_top" in [Fig.S12](#)).
- BD-R (mentioned as "BD\_R\_top" in [Fig.S12](#)).
- BD-NR (mentioned as "BD\_NR\_top" in [Fig.S12](#)).
- Ctrl (mentioned as "Ctrl\_unchanged" in [Fig.S12](#)).

- iv. Visualize overlap between the four sets using R's `upset()` function.
- v. Apply filtering criteria from [Table.1](#):
  - o Slice relevant subsets (reactions).
  - o In [Fig.S12](#), BD relevant subsets are mentioned in blue, BD-R subsets in green, and BD-NR subsets in red. The union set was considered if multiple subsets per phenotype were found.

- vi. Obtain one reaction set for each phenotype (BD/BD-R/BD-NR). Sets may overlap; refer to [Table.1](#) for overlap criteria.
- vii. Perform [Metabolic subSystem Enrichment Analysis \(MSEA\)](#) on the filtered subset of reactions for each of the three phenotypes (BD/BD-R/BD-NR).

Perform step i-vii using this [script in github](#) which also generates [Fig.S12](#). These processes should be iterated for MTA outcomes obtained from 'norm\_t1' and 'norm\_t2' models as well. Modify the script's filename suffix from '\_abs' to '\_norm\_t1' and '\_norm\_t2' to generate results corresponding to the respective conditions.

**7.1.3.2. SCZ-Twin:** This protocol is prepared for replicating [Fig.S15](#), exemplified by analyzing the MTA results from 'abs' models. Similar logic must be extended for 'norm\_t1' ([Fig.S16](#)) and 'norm\_t2' models ([Fig.S17](#)).

- i. Start with six sets i.e., the MTA scores for,
  - o  $iPS\text{-}Ctrl\text{-}b \rightleftharpoons iPS\text{-}ST$ . (one set for either direction).
  - o  $iPS\text{-}Ctrl\text{-}b \rightleftharpoons iPS\text{-}HT$ . (one set for either direction).
  - o  $iPS\text{-}Ctrl\text{-}b \rightleftharpoons Primary\text{-}Ctrl$ . (one set for either direction).
- ii. Identify reactions with top 20% MTA scores i.e., reactions that facilitate metabolic state transformations for " $iPS\text{-}Ctrl\text{-}b \rightleftharpoons iPS\text{-}ST$ ".
  - o For instance, to pinpoint the top 20% of MTA reactions relevant to ST phenotype, run MTA between the  $iPS\text{-}Ctrl\text{-}b$  and  $iPS\text{-}ST$  models. This entails identifying the top 20% of reactions whose knockout transforms  $Ctrl \rightarrow ST$ , as well as the top 20% that transforms  $ST \rightarrow Ctrl$ . Subsequently, take the **union set of the top 20% reactions** from both runs.
- iii. Identify reactions with bottom 80% MTA scores i.e., reactions that do not facilitate metabolic state transformations for " $iPS\text{-}Ctrl\text{-}a \rightleftharpoons iPS\text{-}HT/Primary\text{-}Ctrl$ ".
  - o Similar to the procedure in (ii), except in this case, focus on the **intersection of the bottom 80% reactions** from all four runs, namely  $Ctrl \rightarrow HT$ ,  $HT \rightarrow Ctrl$ ,  $Ctrl \rightarrow Primary$  and  $Primary \rightarrow Ctrl$ .

The above steps (ii, iii) generates two reaction sets for,

- ST (mentioned as "ST\_top" in [Fig.S15](#)).
- Ctrl (mentioned as "Ctrl\_unchanged" in [Fig.S15](#)).

- iv. Visualize overlap between two sets using R's `upset()` function.
- v. Apply filtering criteria from [Table.1](#):
  - o Slice relevant subsets (reactions).
  - o In [Fig.S15](#), ST relevant subsets are mentioned in red. The union set was considered if multiple subsets per phenotype were found.
- vi. Obtain one reaction set for the phenotype (ST). Sets may overlap with BD/BDR/BD-NR; refer to [Table.1](#) for overlap criteria.
- vii. Perform [Metabolic subSystem Enrichment Analysis \(MSEA\)](#) on the filtered subset of reactions for the phenotypes (ST).

Perform step i-vii using this [script in github](#) which also generates [Fig.S15](#). These processes should be iterated for MTA outcomes obtained from 'norm\_t1' and 'norm\_t2' models as well. Modify the script's filename suffix from '\_abs' to '\_norm\_t1' and '\_norm\_t2' to generate results corresponding to the respective conditions.

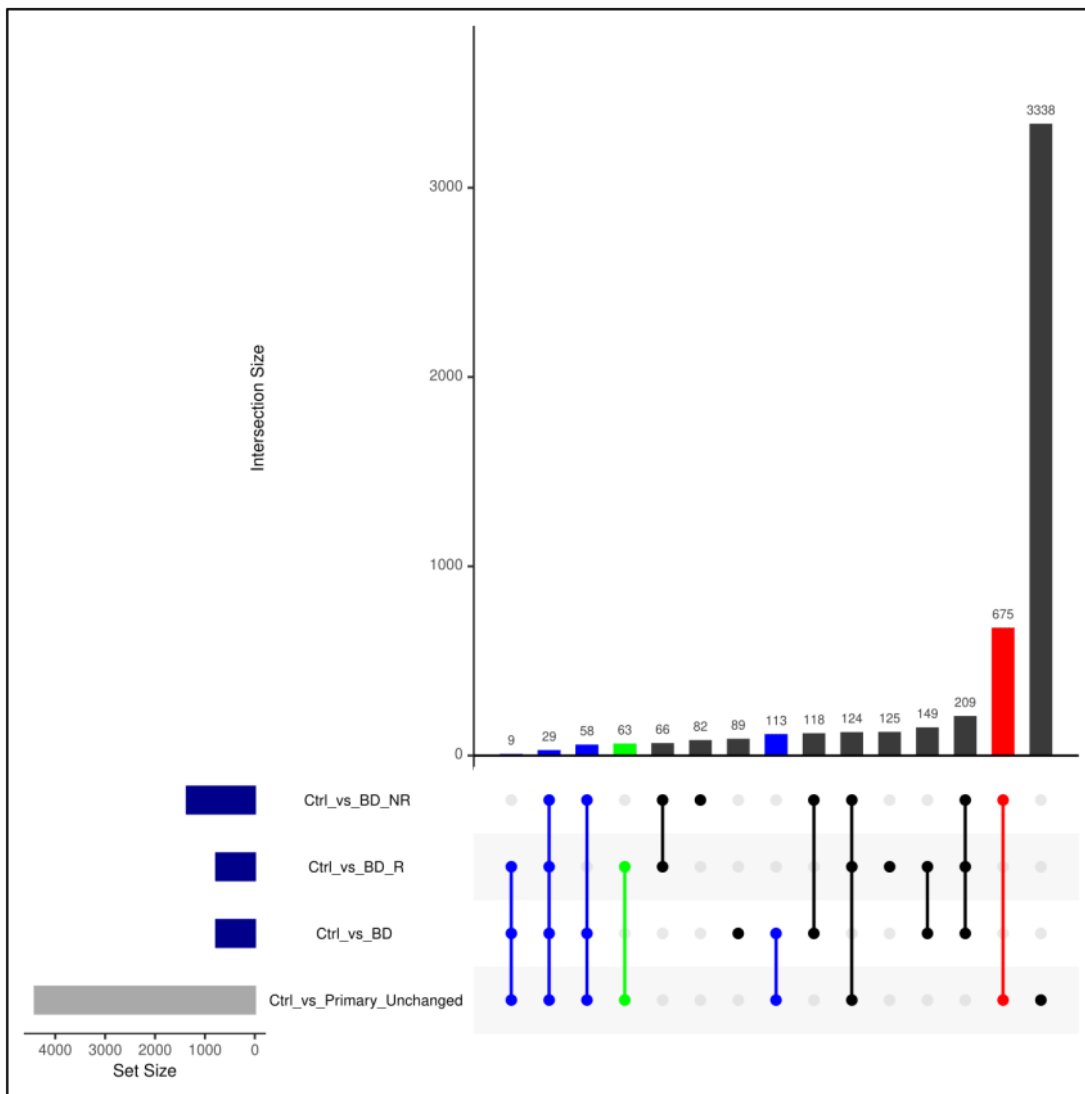


**Figure.S6: Identifying 'BD', 'BD-Responder' and 'BD-NonResponder' relevant reactions by FVA analysis of BD astrocyte (abs) metabolic models.**

UpSet plot depicting the intersections among four reaction sets derived from FVA analysis of BD astrocyte (abs) metabolic models. The reaction sets include 'Ctrl\_vs\_BD' (altered rates between iPS-Ctrl-a and iPS-BD), 'Ctrl\_vs\_BD\_R' (altered rates between iPS-Ctrl-a and iPS-BD-R), 'Ctrl\_vs\_BD\_NR' (altered rates between iPS-Ctrl-a and iPS-BD-NR), and 'Ctrl\_vs\_Primary\_Unc changed' (consistent rates between iPS-Ctrl-a and Primary-Ctrl). Colored intersections represent shortlisted and sliced reactions based on [Table.1](#) criteria. Blue, green, and red intersections denote BD, BD-Responder, and BD-NonResponder subset(s), respectively. For detailed information, refer to [Supplementary Section 7.1](#).

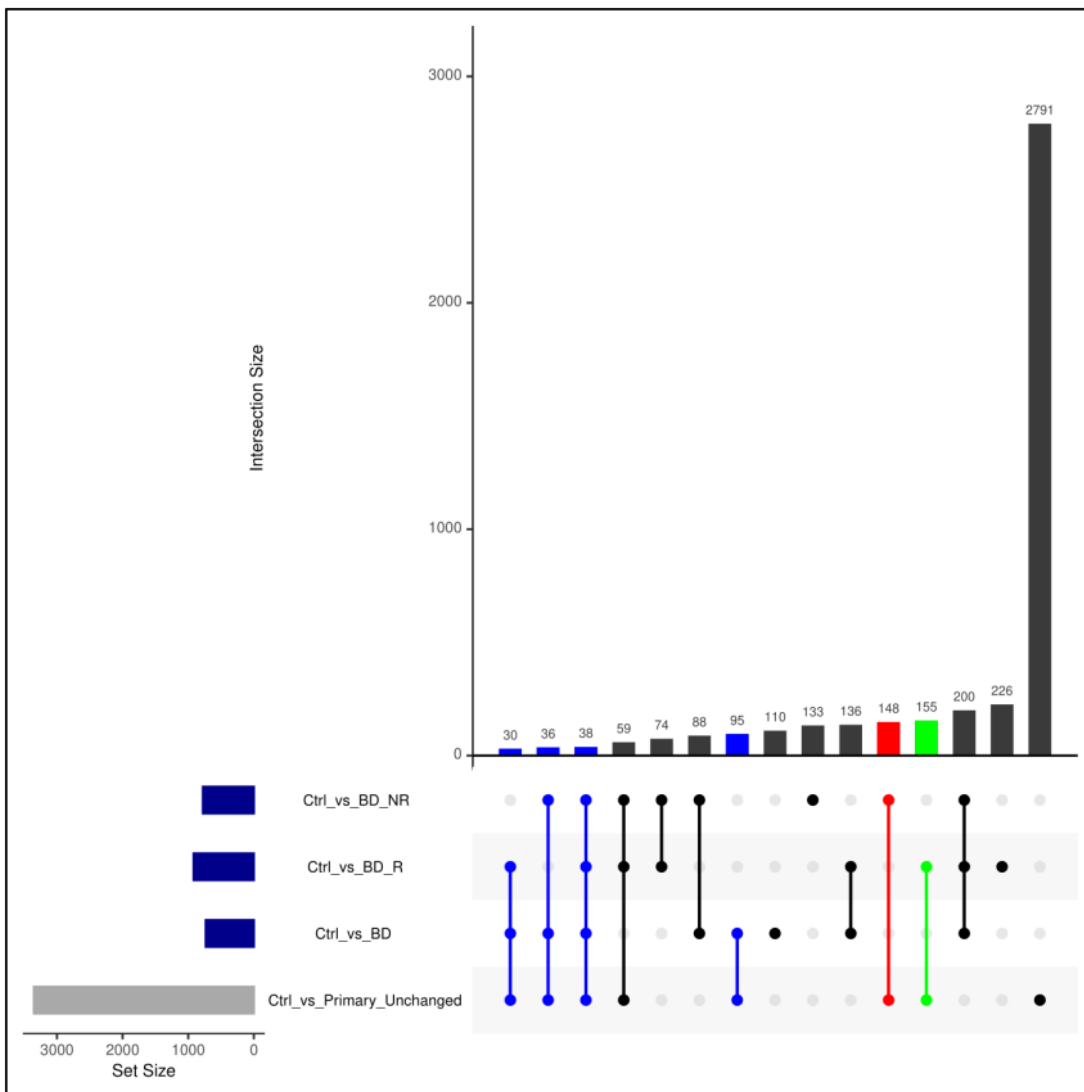


**Figure.S7: Identifying 'BD', 'BD-Responder' and 'BD-NonResponder' relevant reactions by FVA analysis of BD astrocyte (norm-t1) metabolic models.**

UpSet plot depicting the intersections among four reaction sets derived from FVA analysis of BD astrocyte (norm-t1) metabolic models. The reaction sets include 'Ctrl\_vs\_BD' (altered rates between iPS-Ctrl-a and iPS-BD), 'Ctrl\_vs\_BD\_R' (altered rates between iPS-Ctrl-a and iPS-BD-R), 'Ctrl\_vs\_BD\_NR' (altered rates between iPS-Ctrl-a and iPS-BD-NR), and 'Ctrl\_vs\_Primary\_Unc changed' (consistent rates between iPS-Ctrl-a and Primary-Ctrl). Colored intersections represent shortlisted and sliced reactions based on [Table.1](#) criteria. Blue, green, and red intersections denote BD, BD-Responder, and BD-NonResponder subset(s), respectively. For detailed information, refer to [Supplementary Section 7.1](#).

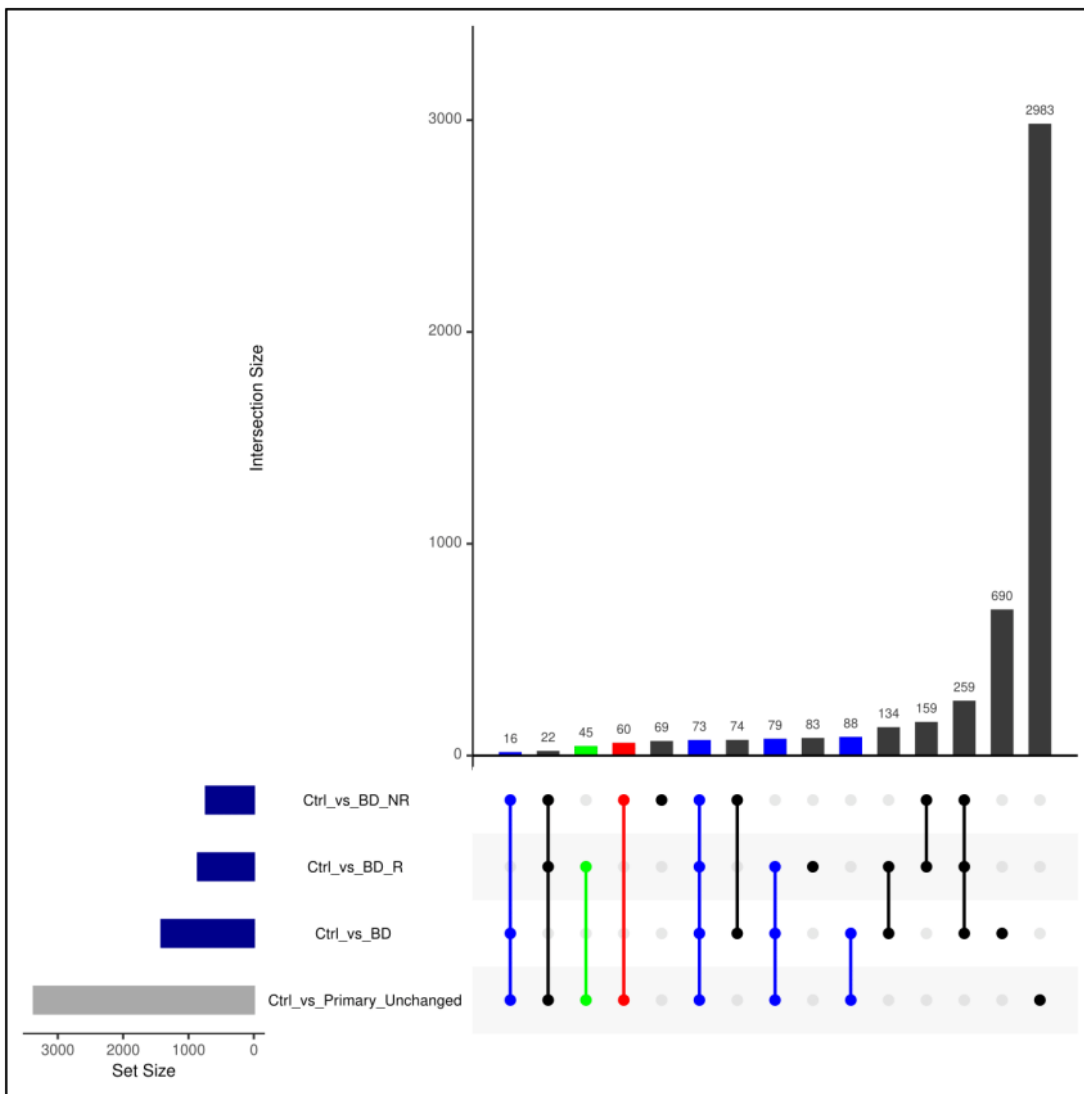


**Figure.S8: Identifying 'BD', 'BD-Responder' and 'BD-NonResponder' relevant reactions by FVA analysis of BD astrocyte (norm-t2) metabolic models.**

UpSet plot depicting the intersections among four reaction sets derived from FVA analysis of BD astrocyte (norm-t2) metabolic models. The reaction sets include 'Ctrl\_vs\_BD' (altered rates between iPS-Ctrl-a and iPS-BD), 'Ctrl\_vs\_BD\_R' (altered rates between iPS-Ctrl-a and iPS-BD-R), 'Ctrl\_vs\_BD\_NR' (altered rates between iPS-Ctrl-a and iPS-BD-NR), and 'Ctrl\_vs\_Primary\_Uncanged' (consistent rates between iPS-Ctrl-a and Primary-Ctrl). Colored intersections represent shortlisted and sliced reactions based on [Table.1](#) criteria. Blue, green, and red intersections denote BD, BD-Responder, and BD-NonResponder subset(s), respectively. For detailed information, refer to [Supplementary Section 7.1](#).

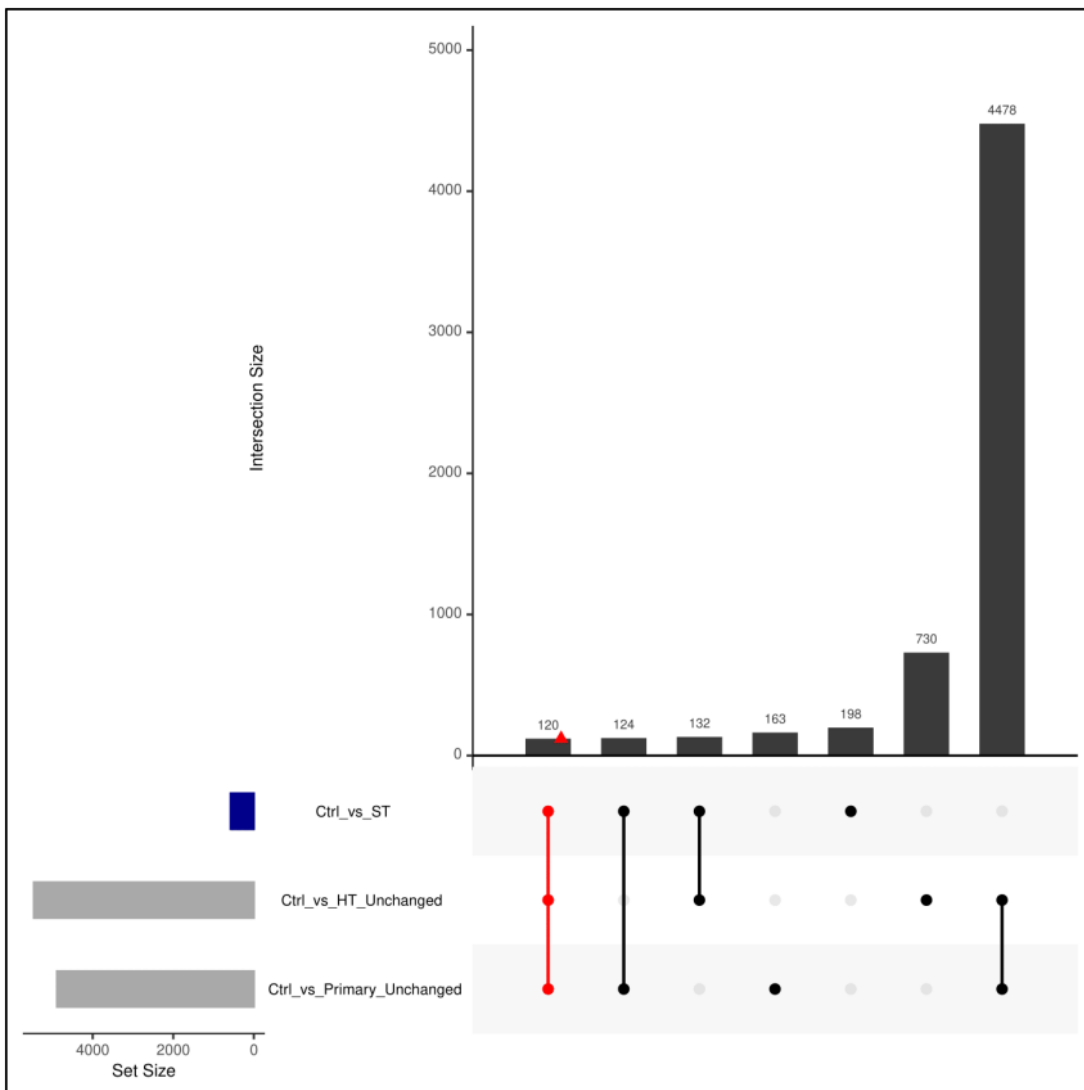


**Figure.S9: Identifying 'SCZ-Twin' relevant reactions by FVA analysis of SCZ astrocyte (abs) metabolic models.**

UpSet plot depicting the intersections among three reaction sets derived from FVA analysis of SCZ astrocyte (abs) metabolic models. The reaction sets include 'Ctrl\_vs\_ST' (altered rates between iPS-Ctrl-b and iPS-ST), 'Ctrl\_vs\_HT\_Uncanged' (consistent rates between iPS-Ctrl-b and iPS-HT), and 'Ctrl\_vs\_Primary\_Uncanged' (consistent rates between iPS-Ctrl-b and Primary-Ctrl). Colored intersections represent shortlisted and sliced reactions based on [Table.1](#) criteria. Red intersections denote SCZ-Twin subset(s). For detailed information, refer to [Supplementary Section 7.1](#).

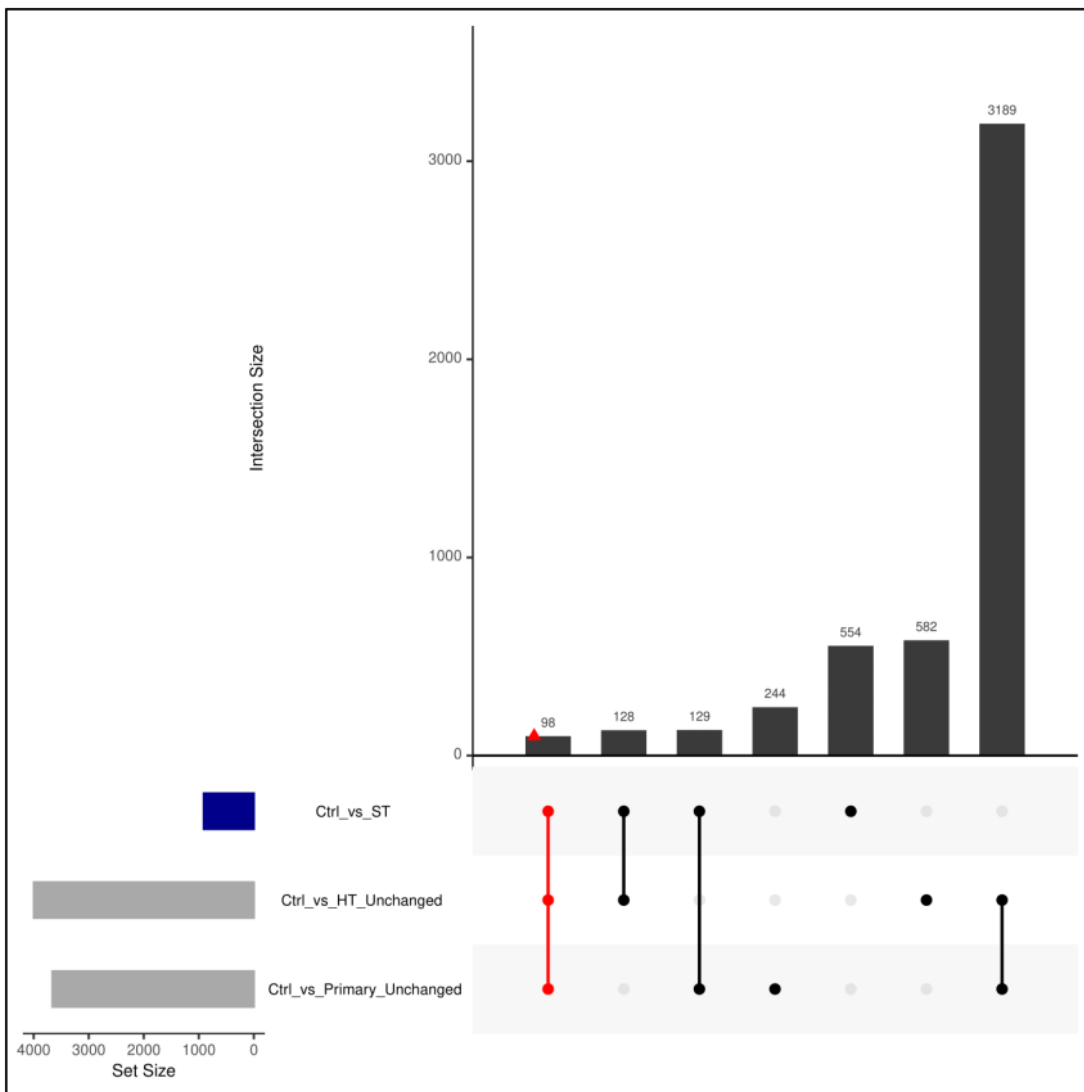


**Figure.S10: Identifying 'SCZ-Twin' relevant reactions by FVA analysis of SCZ astrocyte (norm-t1) metabolic models.**

UpSet plot depicting the intersections among three reaction sets derived from FVA analysis of SCZ astrocyte (norm-t1) metabolic models. The reaction sets include 'Ctrl\_vs\_ST' (altered rates between iPS-Ctrl-b and iPS-ST), 'Ctrl\_vs\_HT\_Uncanged' (consistent rates between iPS-Ctrl-b and iPS-HT), and 'Ctrl\_vs\_Primary\_Uncanged' (consistent rates between iPS-Ctrl-b and Primary-Ctrl). Colored intersections represent shortlisted and sliced reactions based on [Table.1](#) criteria. Red intersections denote SCZ-Twin subset(s). For detailed information, refer to [Supplementary Section 7.1](#).

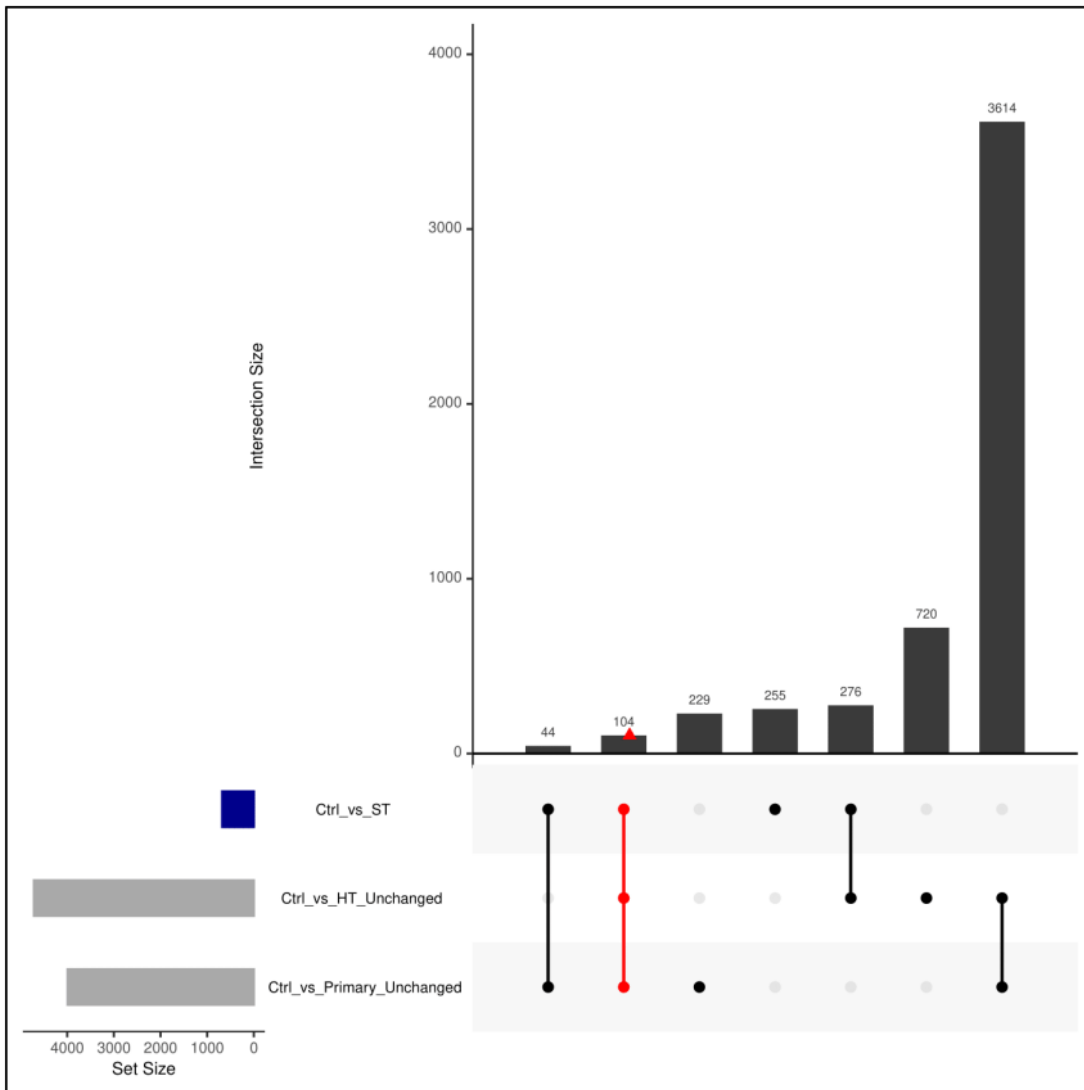


**Figure.S11: Identifying 'SCZ-Twin' relevant reactions by FVA analysis of SCZ astrocyte (norm-t2) metabolic models.**

UpSet plot depicting the intersections among three reaction sets derived from FVA analysis of SCZ astrocyte (norm-t2) metabolic models. The reaction sets include 'Ctrl\_vs\_ST' (altered rates between iPS-Ctrl-b and iPS-ST), 'Ctrl\_vs\_HT\_Uncanged' (consistent rates between iPS-Ctrl-b and iPS-HT), and 'Ctrl\_vs\_Primary\_Uncanged' (consistent rates between iPS-Ctrl-b and Primary-Ctrl). Colored intersections represent shortlisted and sliced reactions based on [Table.1](#) criteria. Red intersections denote SCZ-Twin subset(s). For detailed information, refer to [Supplementary Section 7.1](#).

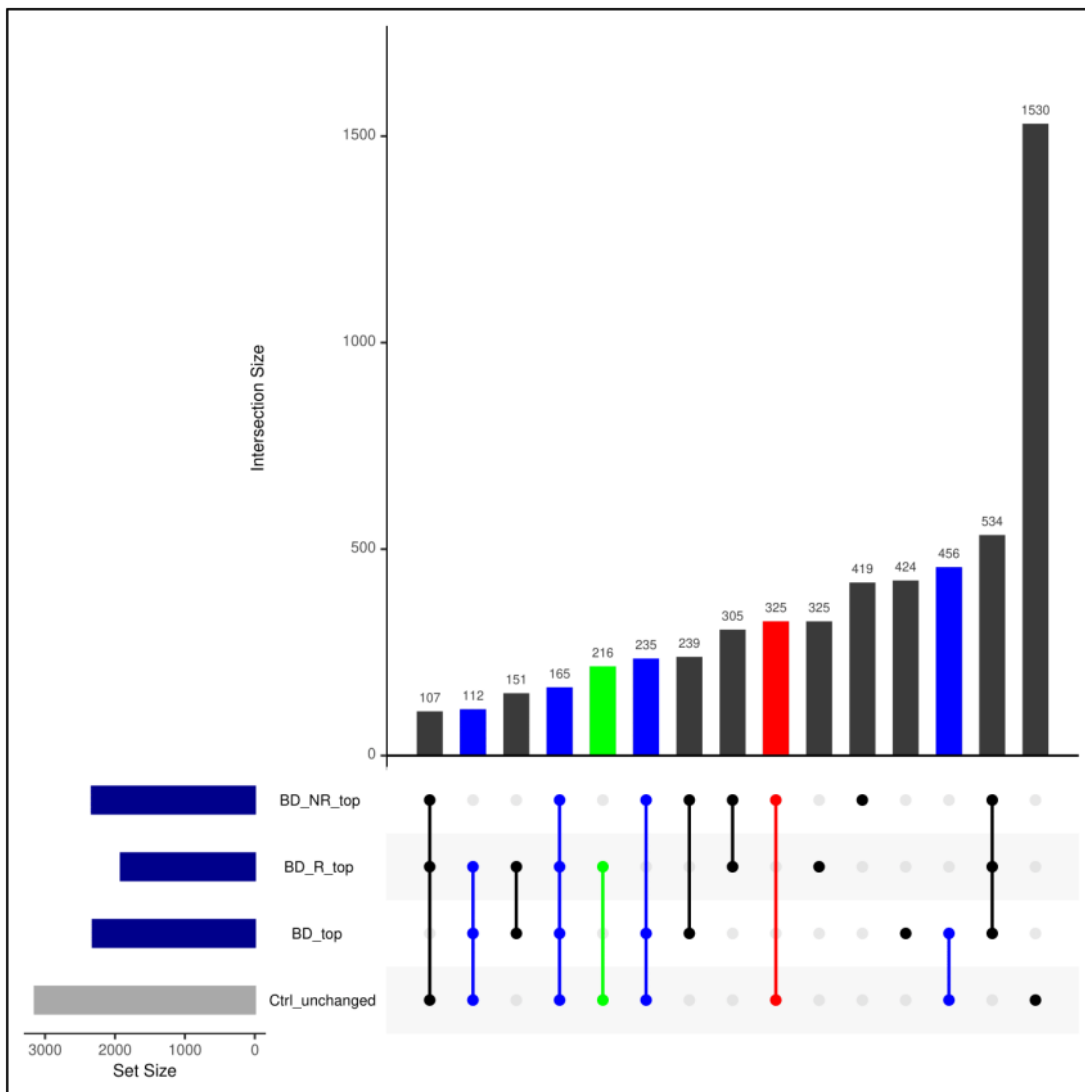


**Figure.S12: Identifying 'BD', 'BD-Responder' and 'BD-NonResponder' relevant reactions by MTA analysis of BD astrocyte (abs) metabolic models.**

UpSet plot depicting the intersections among four reaction sets derived from MTA analysis of BD astrocyte (abs) metabolic models. The reaction sets include 'BD\_top' (transforms iPS-Ctrl-a $\rightleftharpoons$ iPS-BD), 'BD\_R\_top' (transforms iPS-Ctrl-a $\rightleftharpoons$ iPS-BD-R), 'BD\_NR\_top' (transforms iPS-Ctrl-a $\rightleftharpoons$ iPS-BD-NR), and 'Ctrl\_unchanged' (does not transform iPS-Ctrl-a $\rightleftharpoons$ Primary-Ctrl). Colored intersections represent shortlisted and sliced reactions based on [Table.1](#) criteria. Blue, green, and red intersections denote BD, BD-Responder, and BD-NonResponder subset(s), respectively. For detailed information, refer to [Supplementary Section 7.1](#).

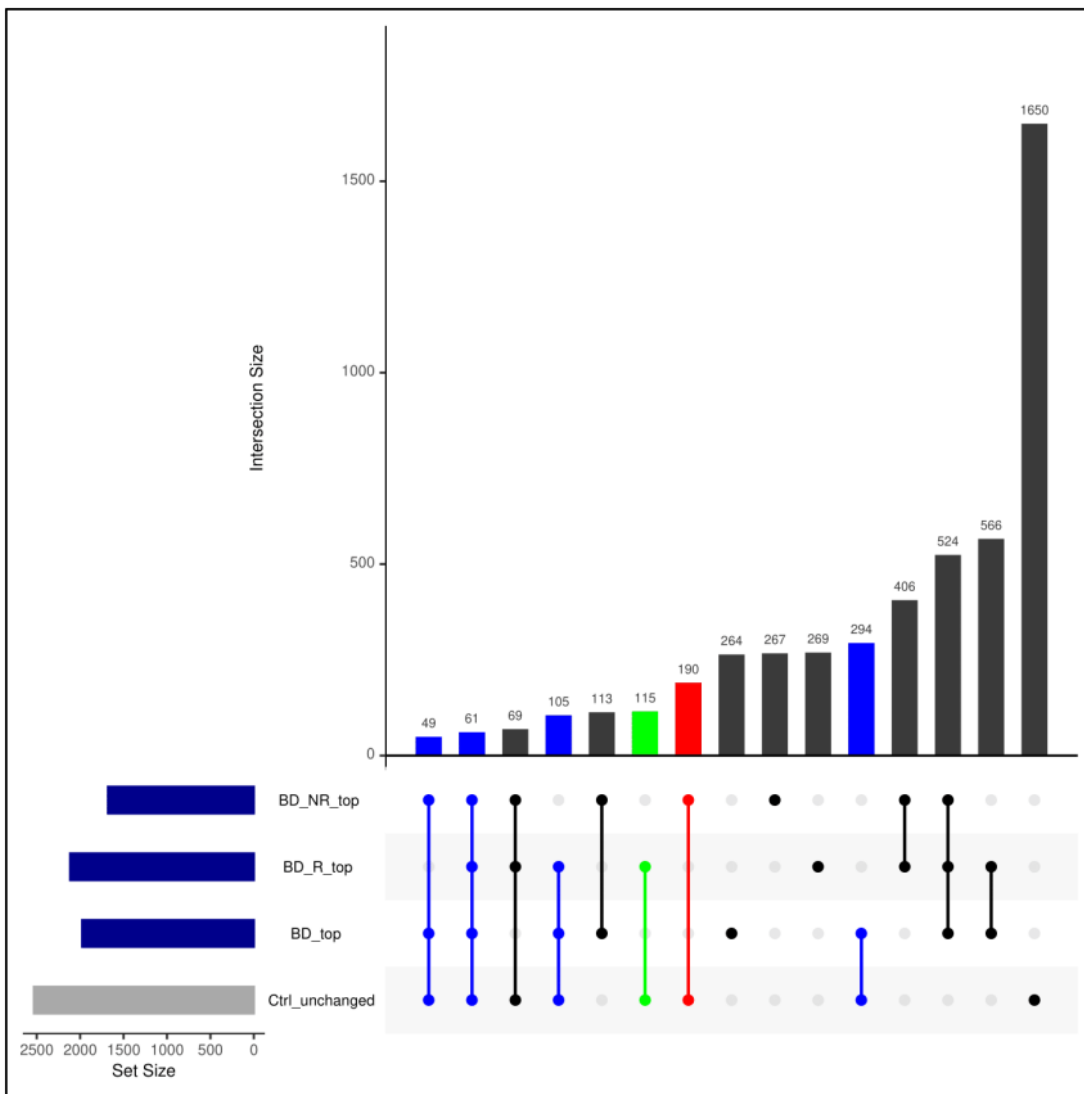


**Figure.S13: Identifying 'BD', 'BD-Responder' and 'BD-NonResponder' relevant reactions by MTA analysis of BD astrocyte (norm-t1) metabolic models.**

UpSet plot depicting the intersections among four reaction sets derived from MTA analysis of BD astrocyte (norm-t1) metabolic models. The reaction sets include 'BD\_top' (transforms iPS-Ctrl-a $\rightleftharpoons$ iPS-BD), 'BD\_R\_top' (transforms iPS-Ctrl-a $\rightleftharpoons$ iPS-BD-R), 'BD\_NR\_top' (transforms iPS-Ctrl-a $\rightleftharpoons$ iPS-BD-NR), and 'Ctrl\_unchanged' (does not transform iPS-Ctrl-a $\rightleftharpoons$ Primary-Ctrl). Colored intersections represent shortlisted and sliced reactions based on [Table.1](#) criteria. Blue, green, and red intersections denote BD, BD-Responder, and BD-NonResponder subset(s), respectively. For detailed information, refer to [Supplementary Section 7.1](#).

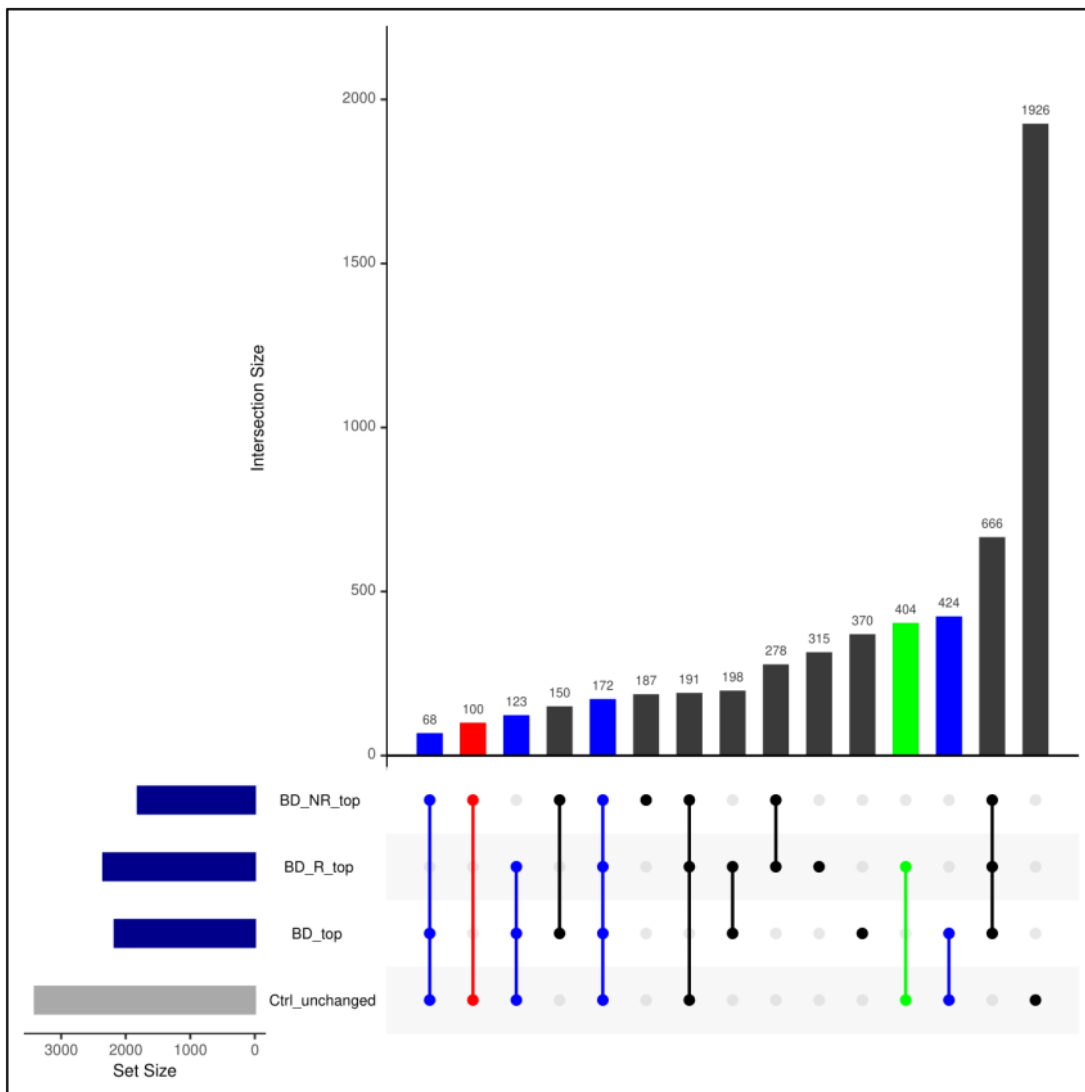


**Figure S14: Identifying 'BD', 'BD-Responder' and 'BD-NonResponder' relevant reactions by MTA analysis of BD astrocyte (norm-t2) metabolic models.**

UpSet plot depicting the intersections among four reaction sets derived from MTA analysis of BD astrocyte (norm-t2) metabolic models. The reaction sets include 'BD\_top' (transforms iPS-Ctrl-a $\rightleftharpoons$ iPS-BD), 'BD\_R\_top' (transforms iPS-Ctrl-a $\rightleftharpoons$ iPS-BD-R), 'BD\_NR\_top' (transforms iPS-Ctrl-a $\rightleftharpoons$ iPS-BD-NR), and 'Ctrl\_unchanged' (does not transform iPS-Ctrl-a $\rightleftharpoons$ Primary-Ctrl). Colored intersections represent shortlisted and sliced reactions based on [Table 1](#) criteria. Blue, green, and red intersections denote BD, BD-Responder, and BD-NonResponder subset(s), respectively. For detailed information, refer to [Supplementary Section 7.1](#).

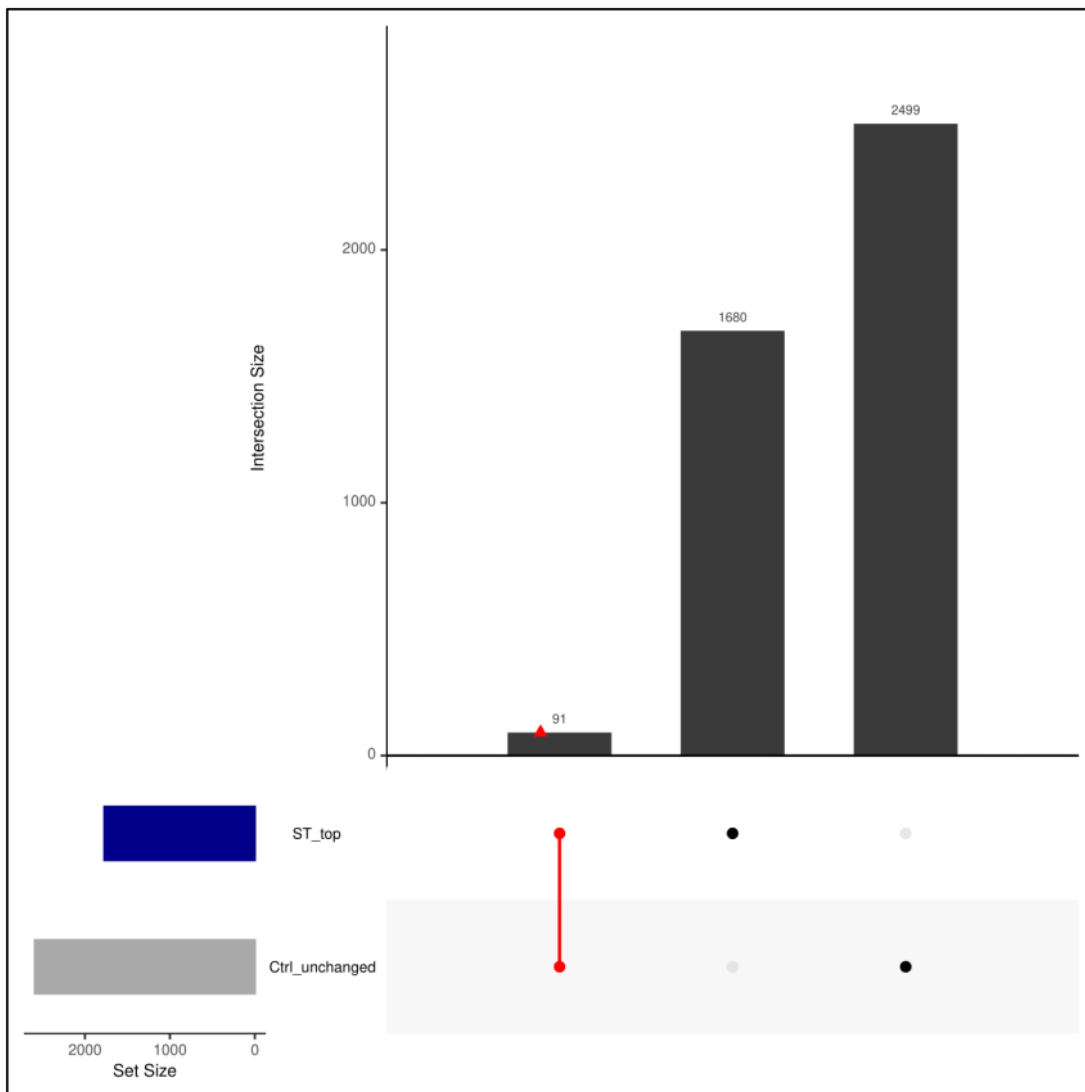


**Figure.S15: Identifying 'SCZ-Twin' relevant reactions by MTA analysis of SCZ astrocyte (abs) metabolic models.**

UpSet plot depicting the intersections among two reaction sets derived from MTA analysis of SCZ astrocyte (abs) metabolic models. The reaction sets include 'ST\_top' (transforms iPS-Ctrl-b*↔*iPS-ST), and 'Ctrl\_unchanged' (does not transform iPS-Ctrl-b*↔*iPS-HT/Primary-Ctrl). Colored intersections represent shortlisted and sliced reactions based on [Table.1](#) criteria. Red intersections denote SCZ-Twin subset(s). For detailed information, refer to [Supplementary Section 7.1](#).

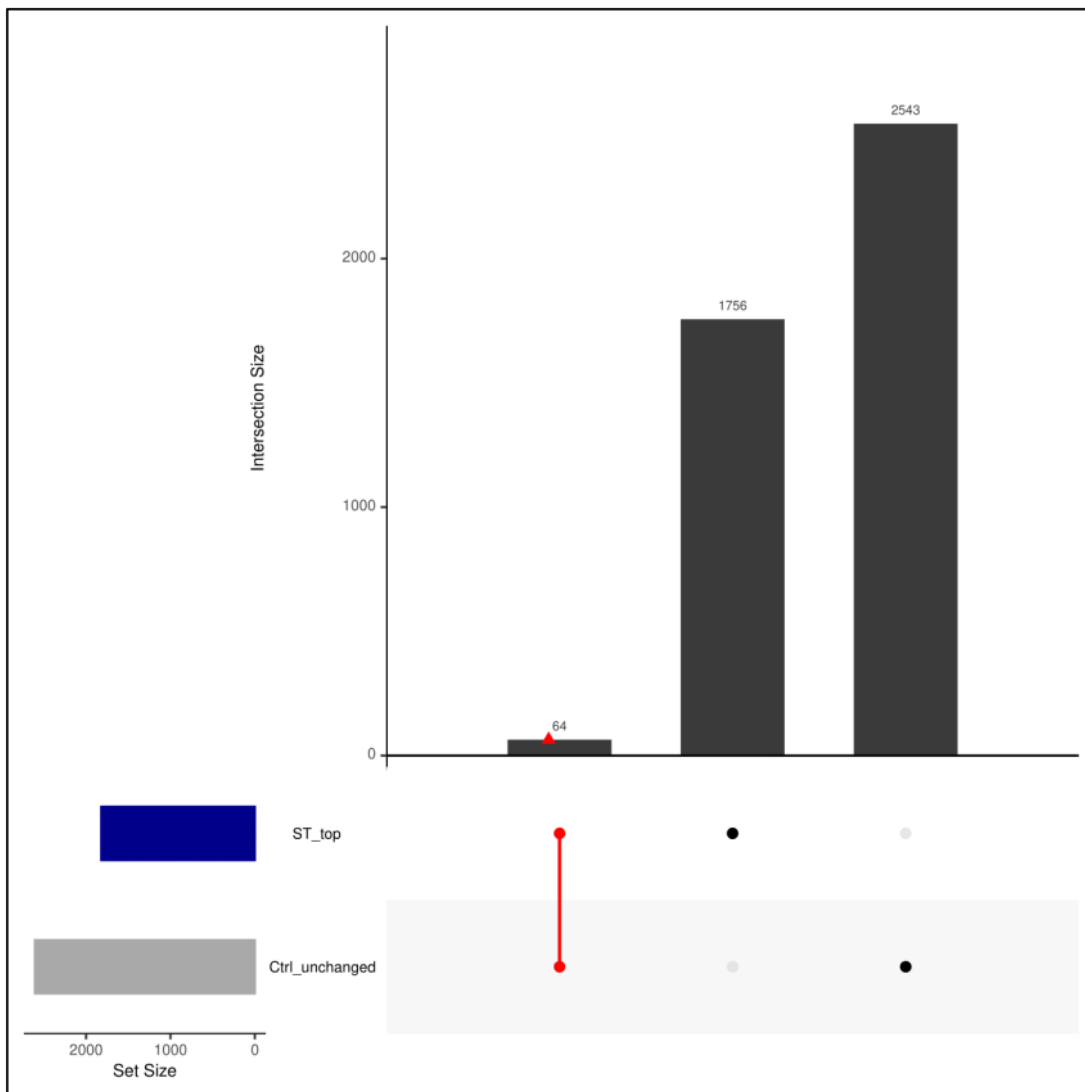


**Figure.S16: Identifying 'SCZ-Twin' relevant reactions by MTA analysis of SCZ astrocyte (norm-t1) metabolic models.**

UpSet plot depicting the intersections among two reaction sets derived from MTA analysis of SCZ astrocyte (norm-t1) metabolic models. The reaction sets include 'ST\_top' (transforms iPS-Ctrl-b $\rightleftharpoons$ iPS-ST), and 'Ctrl\_unchanged' (does not transform iPS-Ctrl-b $\rightleftharpoons$ iPS-HT/Primary-Ctrl). Colored intersections represent shortlisted and sliced reactions based on [Table.1](#) criteria. Red intersections denote SCZ-Twin subset(s). For detailed information, refer to [Supplementary Section 7.1](#).

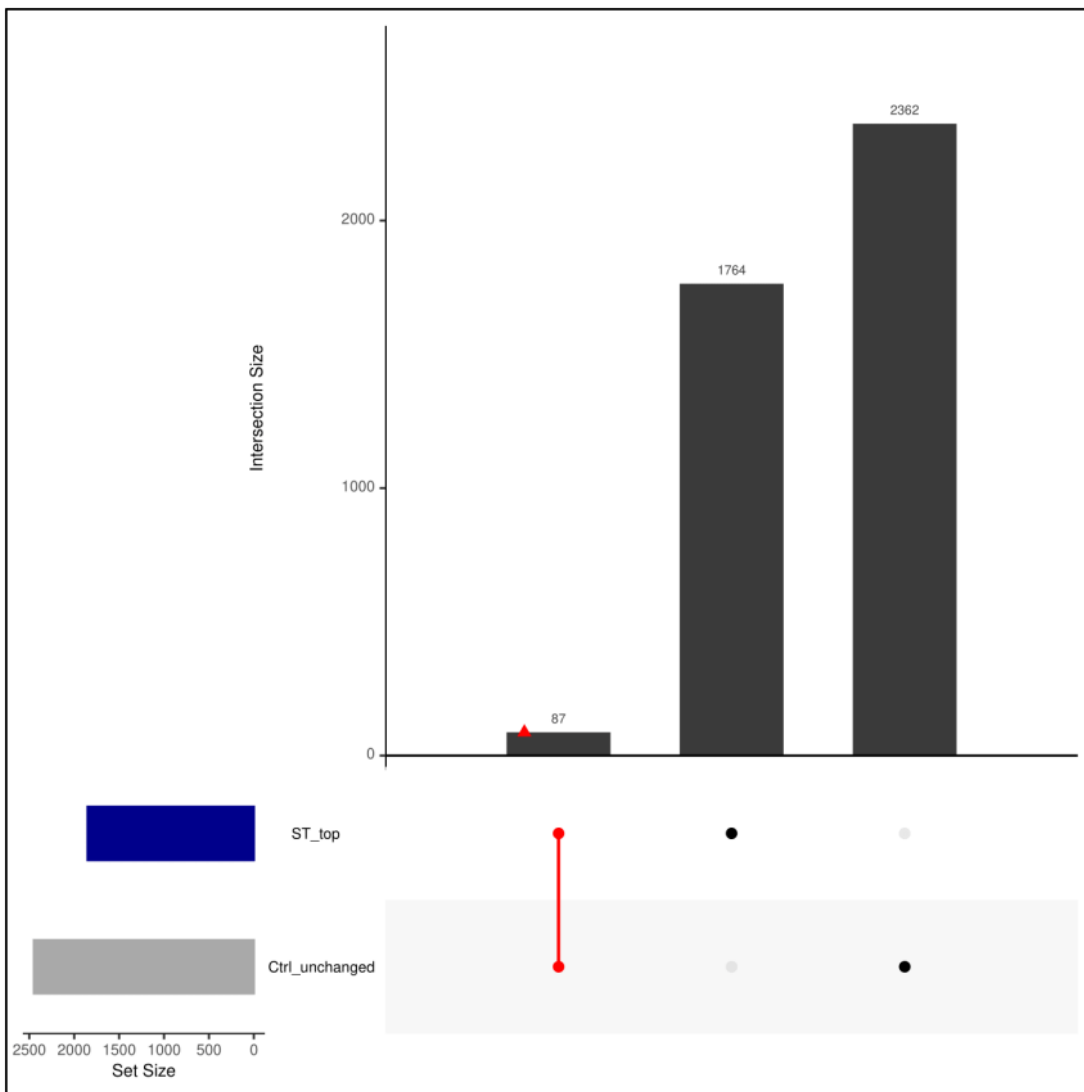


**Figure S17: Identifying 'SCZ-Twin' relevant reactions by MTA analysis of SCZ astrocyte (norm-t2) metabolic models.**

UpSet plot depicting the intersections among two reaction sets derived from MTA analysis of SCZ astrocyte (norm-t2) metabolic models. The reaction sets include 'ST\_top' (transforms iPS-Ctrl-b $\rightleftharpoons$ iPS-ST), and 'Ctrl\_unchanged' (does not transform iPS-Ctrl-b $\rightleftharpoons$ iPS-HT/Primary-Ctrl). Colored intersections represent shortlisted and sliced reactions based on [Table 1](#) criteria. Red intersections denote SCZ-Twin subset(s). For detailed information, refer to [Supplementary Section 7.1](#).

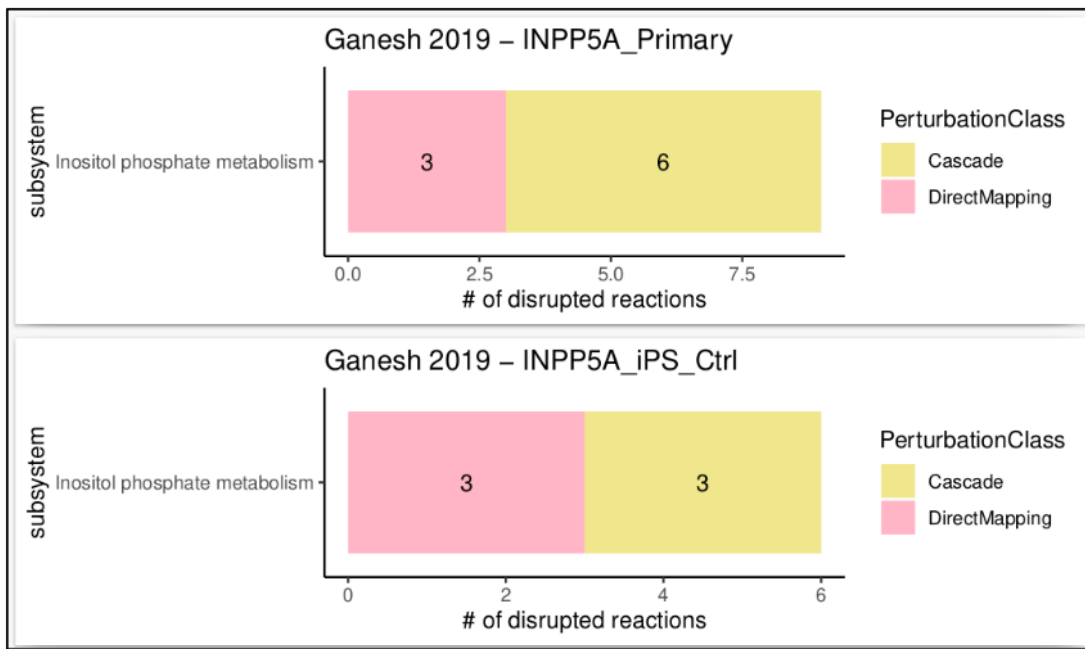


**Figure.S18: The LoF of Inositol Polyphosphate-5-Phosphatase A (*INPP5A*).**

The LoF of *INPP5A*, a gene that directly maps to inositol phosphate metabolism and implicated in SMI<sup>398</sup>, resulted in the disruption of 'Cascade' reactions, also within inositol phosphate metabolism, in either astrocyte metabolic models (Primary-Ctrl and iPS-Ctrl-a).

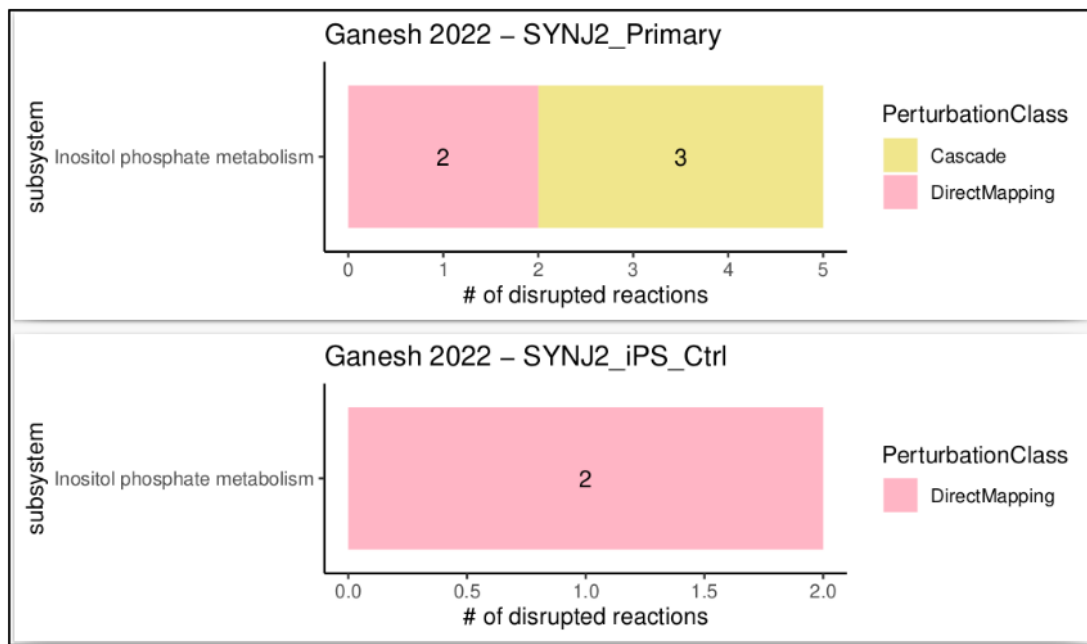


**Figure S19: The LoF of Synaptosomal protein 2 (SYNJ2).**

The LoF of *SYNJ2*, a gene that directly maps to inositol phosphate metabolism and implicated in SMI<sup>397</sup>, resulted in the disruption of 'Cascade' reactions, also within inositol phosphate metabolism, however only in the Primary-Ctrl astrocyte metabolic model, but not in the iPS-Ctrl-a model.

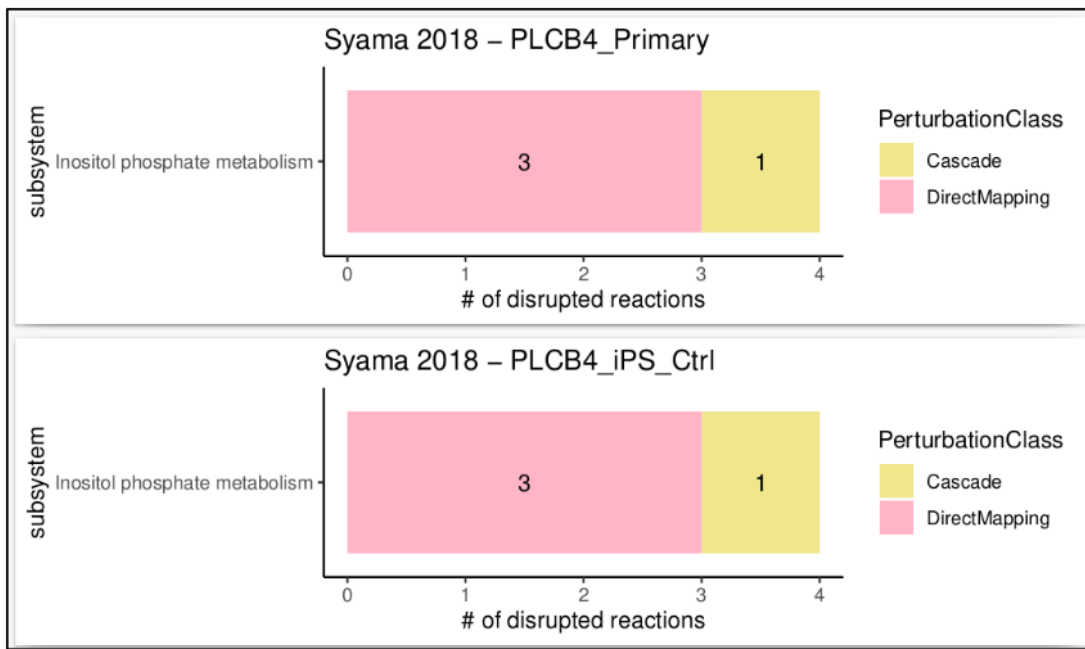


**Figure.S20: The LoF of Phospholipase C Beta 4 (PLCB4).**

The LoF of *PLCB4*, a gene that directly maps to inositol phosphate metabolism and implicated in AD<sup>399</sup>, resulted in the disruption of a single 'Cascade' reaction, also within inositol phosphate metabolism, in either astrocyte metabolic models (Primary-Ctrl and iPS-Ctrl-a).

# Constraint-based modeling of astrocyte metabolism in neuropsychiatric disorders

ORIGINALITY REPORT



PRIMARY SOURCES

- | Rank | Source  | Type            | Percentage |
|------|---|-----------------|------------|
| 1    | <a href="http://www.cell.com">www.cell.com</a>  | Internet Source | 1 %        |
| 2    | <a href="http://www.researchgate.net">www.researchgate.net</a>  | Internet Source | 1 %        |
| 3    | <a href="http://www.wpanet.org">www.wpanet.org</a>  | Internet Source | 1 %        |
| 4    | <a href="http://content.yudu.com">content.yudu.com</a>  | Internet Source | 1 %        |
| 5    | Gilles Bonvento, Juan P. Bolaños. "Astrocyte-neuron metabolic cooperation shapes brain activity", Cell Metabolism, 2021   | Publication     | 1 %        |
| 6    | <a href="http://livrepository.liverpool.ac.uk">livrepository.liverpool.ac.uk</a>  | Internet Source | 1 %        |
| 7    | Feng Cai, Divya Bezwada, Ling Cai, Rohit Mahar et al. "Comprehensive isotopomer analysis of glutamate and aspartate in small tissue samples", Cell Metabolism, 2023 | Publication     | 1 %        |

8	escholarship.org Internet Source	<1 %
9	hdl.handle.net Internet Source	<1 %
10	academic.oup.com Internet Source	<1 %
11	www.nature.com Internet Source	<1 %
12	Michael J. Gandal, Jillian R. Haney, Neelroop N. Parikshak, Virpi Leppa et al. "Shared molecular neuropathology across major psychiatric disorders parallels polygenic overlap", <i>Science</i> , 2018 Publication	<1 %
13	"THE ENZYMATIC RESPONSE OF ASTROCYTES TO VARIOUS IONS IN VITRO", <i>The Journal of Cell Biology</i> , 01/01/1964 Publication	<1 %
14	pharmacometabolomics.duhs.duke.edu Internet Source	<1 %
15	www.ncbi.nlm.nih.gov Internet Source	<1 %
16	www.medrxiv.org Internet Source	<1 %

- 17 Sameer Aryal, Kevin Bonanno, Bryan Song, D.R. Mani, Hasmik Keshishian, Steven A. Carr, Morgan Sheng, Borislav Dejanovic. "Deep proteomics identifies shared molecular pathway alterations in synapses of patients with schizophrenia and bipolar disorder and mouse model", *Cell Reports*, 2023 <1 %  
Publication
- 
- 18 Philip Hasel, Shane A. Liddelow. "Astrocytes", *Current Biology*, 2021 <1 %  
Publication
- 
- 19 Jonathan M. Ghergurovich, Jessica D. Lang, Maren K. Levin, Natalia Briones et al. "Local production of lactate, ribose phosphate, and amino acids by human triple-negative breast cancer", *Med*, 2021 <1 %  
Publication
- 
- 20 [www.biorxiv.org](http://www.biorxiv.org) <1 %  
Internet Source
- 
- 21 Yan Jouroukhin, Yusuke Kageyama, Varvara Misheneva, Alexey Shevelkin et al. "DISC1 regulates lactate metabolism in astrocytes: implications for psychiatric disorders", *Translational Psychiatry*, 2018 <1 %  
Publication
- 
- 22 nbn-resolving.de <1 %  
Internet Source

23	<a href="http://www.omicsdi.org">www.omicsdi.org</a> Internet Source	<1 %
24	<a href="http://www.repository.cam.ac.uk">www.repository.cam.ac.uk</a> Internet Source	<1 %
25	<b>Swagatika Sahoo, Ranjith Kumar Ravi Kumar, Brandon Nicolay, Omkar Mohite et al.</b> <b>"Metabolite systems profiling identifies exploitable weaknesses in retinoblastoma", FEBS Letters, 2018</b> Publication	<1 %
26	<a href="http://www.aseanjournalofpsychiatry.org">www.aseanjournalofpsychiatry.org</a> Internet Source	<1 %
27	<b>Submitted to Cardiff University</b> Student Paper	<1 %
28	<b>Sonja de Zwart, Rachel Brouwer, Christopher Ching, Ole Andreassen et al.</b> "21. ENIGMA-Relatives: The Association Between Familial Risk for Schizophrenia or Bipolar Disorder and Brain Abnormalities", Biological Psychiatry, 2019 Publication	<1 %
29	<b>O. D. Kozenkov, V. V. Gorbunov.</b> "A model for the heat balance of an infinitely long whisker", Inorganic Materials, 2015 Publication	<1 %
30	<a href="http://link.springer.com">link.springer.com</a> Internet Source	

<1 %

- 
- 31 Supreeta Vijayakumar, Claudio Angione. "Protocol for hybrid flux balance, statistical, and machine learning analysis of multi-omic data from the cyanobacterium Synechococcus sp. PCC 7002", STAR Protocols, 2021 <1 %  
Publication
- 
- 32 Elisabeth Yaneske, Guido Zampieri, Loris Bertoldi, Giuseppe Benvenuto, Claudio Angione. "Genome-scale metabolic modelling of SARS-CoV-2 in cancer cells reveals an increased shift to glycolytic energy production", FEBS Letters, 2021 <1 %  
Publication
- 
- 33 Yizhak, Keren, Orshay Gabay, Haim Cohen, and Eytan Ruppin. "Model-based identification of drug targets that revert disrupted metabolism and its application to ageing", Nature Communications, 2013. <1 %  
Publication
- 
- 34 Priyanka Baloni, Cory C. Funk, Jingwen Yan, James T. Yurkovich et al. "Metabolic Network Analysis Reveals Altered Bile Acid Synthesis and Metabolism in Alzheimer's Disease", Cell Reports Medicine, 2020 <1 %  
Publication
-

- 35 Swagatika Sahoo, R Ranjith Kumar, Brandon Nicolay, Omkar Mohite et al. "Metabolite systems profiling identifies exploitable weaknesses in Retinoblastoma", FEBS Letters, 2018  
Publication <1 %
- 36 [www.science.gov](http://www.science.gov) Internet Source <1 %
- 37 [encyclopedia.pub](http://encyclopedia.pub) Internet Source <1 %
- 38 Juan Ricardo Velasco-Álvarez, Nimbe Torres y Torres, Isaac Chairez, José Luis Castrejón-Flores. "Microbiome distribution modeling using gradient descent strategies for mock, in vitro and clinical community distributions", PLOS ONE, 2023  
Publication <1 %
- 39 Gianvito Pio, Paolo Mignone, Giuseppe Magazzù, Guido Zampieri, Michelangelo Ceci, Claudio Angione. "Integrating genome-scale metabolic modelling and transfer learning for human gene regulatory network reconstruction", Bioinformatics, 2021  
Publication <1 %
- 40 Y Sade, L Toker, N Z Kara, H Einat, S Rapoport, D Moechars, G T Berry, Y Bersudsky, G Agam. "IP3 accumulation and/or inositol depletion: <1 %

two downstream lithium's effects that may mediate its behavioral and cellular changes", *Translational Psychiatry*, 2016

Publication

---

- 41 Akriti Srivastava, Pallavi Somvanshi, Bhartendu Nath Mishra. "Reconstruction and visualization of carbohydrate, N-glycosylation pathways in *Pichia pastoris* CBS7435 using computational and system biology approaches", *Systems and Synthetic Biology*, 2012 <1 %
- Publication
- 
- 42 ebin.pub <1 %
- Internet Source
- 
- 43 Bolun Cheng, Chujun Liang, Ping Li, Li Liu, Shiqiang Cheng, Mei Ma, Lu Zhang, Xin Qi, Yan Wen, Feng Zhang. "Evaluating the Genetic Correlations Between Left-Handedness and Mental Disorder Using Linkage Disequilibrium Score Regression and Transcriptome-Wide Association Study", *Biochemical Genetics*, 2020 <1 %
- Publication
- 
- 44 Carla P., Liliana P., M. Margarida C.A. Castro. "Chapter 5 Li<sup>+</sup> in Bipolar Disorder – Possible Mechanisms of Its Pharmacological Mode of Action", *IntechOpen*, 2012 <1 %
- Publication
-

45

Marine P. M. Letertre, Gaud Dervilly, Patrick Giraudeau. "Combined Nuclear Magnetic Resonance Spectroscopy and Mass Spectrometry Approaches for Metabolomics", *Analytical Chemistry*, 2020

Publication

<1 %

46

S.T.R. Moolamalla, P.K. Vinod. "Genome-scale metabolic modelling predicts biomarkers and therapeutic targets for neuropsychiatric disorders", *Computers in Biology and Medicine*, 2020

Publication

<1 %

47

Boaz Styr, Nir Gonen, Daniel Zarhin, Antonella Ruggiero et al. "Mitochondrial Regulation of the Hippocampal Firing Rate Set Point and Seizure Susceptibility", *Neuron*, 2019

Publication

<1 %

48

Hamideh Fouladiha, Sayed-Amir Marashi. "Biomedical applications of cell- and tissue-specific metabolic network models", *Journal of Biomedical Informatics*, 2017

Publication

<1 %

49

Submitted to Management Development Institute Of Singapore

Student Paper

<1 %

50

Submitted to UC, San Diego

Student Paper

<1 %

51	Submitted to University of Cambridge Student Paper	<1 %
52	static-site-aging-prod2.impactaging.com Internet Source	<1 %
53	topsecretapiaccess.dovepress.com Internet Source	<1 %
54	www.frontiersin.org Internet Source	<1 %
55	www2.neuroscience.umn.edu Internet Source	<1 %
56	Submitted to University of Aberdeen Student Paper	<1 %
57	content.iospress.com Internet Source	<1 %
58	uspto.report Internet Source	<1 %
59	www.mdpi.com Internet Source	<1 %
60	journals.plos.org Internet Source	<1 %
61	mdpi-res.com Internet Source	<1 %
62	pure-test.amc.nl Internet Source	<1 %

- 63 Areejit Samal. "Conservation of high-flux backbone in alternate optimal and near-optimal flux distributions of metabolic networks", *Systems and Synthetic Biology*, 05/30/2009 <1 %  
Publication
- 
- 64 Feng Wang, XiuJie Wang, Ying Zhang, Jiarong Yan et al. " SIFHY3 and SIHY5 act compliantly to enhance cold tolerance through the integration of -inositol and light signaling in tomato ", *New Phytologist*, 2022 <1 %  
Publication
- 
- 65 Firoza Mamdani, Iris Jaitovich Groisman, Martin Alda, Gustavo Turecki. "Long-term responsiveness to lithium as a pharmacogenetic outcome variable: Treatment and etiologic implications", *Current Psychiatry Reports*, 2003 <1 %  
Publication
- 
- 66 Scott A Becker, Adam M Feist, Monica L Mo, Gregory Hannum, Bernhard Ø Palsson, Markus J Herrgard. "Quantitative prediction of cellular metabolism with constraint-based models: the COBRA Toolbox", *Nature Protocols*, 2007 <1 %  
Publication
- 
- 67 Suthat Phaiphinit, Sittiporn Pattaradilokrat, Chidchanok Lursinsap, Kitiporn Plaimas. "In <1 %

silico multiple-targets identification for heme detoxification in the human malaria parasite *Plasmodium falciparum*", *Infection, Genetics and Evolution*, 2016

Publication

68	<a href="http://aacrjournals.org">aacrjournals.org</a>	<1 %
69	<a href="http://archive.org">archive.org</a>	<1 %
70	<a href="http://dspace.cuni.cz">dspace.cuni.cz</a>	<1 %
71	<a href="http://dspace.uib.es">dspace.uib.es</a>	<1 %
72	<a href="http://ladd00.triumf.ca">ladd00.triumf.ca</a>	<1 %
73	<a href="http://www.diva-portal.org">www.diva-portal.org</a>	<1 %
74	<a href="http://www2.mdpi.com">www2.mdpi.com</a>	<1 %
75	"Computational Approaches to Dissect and Understand Mechanisms of Adaptation", <i>Molecular Mechanisms in Plant Adaptation</i> , 2015.	<1 %
76	Andrew Walakira, Damjana Rozman, Tadeja Režen, Miha Mraz, Miha Moškon. "Guided	<1 %

extraction of genome-scale metabolic models for the integration and analysis of omics data", Computational and Structural Biotechnology Journal, 2021

Publication

---

- 77 Ankur Gupta, Ajay Kumar, Rajat Anand, Nandadulal Bairagi, Samrat Chatterjee. "Genome scale metabolic model driven strategy to delineate host response to Mycobacterium tuberculosis infection", Molecular Omics, 2021 <1 %
- Publication
- 
- 78 David Kalman, Austin Lee, Edward Chan, Donald R. Miller, Avron Spiro, Xinhua S. Ren, Lewis E. Kazis. "Alcohol Dependence, Other Psychiatric Disorders, and Health-Related Quality of Life: A Replication Study in a Large Random Sample of Enrollees in the Veterans Health Administration", The American Journal of Drug and Alcohol Abuse, 2004 <1 %
- Publication
- 
- 79 Eagleman, David, Downar, Jonathan. "Brain and Behavior", Brain and Behavior, 2023 <1 %
- Publication
- 
- 80 Shoval Lagziel, Won Dong Lee, Tomer Shlomi. "Studying metabolic flux adaptations in cancer through integrated experimental- <1 %

computational approaches", BMC Biology,  
2019

Publication

---

- 81 insight.jci.org <1 %  
Internet Source
- 82 openresearch.surrey.ac.uk <1 %  
Internet Source
- 83 www.mintankesmie.no <1 %  
Internet Source
- 84 Marja Koskuvi, Šárka Lehtonen, Kalevi Trontti, Meike Keuters et al. "Patient iPSC-astrocytes show transcriptional and functional dysregulation in schizophrenia", Cold Spring Harbor Laboratory, 2020  
Publication
- 85 Nathan G. Skene, Julien Bryois, Trygve E. Bakken, Gerome Breen et al. "Genetic identification Of brain cell types underlying schizophrenia", Cold Spring Harbor Laboratory, 2017  
Publication
- 86 Niccolo Tesi, Marc Hulsman, Sven van der Lee, Iris Jansen et al. "The effect of Alzheimer's disease-associated genetic variants on longevity", Cold Spring Harbor Laboratory, 2021  
Publication

87

Ole A. Andreassen, Guy F.L. Hindley, Oleksandr Frei, Olav B. Smeland. "New insights from the last decade of research in psychiatric genetics: discoveries, challenges and clinical implications", World Psychiatry, 2023

<1 %

Publication

---

88

Xiao-Yi Xiong, Yong Tang, Qing-Wu Yang. "Metabolic changes favor the activity and heterogeneity of reactive astrocytes", Trends in Endocrinology & Metabolism, 2022

<1 %

Publication

---

89

Cholsoon Jang, Li Chen, Joshua D. Rabinowitz. "Metabolomics and Isotope Tracing", Cell, 2018

<1 %

Publication

---

90

Timothy A. Thornton. "Statistical Methods for Genome-Wide and Sequencing Association Studies of Complex Traits in Related Samples", Current Protocols in Human Genetics, 2015

<1 %

Publication

---

Exclude quotes

Off

Exclude matches

Off

Exclude bibliography

Off